This document is confidential and is proprietary to the American Chemical Society and its authors. Do not copy or disclose without written permission. If you have received this item in error, notify the sender and delete all copies.

The Structural Basis of Sirtuin 6-Catalyzed Nucleosome Deacetylation

Journal:	Journal of the American Chemical Society
Manuscript ID	ja-2022-13512a.R3
Manuscript Type:	Article
Date Submitted by the Author:	n/a
Complete List of Authors:	Wang, Zhipeng; Harvard Medical School, Department of Medicine Markert, Jonathan; Harvard Medical School, Cell Biology Whedon, Samuel; Harvard Medical School, Medicine Yapa Abeywardana, Maheeshi; Harvard Medical School, Medicine and BCMP Lee, Kwangwoon; Harvard Medical School Jiang, Hanjie; Harvard Medical School, Medicine and BCMP Suarez, Carolay; Harvard Medical School, Medicine and BCMP Lin, Hening; Cornell University, Chemistry and Chemical Biology; Farnung, Lucas; Harvard Medical School, Cell Biology Cole, Philip; Harvard Medical School, Medicine and BCMP

SCHOLARONE™ Manuscripts

The Structural Basis of Sirtuin 6-Catalyzed Nucleosome Deacetylation

Zhipeng A. Wang,^{†,‡,#} Jonathan W. Markert,^{§,#} Samuel D. Whedon,^{†,‡,#} Maheeshi Yapa Abeywardana,^{†,‡} Kwangwoon Lee,^{†,‡} Hanjie Jiang,^{†,‡} Carolay Suarez,^{†,‡} Hening Lin,[^] Lucas Farnung,^{§,*} and Philip A. Cole, ^{†,‡,*}

- † Division of Genetics, Department of Medicine, Brigham and Women's Hospital, Boston, MA, 02115, United States;
- [‡] Department of Biological Chemistry and Molecular Pharmcology, Harvard Medical School, Boston, MA, 02115, United States;
- § Department of Cell Biology, Blavatnik Institute, Harvard Medical School, Boston, MA, 02115, United States;
- ^ Howard Hughes Medical Institute; Department of Chemistry and Chemical Biology, Cornell University, Ithaca, NY, 14853, United States

KEYWORDS: Sirtuin 6, Histone, Nucleosome, Cryo-EM, NAD.

ABSTRACT: The reversible acetylation of histone lysine residues is controlled by the action of acetyltransferases and deacetylases (HDACs) which regulate chromatin structure and gene expression. The sirtuins are a family of NAD-dependent HDAC enzymes and one member, sirtuin 6, Sirt6, influences DNA repair, transcription, and aging. Here we demonstrate that Sirt6 is efficient at deacetylating several histone H3 acetylation sites, including its canonical site Lys9, in the context of nucleosomes but not free acetylated histone H3 protein substrates. By installing a chemical warhead at the Lys9 position of histone H3, we trap a catalytically poised Sirt6 in complex with a nucleosome and employ this in cryo-EM structural analysis. The structure of Sirt6 bound to a nucleosome reveals extensive interactions between distinct segments of Sirt6 and the H2A/H2B acidic patch and nucleosomal DNA, which accounts for the rapid deacetylation of nucleosomal H3 sites and the disfavoring of histone H2B acetylation sites. These findings provide a new framework for understanding how HDACs target and regulate chromatin.

INTRODUCTION

Reversible lysine acetylation modifications on histones and other proteins are a major and critical class of post-translational modifications that regulate chromatin structure, gene expression, and numerous biological processes (Figure 1A). In humans, there are 18 established histone deacetylases (HDACs, aka KDACs), which include 11 metallohydrolase HDACs² and 7 NAD-dependent HDACs known as sirtuins. The dysregulation of HDACs in cancer and other diseases has led to drug discovery efforts to identify HDAC modulators and several metallohydrolase HDAC inhibitors are approved for the treatment of cutaneous T cell lymphoma and other malignancies. Sirtuin inhibitors⁵ and activators⁶ have also been intensively pursued for various therapeutic applications.

Although the site-specificities of particular HDACs for various histone acetylation sites has been identified, the mechanistic details of how deacetylation occurs in the context of chromatin are generally lacking. In this study, we focus on sirtuin 6, Sirt6. Sirt6 is a 355 amino acid-long enzyme that has been shown to play a critical role in DNA damage response, modulating transcriptional pause release, and has been found to show altered activity in various diseases. Increased Sirt6 activity has been shown to enhance lifespan in Drosophila and mice, and DNA sequence polymorphisms in humans have been correlated with altered longevity. As a result, there has been an effort to develop Sirt6 allosteric activator small molecules such as MDL-800¹³ that are hypothesized to impede biological aging.

Sirt6 can catalyze at least three distinct reaction types: Lys deacetylation, long chain Lys deacylation¹⁴, and ADPribosylation. 15 However Sirt6's specific activity and selectivity for different histone lysine sites, 16 how these activities are regulated, 17 and the connections between enzymatic activities and biological function¹⁸ are unclear.¹⁹ Sirt6 has been reported to be poor at deacetylation of free histone tail peptides^{14, 20} but in cellular studies, Sirt6 has a documented preference for cleavage of Lys9 acetylation of histone H3 (H3K9ac),²¹ leading to the hypothesis that Sirt6 can deacetylate histones more efficiently in chromatin substrates.²² Several X-ray structures of histone peptides in complex with Sirt6 have been reported, 14, 23 but the molecular recognition of nucleosome substrates by Sirt6 has been poorly understood.²⁴ Sirt6 appears to have relatively high affinity for nucleosomes (nanomolar K_D values) which is partially mediated by the H2A/H2B "acidic patch" as well as nucleosomal DNA, though the structural details of these interactions are lacking.²⁴ Here we have analyzed site-specifically acetylated nucleosomes as substrates to assess the rate of deacetylation of a range of Lys sites in histone H3 and histone H2B. Moreover, we have used protein semisynthesis to prepare a Lys9-thiocarbonyl derivatized nucleosome to trap a Sirt6nucleosome complex. This approach facilitated the structural determination of Sirt6 bound to nucleosome in a catalytically poised conformation.

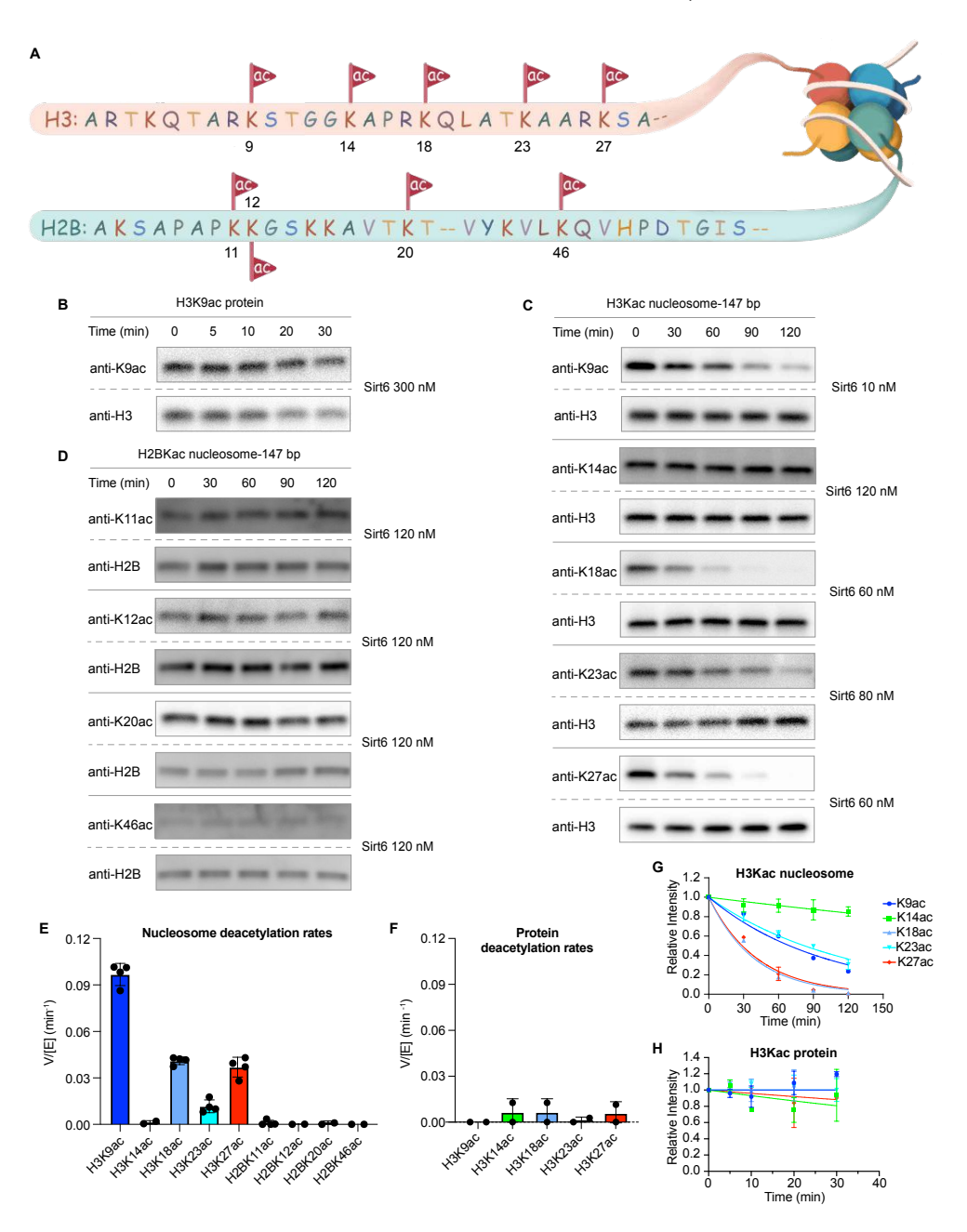


Figure 1. Sirt6 nucleosome deacetylation kinetics. (A) Illustration of histone H3 and H2B N-terminal acetylation sites and surrounding sequence. (B) Western blot analysis of Sirt6 deacetylation of free H3K9ac protein. Enzyme concentrations (right) were selected to maintain diminishing H3K9ac intensity in the antibody linear range. (C) Western blot analysis of Sirt6 deacetylation of multiple nucleosome H3Kac sites. Enzyme concentrations (right) were selected to maintain diminishing H3K9ac intensity in the antibody linear range. (D) Western blot analysis of Sirt6 deacetylation of multiple nucleosome H2BKac sites. Enzyme concentrations (right) were selected to maintain diminishing H2BK9ac intensity in the antibody linear range. (E) Comparison of Sirt6 V/[E] for different nucleosome H3Kac and H2BKac sites. (F) Comparison of Sirt6 V/[E] for different free protein H3Kac sites (G) Deacetylation rate curve fitting for different nucleosome H3Kac sites. (H) Deacetylation rate curve fitting for different free protein H3Kac sites (n=2-4).

RESULTS

Sirt6 deacetylation of acetylated nucleosome substrates.

To understand the site- and substrate-selectivity of Sirt6 required access to chemically defined protein substrates for enzymology. Scarless semisynthetic histone H3 and H2B containing known acetylations at specific sites (Figure 1A) were prepared using engineered sortase enzymes and synthetic tail peptides as previously described (Figure S1).²⁵ For histone H3, we produced K9ac, K14ac, K18ac, K23ac, and K27ac forms and for H2B, we

generated K11ac, K12ac, K20ac, and K46ac forms (Figure S1). The modified histone H3s were assembled into octamers with unmodified recombinant histones H2A, H2B, and H4, and modified H2Bs incorporated into octamers with unmodified recombinant H2A, H3, and H4. Octamers were assembled into nucleosomes with either 147 bp or 185 bp DNA (nucleosome-147 and nucleosome-185),²⁶ and purified by anion exchange chromatography.²⁷ Acetylated histone protein and nucleosomes were analyzed as substrates of purified Sirt6 (Figure S2) using

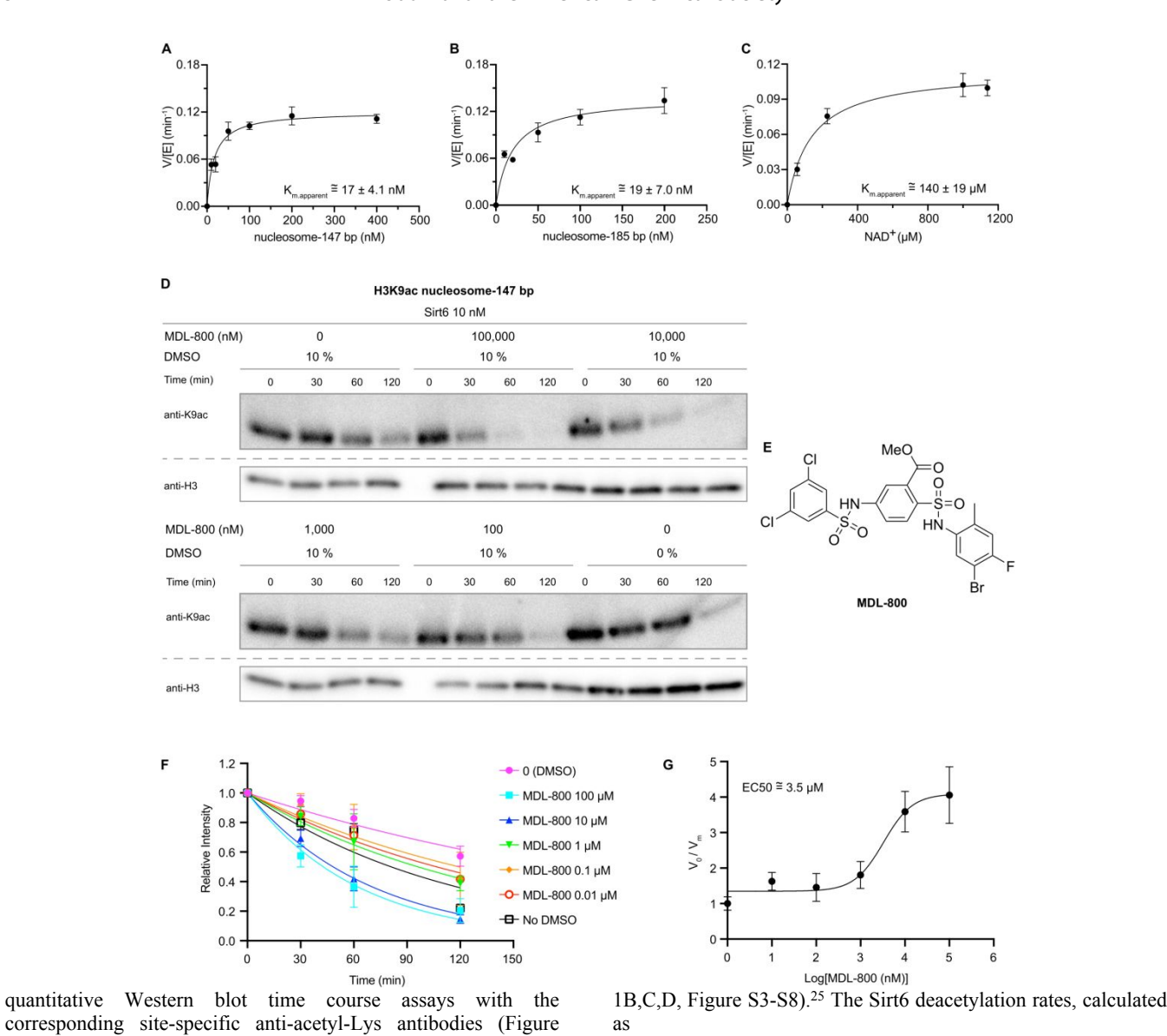
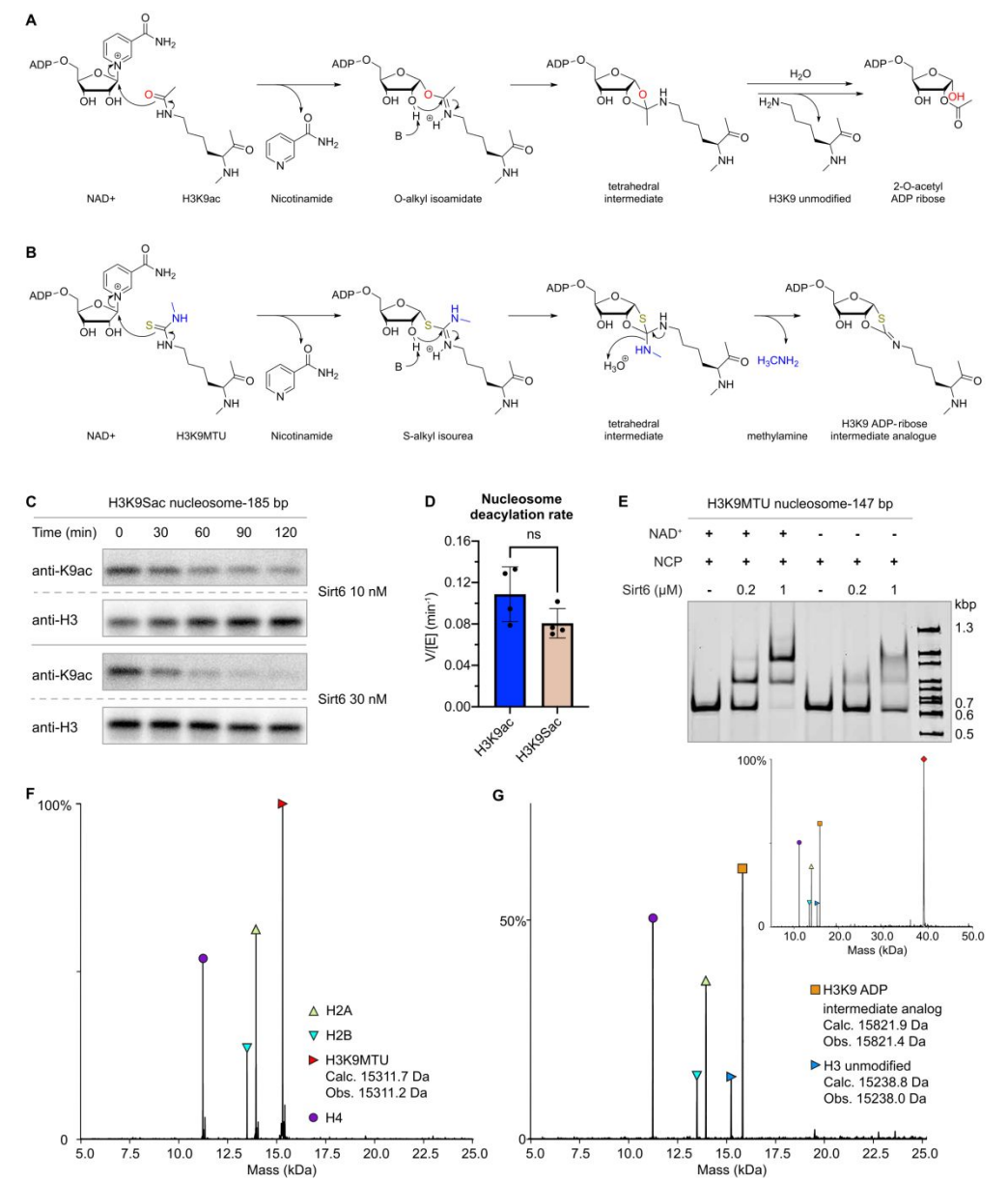


Figure 2. Determination of Sirt6 apparent substrate Km values and allosteric activation by MDL-800. (A) Sirt6 V/[E] vs. 147 bp H3K9ac nucleosome substrate. (B) Sirt6 V/[E] vs. 185 bp H3K9ac nucleosome substrate. (C) Sirt6 V/[E] vs. NAD with 147 bp H3K9ac nucleosome substrate. (D) Western blot analysis of the effect of MDL-800 on Sirt6 deacetylation of H3K9ac 147 bp nucleosome substrates with DMSO as the vehicle control, as DMSO caused a slight rate reduction. (E) MDL-800 structure. (F) Fitting Sirt6 deacetylation rates at different concentrations of MDL-800. (G) MDL-800 activation curve (n=2-3).

velocity/enzyme concentration (V/[E]), are shown in Figure 1E and 1F. Three of the H3 acetylated nucleosome forms revealed robust deacetylation including H3K9ac, H3K18ac, and H3K27ac with V/[E] of 0.1, 0.04, and 0.04 min⁻¹, respectively. The rate of nucleosome H3K9ac deacetylation is comparable to the reported rate of one of the faster class I HDAC1 complexes, CoREST, and faster than recently reported for Sirt1 (V/[E]<0.001 min⁻¹), Sirt2 (0.03 min⁻¹), Sirt3 (0.006 min⁻¹), and Sirt5 (<0.001 min⁻¹).²⁵ In contrast to H3K9ac, H3K18ac, and H3K27ac substrates, Sirt6-mediated deacetylation of H3K23ac (V/[E] 0.011 min⁻¹) and H3K14ac (0.0012 min⁻¹) nucleosome substrates, while detectable, was considerably slower (Figure 1E,G, Table S1). Surprisingly, acetylated H2B nucleosomes were not observed to undergo Sirt6-mediated deacetylation at any of the four sites investigated (V/[E])

<0.001 min⁻¹) (Figure 1D,E). Moreover, neither histone H3 nor H2B free protein were detectably deacetylated by Sirt6 (V/[E] <0.01 min⁻¹) (Figure 1F,H, Figure S7,S8, Table S1). The marked preference of Sirt6 for H3 acetylated nucleosomes over either H2B nucleosomes or free histone proteins starkly contrasts with other sirtuins (Sirt1, Sirt2, Sirt3, and Sirt5)²⁵ and HDAC complexes (CoREST, MIDAC, Sin3, NuRD, MIER, RERE, and SMRT)²⁸, which generally deacetylate free histone protein faster than nucleosomes, and show little preference between nucleosomes with acetylated H3 or H2B.

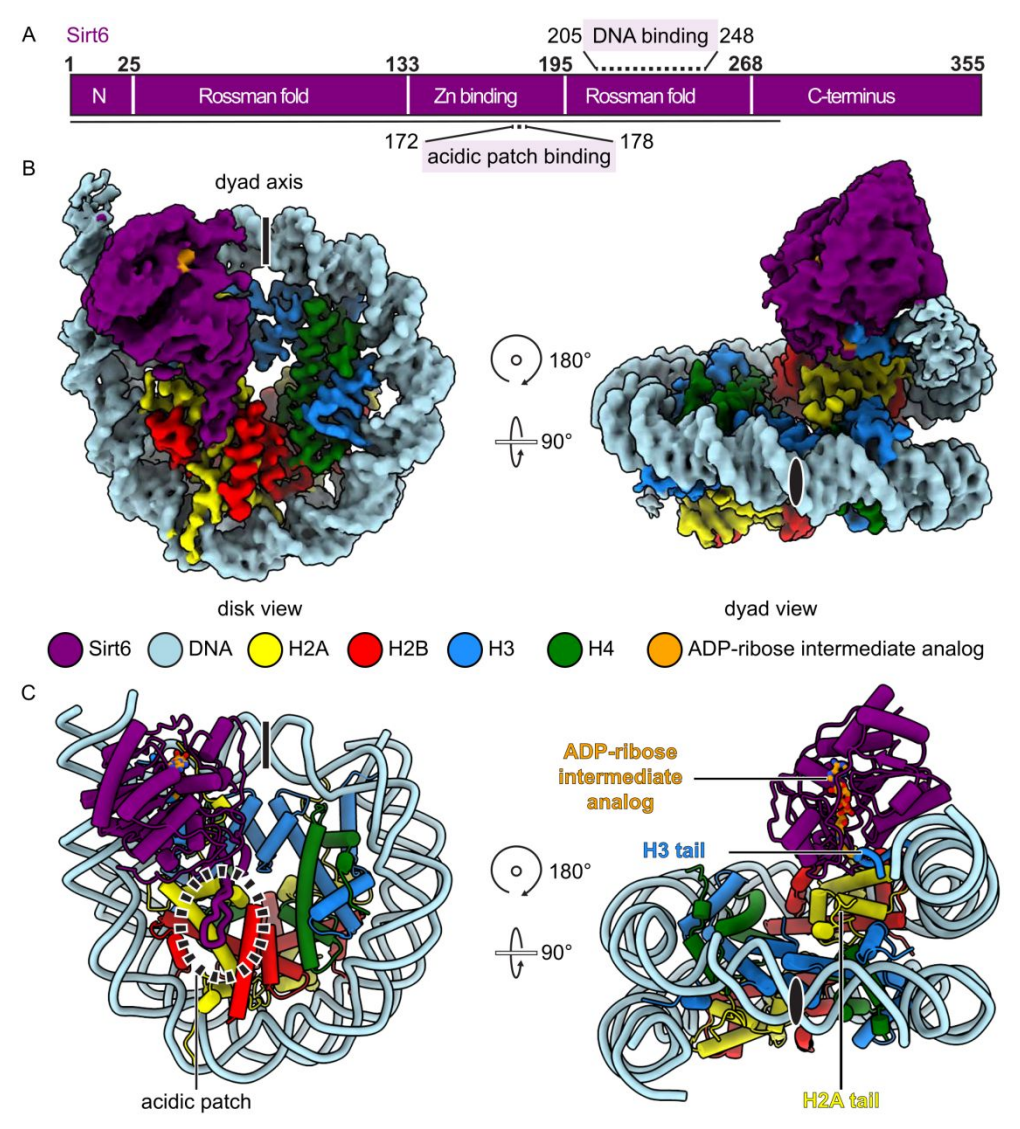
To further characterize H3K9ac nucleosome deacetylation by Sirt6, we examined the substrate concentration dependence and



derived an apparent K_m in the range of 17-19 nM, independent of DNA length (Figure 2A,B, Figure S9,10). This apparent K_m is in the same range as the previously reported K_d value of nucleosome binding to Sirt6.²⁴ It has been reported that sirtuin family members²⁹ exhibit different NAD binding modes³⁰ with NAD affinities depending on the specific acyl-Lys substrate³¹. We determined the NAD concentration dependence here with

nucleosomal substrate, which showed an apparent K_m of $\sim\!150~\mu M$ (Figure 2C, Figure S11), significantly larger than the K_m of NAD obtained with a peptide substrate $(\sim\!15~\mu M).^{32}$ We also explored the influence of ionic strength by varying the reaction NaCl concentration. We observed a sharp decline in Sirt6-catalyzed deacetylation rate with increasing NaCl, indicating the importance of ionic interactions in the binding

Figure 3. Covalent capture of Sirt6 by cofactor crosslinking with ADP-ribose intermediate analogues. (A) Sirtuin deacylation mechanism illustrating proposed O-alkyl isoamidate (PDBID: 4BVE)³³ and tetrahedral intermediates (PDBID: 4F56),³⁴ and observed products (PDBID: 2H59).³⁵ (B) Proposed mechanism of N-methyl thiourea reaction and ADP-ribose intermediate analog. (C) Dethioacetylation of 185 bp H3K9 thioacetyl nucleosomes. (D) Comparison of H3K9 deacetylation and dethioacetylation rates employed an unpaired t-test with a two-tailed P value (ns p>0.1) (n=4). (E) Electrophoretic mobility shift assay of 185 bp H3K9 N-methyl thiourea nucleosome substrates with increasing concentrations of Sirt6, and in the presence or absence of NAD+(n=2). Shifted bands likely correspond to either one (middle) or two (upper) molecules of sirtuins binding to one nucleosome. (F) Deconvoluted intact ESI-MS of H3K9MTU (red triangle; Calculated: 15311.72 Da; Observed: 15311.2 Da) nucleosomes including H4 (purple circle; Calculated: 11236.15 Da; Observed: 11235.5 Da), H2A (upward-pointed yellow green triangle; Calculated 13950.20; Observed: 13949.6 Da) and H2B (downward-pointed cyan triangle; Calculated:



13493.68 Da; Observed: 13493.1 Da) prior to Sirt6 treatment. (G) Deconvoluted intact ESI-MS of H3K9MTU nucleosomes including H4, H2A and H2B following treatment with Sirt6 in the presence of NAD. Masses corresponding to deacylation product (rightward-pointed green triangle) and Nε-1,3-oxathiolan-2-ylidene amine product (orange square) are illustrated, along with the Sirt6 mass (red diamond, inset; Calculated: 39090.82 Da; Observed: 39087.1 Da).

and/or deacetylation process (Figure S12). Prior reports that DNA stimulates sirtuin activity prompted our evaluation of linker DNA outside of the core 147 bp Widom 601 sequence. We assessed the deacetylation of H3K9ac nucleosomes containing 185 bp DNA and found that Sirt6 deacetylatese 147 bp and 185 bp nucleosomes at similar rates (Figure S10). As mentioned, MDL-800 is reported to be an allosteric activator of Sirt6 and as such we evaluated that

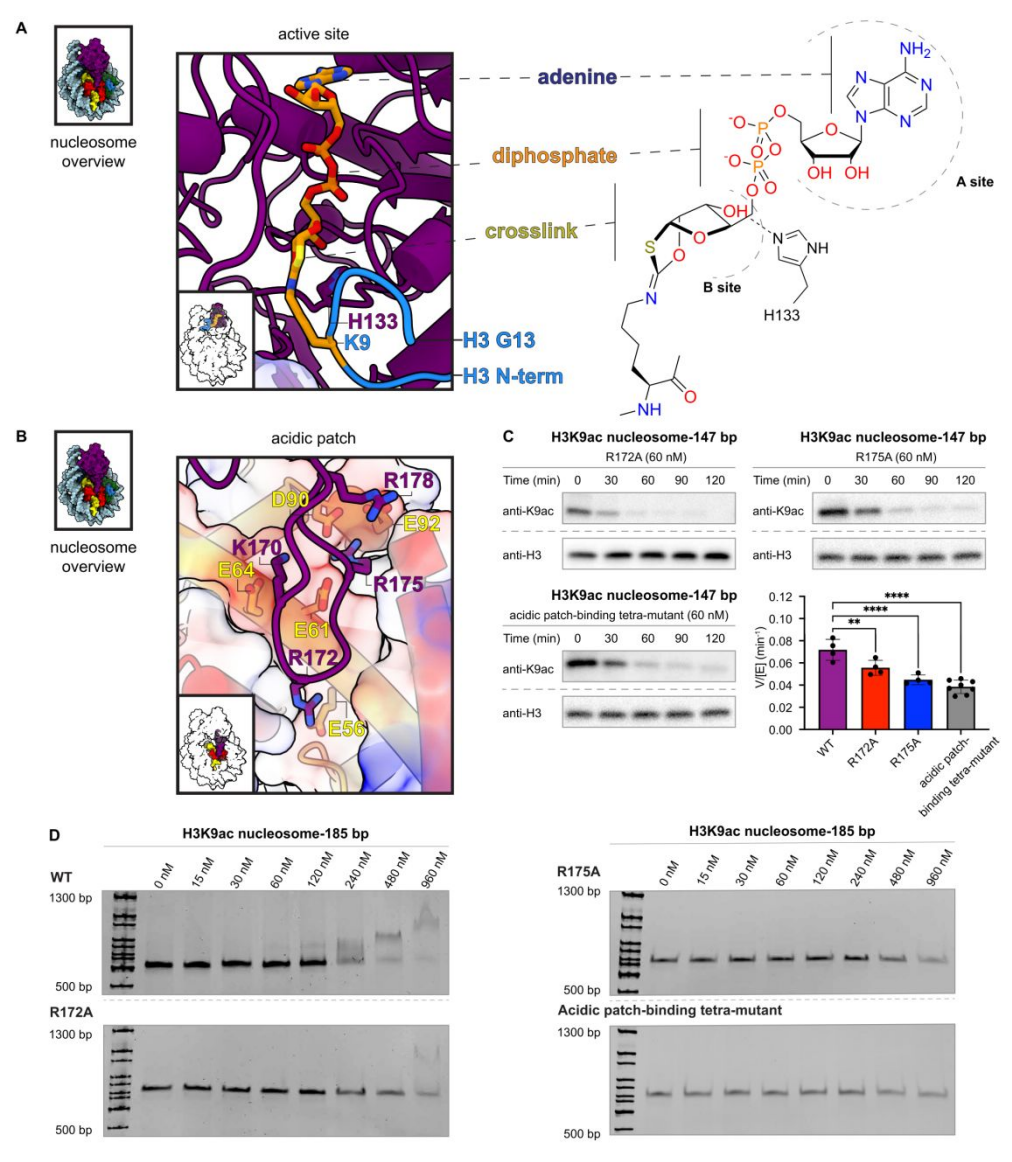
here. Using H3K9ac 147 bp nucleosomes at 20 nM (close to the apparent $K_{\rm m}$), we observed an MDL-800 concentration dependent stimulation of Sirt6 deacetylation activity with a ~4-fold maximal effect and an EC50 of ~3.5 μM relative to DMSO vehicle control (Figure 2D-G, Figure S13). These results indicate that MDL-800 is

Figure 4. Cryo-EM structure of Sirt6-Nucleosome complex. (A) Domain map of Sirt6 with acidic patch-binding loop (170-178) and DNA-binding (205-248) regions highlighted. Modeled region is indicated as black line. (B) Complex density map. Dyad axis indicated as line or black oval. (C) Structure of Sirt6-nucleosome complex, showing the H2A C-terminal tail.

an allosteric activator for both peptide substrates and physiologically relevant acetylated nucleosome substrates (Figure 2, Table S1).

Thiocarbonyl nucleosomes and Sirt6 interactions. To investigate the structural basis for the selective Sirt6 deacetylation of H3Kac

nucleosome substrates, we prepared nucleosomes modified with thiocarbonyl groups at the H3K9 position.³⁶ Thioacetyl (Sac) and methyl-thiourea (MTU) functionalities were installed using sortase-mediated histone H3 semisynthesis.³⁷ Both Sac³⁸ and MTU³⁹ groups have previously been installed in synthetic peptides,

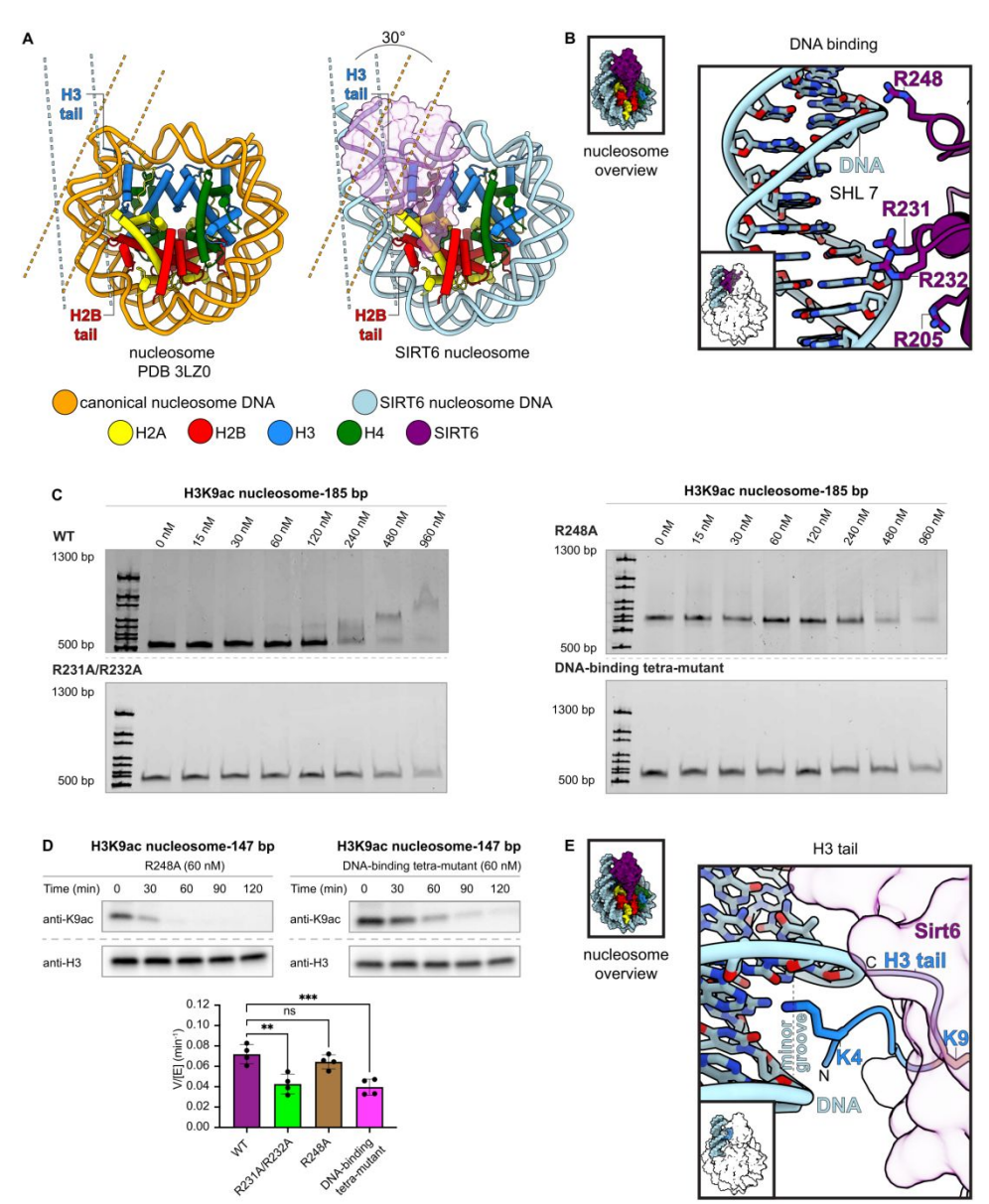


leading to potent sirtuins inhibitors⁴⁰. Thiocarbonyls can trap enzyme-substrate complexes due to slow turnover of ADPthiogylcoside intermediates (Figure 3A,B, Figure S14)⁴¹. Such chemical traps have aided in the structural determination of sirtuins bound to the peptide substrate analogs. Unexpectedly, the H3K9-Sac nucleosomes were efficiently cleaved by Sirt6, rendering them ineffective for covalent capture (Figure 3C,D, Figure S15). In contrast, H3K9-MTU appeared more resistant to removal by Sirt6, and nucleosome electrophoretic mobility shift assays (EMSAs) revealed the formation of two sharp, higher molecular weight bands that were presumed to have one or two Sirt6 polypeptides tightly bound to the nucleosome (Figure 3E). This EMSA behavior was dependent on the presence of NAD, consistent with the predicted formation of a covalent adduct between the MTU group and ADPribose. Characterization of the four histones by intact mass spectrometry revealed that the H3 alone displayed a 511 Da increase compared to the H3K9-MTU starting material (Figure 3F, Figure S16). Based on the increased molecular weight of the modified H3 and the generally accepted sirtuin catalytic mechanism, the deconvoluted product mass of 15,822 Da corresponds to the chemical structure of a Lys Nɛ-1,3-oxathiolan-2-yliden amine ADP-ribose adduct (ADP-ribose intermediate analog) formed after elimination of methylamine (Figure 3G). This adduct appears to be an analog of a cyclic intermediate proposed for the catalytic steps of the deacetylation process (Figure 3A,B) and the capacity to eliminate methylamine allows for the stable modified H3 to be isolable. It is noteworthy that there was little unreacted H3K9-MTU protein visible suggesting a robust conversion to the ADP-ribose intermediate analog.

Cryo-EM structural analysis of the Sirt6 nucleosome complex. Encouraged by these findings with the H3K9-MTU

Figure 5. Cofactor crosslink and interactions between Sirt6 and the H2A/H2B acidic patch. (A) Sirt6 active site with modelled K9 Nε-1,3-oxathiolan-2-ylidene amine linkage to ADP-ribose. Histone H3 T3 through G13 are modelled (blue) based on an existing crystal structure (PDBID: 5Y2F).¹³ (B) Residues involved in interaction between Sirt6 (K170, R172, R175, R178) and H2A (E56, E61, E64, D90, E92). (C) Effect of point mutations to the acidic patch-binding loop on Sirt6 deacetylation of H3K9ac nucleosomes. R172A (top left, n=4), R175A (top right, n=4), and K170A/R172A/R175A/R178A (bottom left, n=8) each significantly decreased (** p=0.0089; **** p<0.0001) using an ordinary one-way ANOVA with multiple comparisons with the WT Sirt6 deacetylation rate (bottom right, n=4). (D) Electrophoretic mobility

shift assay of acidic patch-binding point mutants. WT Sirt6 (top left) induces a change in nucleosome migration at the final two concentrations



(480 nM and 960 nM). R172A (lower left), R175A (upper right) and K170A/R172A/R175A/R178A (bottom right) show only a slight change in nucleosome intensity at the final concentration (960 nM).

nucleosome/Sirt6 reaction, we used single-particle cryo-EM to analyze the structure of the macromolecular complex (Figure 4). We reconstituted a H3K9-MTU nucleosome with 20 base pairs of extranucleosomal DNA on both sides for a total construct length of 185 base pairs for the nucleosome and prepared the H3K9-MTU nucleosome-Sirt6 complex in the presence of NAD using size exclusion chromatography (Figure S17). Peak fractions containing the H3K9-MTU nucleosome-Sirt6 complex were mildly cross-linked with glutaraldehyde and then prepared for single-particle cryo-EM. Single-particle cryo-EM data were collected on a Titan Krios microscope with a K3 direct electron detector and energy filter (Methods). The cryo-EM data was subsequently processed and analyzed (Figure S18,S19). The structure of Sirt6 bound to the

H3K9-MTU nucleosome was determined from 95,205 particles with an overall resolution of 3.1 Å (Figure 4B, Table S2). The nucleosome was resolved to a resolution of 3-5 Å and Sirt6 to resolutions of 3-6 Å (Figure S19). A known crystal structure of the nucleosome⁴² and a previously reported crystal structure of Sirt6¹³ were docked into the density and locally adjusted. Additional extranucleosomal DNA was only visible on the Sirt6 bound site and the DNA was extended to accommodate an additional three base pairs. We docked the N-terminus of Sirt6 from an AlphaFold2 model⁴³, which sits on top of the Sirt6 hydrophobic pocket that is formed by the Sirt6 Rossman fold and the zinc-binding domain (Figure 4C). Only a small part of the Sirt6 C-terminus could not be resolved (Figure 4). In our structure, Sirt6 sits on top of the

Figure 6. Interactions between Sirt6 and nucleosome entry site DNA. (A) Comparison of canonical nucleosome structure (left) and Sirt6-bound nucleosome (right) illustrating the unwinding of entry site DNA that accompanies Sirt6 binding. The different positions of H3 and H2B tails are illustrated. (B) Residues involved in interaction between Sirt6 (R205, R231, R232, R248) and DNA. (C) Electrophoretic

mobility shift assay of DNA-binding point mutants. WT Sirt6 (top left) induces a change in nucleosome migration at the highest two concentrations (480 nM and 960 nM). R231A/R232A (lower left), R248A (upper right) and R205A/R231A/R232A/R248A (bottom right) show little change in migration up to 960 nM. (D) Effect of point mutations to the DNA-binding residues on Sirt6 deacetylation of H3K9ac nucleosomes. R231A/R232A (supplement, n=4) and R205A/R231A/R232A/R248A (top right, n=4), each significantly decreased (** p=0.0011; *** p<0.0005), while R248A (top left, n=4) does not significantly decrease the rate (ns p>0.1) using an ordinary one-way ANOVA with multiple comparisons with the WT Sirt6 deacetylation rate (bottom, n=4). (E) Interaction between H3K4 and the minor groove of DNA at SHL 6.5.

nucleosomal disc above the H2A C-terminus docking domain and the H3 aN helix next to the nucleosomal DNA at SHL 6 to 7. Sirt6 is relatively unaltered compared to published crystal structures with a root mean square deviation of 1.723 Å. After completing the structural model of the nucleosome and Sirt6, we observed additional density that allowed us to build the ADP-ribose intermediate analog and H3 tail residues 3-13 into our density (Figure 5A). The ADP-ribose intermediate analog moiety is bound in the Sirt6 Rossman fold and the histone tail is positioned between nucleosomal DNA at superhelical location 6.5 and Sirt6, positioning the substrate H3K9 lysine for insertion into the Sirt6 active site proximal to Sirt6 residue His133. The nucleosome-Sirt6 structure was refined and showed good stereochemistry (Table S2,S3).

Multivalent interactions of Sirt6 with the nucleosome. In our structure, a single copy of Sirt6 sits on top of the nucleosomal disk and interacts with histones and nucleosomal DNA to form multiple contacts with the nucleosome (Figure 5,6). First, Sirt6 interacts with the acidic patch of the nucleosome (Figure 5B). Specifically, Sirt6 has a zinc-binding domain with a unique insertion between the third and fourth cysteines of the zinc cluster. 44 This insertion is unique to Sirt6 among all sirtuins (Figure S20).44 The ten amino acid long extension forms an approximately 15 Å long loop and is enriched in basic amino acids (Sirt6 residues K170, R172, R175, R178). In our structure, the loop binds the acidic patch of the nucleosome, confirming biochemical observations.²⁴ The interactions are mediated via Sirt6 residues K170, R172, R175. K170 contacts H2A residue E64, Sirt6 R172 inserts into the acidic patch and contacts H2A E56, and Sirt6 R175 binds H2A residues E61, D90, and E92 (Figure 5B). This configuration is similar to other arginine anchors that bind the acidic patch.⁴⁵ To test the importance of this interaction, we generated multiple Sirt6 mutants that disrupt the binding to the acidic patch. These mutations include a R172A mutant, a R175A mutant, and a mutant with K170A, R172A, R175A, and R178A. All three mutants showed a decreased deacetylase activity and reduced ability to bind the nucleosome (Figure 5C,D, Figure S21,S23).45

Second, we observe that 15 base pairs of nucleosomal DNA from SHL 5.5 to SHL 7 are unwrapped from the histone octamer by approximately 30° compared to a canonical nucleosome (Figure 6A). Sirt6 interacts with the unwrapped DNA via multiple arginine residues. Sirt6 arginine residues 205, 231, and 232 contact the phosphate backbone of the unwrapped DNA at SHL 6.5 and Sirt6 R248 is located in close proximity to the phosphate backbone at SHL 7 (Figure 6B). Confirming our structural observations, mutation of R231 and R232 to alanines or mutation of all identified DNA interacting Sirt6 residues to alanines results in a significant reduction of deacetylase activity and a reduced affinity to the nucleosomal substrate. Notably, disruption of just Sirt6 R248 does not show a significant reduction of H3K9 Sirt6 deacetylase activity but does appear to weaken nucleosome affinity. (Figure 6C and 6D, Figure S22,S23). Because the H3 histone tail is clamped between the two DNA gyres in canonical nucleosome conformations, it is

likely that the unwrapping of nucleosomal DNA and the stabilization of this unwrapped conformation by Sirt6 plays an important role in facilitating access of Sirt6 to the acetylated H3 tail. Due to the positioning of Sirt6 on the nucleosomal disk, unwrapping of the DNA is likely required to release the H3 tail from its DNA clamp between the two DNA gyres, which then allows H3K9ac to enter the Sirt6 active site.

Third, Sirt6 is located above the C-terminus of H2A and H2A residues 119–122 reach toward the N-terminal region of Sirt6 (residues 8-11), forming an additional interaction surface. Together, Sirt6 recognizes the nucleosomal substrate through multiple interactions, allowing Sirt6 to be optimally positioned to catalyze the deacylation of acetylated histone H3 lysine residues. Our structural findings do not rule out binding of a second Sirt6 copy on the opposite side of the nucleosome as suggested biochemically.

Interaction of SIRT6 with a catalytic intermediate analog of H3K9ac deacylation We observe density for the ADP-ribose intermediate analog formed during the deacylation of H3K9 including H3 histone tail residues 3-13. Similar to other sirtuins and as previously observed, the adenosine moiety of the cofactor analog binds in the A site and the reactive ribose moiety binds in the B site⁴⁶ in close proximity to the important catalytic Sirt6 residue His133⁶ (Figure 5A). The resolved part of the H3 histone tail extends from the unwrapped DNA towards the active site of Sirt6 to insert H3 residue Lys9 into the Sirt6 active site, facilitating deacylation. Similar to previous crystal structures, ¹⁴ our structure confirms that Sirt6 can accommodate larger lysine acylations in its hydrophobic pocket and is likely able to complete their deacylation.

We observe the H3 tail residues T3-R8 projecting from the unwrapped DNA to the Sirt6 active site. Notably, H3 residue K4 inserts itself into the minor groove of DNA at SHL 6.5 (Figure 6E). It is likely this interaction with DNA helps stabilize the H3 tail in the proper orientation to ensure placement of H3K9 into the active site of SIRT6.

We do not observe density for H3 tail residues K14 through P38 in our reconstruction, likely due to their inherent flexibility. However, the distance between resolved H3 residues 13 and 39 is only ~20 Å. As such, our model suggests that Sirt6 binding and deacetylation of other residues within the H3 tail such as H3K27 can reach the active site of Sirt6 in the observed conformation, consistent with our biochemical observations (Fig. 1)

DISCUSSION

As critical enzymes that regulate gene regulation and established therapeutic targets, HDACs have been intensively studied since their original molecular identification over two decades ago.⁴⁷ Nevertheless, how the metallohydrolase HDACs or the NAD-dependent sirtuins target acetyl-Lys sites for removal from chromatin has been unclear. In this study, we employed a series of site-specifically H3- and H2B-acetylated nucleosomes to assess how nucleosome substrates compare to free histone protein as Sirt6 substrates. Two principal features of selectivity were observed for

Sirt6 mediated deacetylation. First, H3 tail acetylated nucleosome substrates are far superior to histone N-tail H2B acetylated nucleosome substrates, and second, H3 tail acetylated nucleosome substrates are much more rapidly processed than free histone H3 and H2B protein acetylated substrates. Our cryo-EM analysis of the Sirt6-nucleosome complex readily explains both of these selectivity features. The extensive and intimate interactions between the nucleosome and Sirt6 position the H3 tail in a suitable orientation for active site entry whereas the H2B tail appears to extend away from the Sirt6 catalytic site. This also explains why Sirt6 only exhibits deacylation activity with H2B peptide substrates and not on nucleosomal substrates. 14

The cryo-EM structure reconstructed here is effectively modeled with X-ray crystal structures that include both H3K9 modified tail peptide as well as MDL-800 allosteric ligand. This structure can therefore be used to discern the basis for the increased cleavage rates of Sirt6 at H3K9ac, H3K18ac, and H3K27ac relative to H3K23ac and H3K14ac, agreeing with the general selectivity observed in cell experiments as a H3K9ac and H3K18ac deacetylase. 48 A common element of H3K9, H3K18, and H3K27 is an Arg residue preceding the targeted Lys. The Sirt6 X-ray structure shows that Arg8 is nicely accommodated by the peptide substrate binding site whereas a Thr preceding Lys23 and especially the small residue Gly preceding Lys14 would appear to be poorer fits. It is interesting that Lys14 acetylation is generally the most difficult to remove among metallohydrolase HDACs and sirtuins and this could account for its high prevalence across chromatin. H3K27ac is an apparently novel Sirt6 deacetylation site that should be considered in future studies.8 Notably, we also observe that H3 residue K4 inserts into the DNA minor groove at SHL 6.5. Because H3K4 can be post-translationally modified (e.g., methylated), future studies should consider how these modifications impact Sirt6 deacylation activity of H3K9.

That MDL-800 can accelerate nucleosome deacetylation *in vitro* reinforces the idea that it acts to stimulate Sirt6 *in vivo*. Agents that activate Sirt6 and other sirtuins are proposed to slow down the aging process, and we would suggest that examining their behavior in a purified system with nucleosome substrates as employed here can help select for the most promising agents.

Although to our knowledge this study describes the first high resolution structure of an HDAC in complex with a nucleosome, there are several enzyme-nucleosome complexes previously determined.^{45, 49–51} A common theme for nucleosome binding proteins is that they involve the H2A/H2B acidic patch by employing one or more basic residues.^{52, 53} That is certainly the case with Sirt6. Some specialized features regarding DNA binding and H2A C-terminal contact also appear to be facets of Sirt6/nucleosome interaction and allow a targeted recruitment to the nucleosome and positioning of Sirt6 on the substrate to facilitate histone deacylation. Though unexplored in this study, the proximity of the H2A C-tail to the Sirt6 active site suggests a possible H2A deacylase role that fits the function of Sirt6 in safeguarding genome integrity.⁵⁴

Chemical trapping functionalities like norleucine for histone methyltransferases⁵⁵, methionine for LSD1 histone demethylase⁵¹, and CoA for histone acetyltransferases⁵⁶ have proven effective for structural analysis of these enzymes. The use of a thiourea as performed in this work rather than a thioacetyl to trap Sirt6-nucleosome interactions may be of general advantage for the sirtuin family in analyzing nucleosome interactions. We also propose that this approach of incorporating warheads like hydroxamic acids⁸ for metallohydrolase HDACs may facilitate structural determination of these enzymes bound to nucleosomes.

EXPERIMENTAL METHODS

Cloning, expression, and purification of Sirt6. The His-Sirt6 plasmid previously reported⁵⁷ was employed after a TEV cleavage site was inserted between the His-tag and Sirt6 sequence along with an N-terminal Cys. All subsequent constructs were generated by Q5 site-directed mutagenesis (New England Biolabs). Sirt6 constructs were expressed in LOBSTR E. coli strain derived from Rosetta (DE3) in LB media supplemented with 50 mg/L kanamycin. Cells were grown at 37 °C, 200 rpm to an OD600 of 0.6, and overexpression was induced with the addition of isopropyl β-D-1thiogalactopyranoside to 0.5 mM. Cells were grown for a further 18 h at 25 °C, 200 rpm. Pelleted cells were resuspended in ice cold lysis buffer (20 mM Tris, 500 mM NaCl, 20 mM imidazole, pH 7.5) and then lysed by passage through a French press. Lysate was clarified by centrifugation at 13,000 × g, 4 °C. Lysate supernatant was applied to pre-equilibrated Ni-NTA resin (2 mL resin bed volume / 1 L culture) and incubated 1 h at 4 °C. The resin was drained and was washed with 10 column volumes of wash buffer (20 mM Tris, 500 mM NaCl, 50 mM imidazole, 0.5 mM TCEP, pH 7.5), followed by 25 column volumes of high-salt wash buffer (20 mM Tris, 2 M NaCl, 20 mM imidazole, pH 7.5), then eluted with 10 column volumes of elution buffer (20 mM Tris, 500 mM NaCl, 200 mM imidazole, 0.5 mM TCEP, pH 7.5). The elution was concentrated by spin concentrator (Amicon, 10 kDa MWCO, 4,000 rpm, 4 °C) and mixed with TEV protease (~1 mg/mL), before overnight dialysis at 4 °C (dialysis buffer: 20 mM Tris, 150 mM NaCl, 20 mM imidazole, 0.5 mM TCEP, pH 7.5. Uncleaved protein was removed by a second passage over Ni-NTA resin (1 h incubation at 4 °C). The flow through was diluted with 10 mL Heparin buffer A (50 mM Tris, 150 mM NaCl, 5 % glycerol, 0.5 mM TCEP, pH 7.5), and concentrated by spin concentrator (10 kDa MWCO, 4,000 rpm, 4 °C). Concentrated sample was applied to a Heparin column (1 mL), and eluted with a linear gradient from 0-50 % Heparin buffer B (50 mM Tris, 2000 mM NaCl, 5 % glycerol, 0.5 mM TCEP, pH 7.5) over 20 column volumes at a flow rate of 0.6 mL/min. Elution fractions were checked by Coomassie-staining following SDS-PAGE (6-20 %), and pure fractions were collected and concentrated. This material was further purified by size exclusion using a Superdex200 increase 10/300 GL column (Cytiva) with Superdex running buffer (50 mM Tris, 150 mM NaCl, 0.5 mM TCEP, pH 7.5). Elution fractions were checked by SDS-PAGE, and the pure fractions were combined and concentrated to ~40 μM. Coomassie-staining after SDS-PAGE was used for densitometry and quality check for WT Sirt6 and all the Sirt6 mutants. WT Sirt6 was characterized by intact ESI-MS (Q Exactive, Thermo Scientific) and deconvoluted using UniDec.⁵⁸ All Sirt6 constructs were aliquoted and flash-frozen in liquid nitrogen, then stored at -80 °C prior to use.

General deacetylation assay and conditions. Free histone protein (H3K9ac, H3K14ac, H3K18ac, H3K23ac, H3K27ac, H2BK11ac, H2BK12ac, H2BK20ac, and H2B46ac; final 1.0 µM) or nucleosomes (H3K9ac, H3K9Sac, H3K14ac, H3K18ac, H3K23ac, H3K27ac, H2BK11ac, H2BK12ac, H2BK20ac, and H2B46ac; final 100 nM) were diluted in Sirt6 reaction buffer (50 mM HEPES at pH 7.5, 1 mM DTT, 0.2 mg/mL BSA, and 1 mM NAD). This solution was kept on ice until the reaction start. Reactions were commenced by addition of Sirt6, after which samples were incubated at 37 °C. At each indicated time point a small volume was removed from the reaction. For typical nucleosome assays time points were taken at 0, 30, 60, 90, 120 min. Each quenched sample was boiled for 3-5 min at 95 °C and resolved on a 4-20 % gradient SDS-PAGE gel at 180 Volts for ~25 min. Gels were transferred semi dry onto nitrocellulose membrane by iBlot with P3 (20 V) for 5.0 min. Membranes were blocked for 1 h with 5% BSA in TBST. then incubated overnight with primary antibody. Site-specific antibodies for H3, acetylated H3, H2B, acylated H2B are listed in the key materials table. After washing, HRP linked secondary antibody was applied for 1 h at room temperature. Membranes were washed and treated with ECL substrate reagent, then visualized with a G:BOX mini gel imager (Syngene). Band intensity was quantified by ImageJ (imagej.nih.gov/ij/). All intensity values were divided by the intensity value at time 0 to get relative intensity, and then fit to a single-phase exponential decay curve with constraints Y0=1, Plateau=0 (GraphPad Prism 9). For assays with free histone protein substrates the decrease in anti-H3 or anti-H2B signal was accounted for by normalizing the PTM signal relative to the corresponding total histone signal at each time point. Each plotted point represents at least 2 replicates. The kinetic parameter V/[E] was calculated using GraphPad Prism 9. All the Km measurements and activator assays were done with similar procedures.

Cryo-EM structural analysis of the Sirt6 nucleosome complex. Sirt6-H3K9MTU complexes were mixed with NAD and purified by size exclusion chromatography. Purified complex was mildly cross-linked with glutaraldehyde and dialyzed prior to vitrification onto cryo-EM grids. A 15,192 micrograph dataset and a second dataset with 6,922 micrograph and 30° tilt were both collected on a Titan Krios equipped with a BioQuantum energy filter and Gatan K3 direct electron detector. A total of 2,507,720 particles were picked from the first dataset and 1,556,859 particles were collected from the second dataset. Both datasets were combined and after several rounds of 3D classification in cryoSPARC, 95,205 particles were refined to a final resolution of 3.1 Å (map A). Further classification of the particles resulted in a second map with better resolved Sirt6 and H3 tail features. This second map (map B) was refined to 3.3 Å and aided in model building. The model was built by first rigid-body fitting in the nucleosome (PDB 3LZ0),⁴² Sirt6 (PDB 5Y2F)¹³, Sirt6 residues 1-16 (AlphaFold2, AF-Q8N6T7-F1), and the H3 tail (PDB 5Y2F). The ADP-ribose intermediate analog was modeled based on NAD⁺ (PDB 5Y2F) and placed into the extra density. Local adjustments were made in Coot⁵⁹ and further refined with Phenix.60

Sirt6 mutants activity and EMSA. Nucleosome binding of Sirt6 constructs was assessed by electrophoretic mobility shift assay (EMSA). Sirt6 constructs were diluted to a working concentration of 9.6 μM , then serially diluted to 4800, 2400, 1200, 600, 300, 150, 75, and 0 nM. H3K9ac nucleosome-185 bp was diluted in Sirt6 binding buffer, then combined with Sirt6 enzyme to a final nucleosome concentration of 20 nM. NAD was added to a concentration of 150 μM and mixed. Samples were prepared such that the final Sirt6 concentrations were 960, 480, 240, 120, 60, 30, 15, 0 nM. Samples were incubated for 30 min on ice, followed by native electrophoresis on a 4-20 % TBE gel run at 130 Volts for 110 min on ice.

ASSOCIATED CONTENT

Supporting Information

The Supporting Information is available free of charge on the ACS Publications website at DOI:

Additional experimental details, materials, methods, and supporting figures (PDF)

Structural coordinates and EM maps are available under accession codes PDB 8F86 and EMDB-28915.

AUTHOR INFORMATION

Corresponding Authors

Lucas Farnung – Department of Cell Biology, Blavatnik Institute, Harvard Medical School, Boston, Massachusetts 02115, United States; orcid.org/0000-0002-8200-2493; Email: Lucas Farnung@hms.harvard.edu

Philip A. Cole – Division of Genetics, Department of Medicine, Brigham and Women's Hospital, Boston, Massachusetts 02115, United States; Department of Biological Chemistry and Molecular Pharmacology, Harvard Medical School, Boston, Massachusetts 02115, United States; orcid.org/0000-0001-6873-7824; Email: pacole@bwh.harvard.edu

Authors

Zhipeng A. Wang – Division of Genetics, Department of Medicine, Brigham and Women's Hospital, Boston, Massachusetts 02115, United States; Department of Biological Chemistry and Molecular Pharmacology, Harvard Medical School, Boston, Massachusetts 02115, United States; orcid.org/0000-0002-5693-7359

Jonathan W. Markert – Department of Cell Biology, Blavatnik Institute, Harvard Medical School, Boston, Massachusetts 02115, United States; orcid.org/0000-0003-3292-2379

Samuel D. Whedon – Division of Genetics, Department of Medicine, Brigham and Women's Hospital, Boston, Massachusetts 02115, United States; Department of Biological Chemistry and Molecular Pharmacology, Harvard Medical School, Boston, Massachusetts 02115, United States; orcid.org/0000-0002-3745-5645

Maheeshi Yapa Abeywardana – Division of Genetics, Department of Medicine, Brigham and Women's Hospital, Boston, Massachusetts 02115, United States; Department of Biological Chemistry and Molecular Pharmacology, Harvard Medical School, Boston, Massachusetts 02115, United States; orcid.org/0000-0002-9773-2587

Kwangwoon Lee – Division of Genetics, Department of Medicine, Brigham and Women's Hospital, Boston, Massachusetts 02115, United States; Department of Biological Chemistry and Molecular Pharmacology, Harvard Medical School, Boston, Massachusetts 02115, United States; orcid.org/0000-0002-2021-5186

Hanjie Jiang – Division of Genetics, Department of Medicine, Brigham and Women's Hospital, Boston, Massachusetts 02115, United States; Department of Biological Chemistry and Molecular Pharmacology, Harvard Medical School, Boston, Massachusetts 02115, United States

Carolay Suarez – Division of Genetics, Department of Medicine, Brigham and Women's Hospital, Boston, Massachusetts 02115, United States; Department of Biological Chemistry and Molecular

Pharmacology, Harvard Medical School, Boston, Massachusetts 02115. United States

Hening Lin – Howard Hughes Medical Institute; Department of Chemistry and Chemical Biology, Cornell University, Ithaca, New York 14853, United States; orcid.org/0000-0002-0255-2701

Author Contributions

*These authors contributed equally.

Notes

P.A.C. is a cofounder of Acylin Therapeutics which is involved in developing epigenetic agents and has been a consultant for the pharmaceutical companies Abbvie and Constellation.

ACKNOWLEDGMENT

The authors would like to thank James Lee from MBCF of Dana-Farber Cancer Institute for MALDI, Brad Palanski for technical support, Yi Zheng for illustrations (www.yizhengillustration.com), Marty Taylor and Maggie Chen for advice. The authors acknowledge NIH (GM62437 to P.A.C.), NSF2127882, LLS, American Cancer Society (PF-20-105-01-DMC to S.D.W), American Heart Association (Postdoctoral fellowship award 826614 to K. L) for financial support. L.F. is supported by the Dorsett L. Spurgeon, MD (HMS 1929) Distinguished Research Award at Harvard Medical School, by The Smith Family Awards Program for Excellence in Biomedical Research, and the Damon Runyon-Rachleff Innovation Award. C.S. is supported by the DF/HCC SPARC Program. We thank The Harvard Cryo-EM Center for Structural Biology at Harvard Medical School for support with data collection.

REFERENCES

- (1) Dancy, B. M.; Cole, P. A. Protein lysine acetylation by p300/CBP. *Chem Rev.* **2015**, *115* (6), 2419–2452.
- (2) Lee, K.; Whedon, S. D.; Wang, Z. A.; Cole, P. A. Distinct biochemical properties of the class I histone deacetylase complexes. *Curr Opin Chem Biol.* **2022**, *70*, 102179.
- (3) Jing, H.; Lin, H. Sirtuins in epigenetic regulation. *Chem Rev.* **2015**, *115* (6), 2350–2375.
- (4) Shiota, H.; Alekseyenko, A. A.; Wang, Z. A.; *et al.* Chemical Screen Identifies Diverse and Novel Histone Deacetylase Inhibitors as Repressors of NUT Function: Implications for NUT Carcinoma Pathogenesis and Treatment. *Mol Cancer Res.* **2021**, *19* (11), 1818–1830.
- (5) Jing, H.; Hu, J.; He, B.; *et al.* A SIRT2-Selective Inhibitor Promotes c-Myc Oncoprotein Degradation and Exhibits Broad Anticancer Activity. *Cancer Cell.* **2016**, *29* (3), 297–310.
- (6) Klein, M. A.; Denu, J. M. Biological and catalytic functions of sirtuin 6 as targets for small-molecule modulators. *J Biol Chem.* **2020**, *295* (32), 11021–11041.
- (7) Wang, Z. A.; Cole, P. A. The Chemical Biology of Reversible Lysine Post-translational Modifications. *Cell Chem Biol.* **2020**, *27* (8), 953–969.
- (8) Wu, M.; Hayward, D.; Kalin, J. H.; Song, Y.; Schwabe, J. W.; Cole, P. A. Lysine-14 acetylation of histone H3 in chromatin confers resistance to the deacetylase and demethylase activities of an epigenetic silencing complex. *eLife*. **2018**, *7*, e37231.
- (9) Toiber, D.; Erdel, F.; Bouazoune, K.; *et al.* SIRT6 recruits SNF2H to DNA break sites, preventing genomic instability through chromatin remodeling. *Mol Cell.* **2013**, *51* (4), 454–468.
- (10) Taylor, J. R.; Wood, J. G.; Mizerak, E.; *et al.* Sirt6 regulates lifespan in Drosophila melanogaster. *Proc Natl Acad Sci U S A.* **2022**, *119* (5), 1–9. (11) Kanfi, Y.; Naiman, S.; Amir, G.; *et al.* The sirtuin SIRT6 regulates lifespan in male mice. *Nature.* **2012**, *483* (7388), 218–221.
- (12) Hirvonen, K.; Laivuori, H.; Lahti, J.; Strandberg, T.; Eriksson, J. G.; Hackman, P. SIRT6 polymorphism rs117385980 is associated with longevity and healthy aging in Finnish men. *BMC Med Genet.* **2017**, *18* (1), 1–5.
- (13) Huang, Z.; Zhao, J.; Deng, W.; et al. Identification of a cellularly active

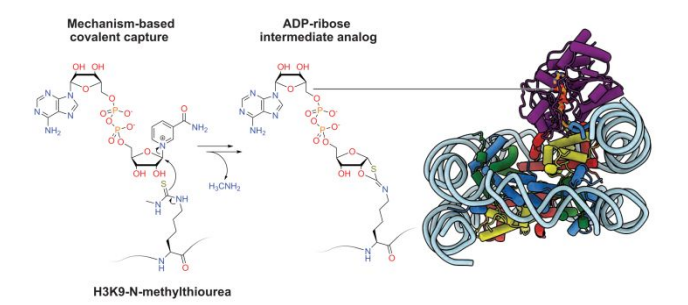
60

- SIRT6 allosteric activator. *Nat Chem Biol.* **2018**, *14* (12), 1118–1126.
- (14) Jiang, H.; Khan, S.; Wang, Y.; *et al.* SIRT6 regulates TNF- α secretion through hydrolysis of long-chain fatty acyl lysine. *Nature.* **2013**, *496* (7443), 110–113.
- (15) Liszt, G.; Ford, E.; Kurtev, M.; Guarente, L. Mouse Sir2 homolog SIRT6 is a nuclear ADP-ribosyltransferase. *J Biol Chem.* **2005**, *280* (22), 21313–21320.
- (16) Tasselli, L.; Xi, Y.; Zheng, W.; et al. SIRT6 deacetylates H3K18ac at pericentric chromatin to prevent mitotic errors and cellular senescence. Nat Struct Mol Biol. 2016, 23 (5), 434–440.
- (17) Rezazadeh, S.; Yang, D.; Tombline, G.; *et al.* SIRT6 promotes transcription of a subset of NRF2 targets by mono-ADP-ribosylating BAF170. *Nucleic Acids Res.* **2019**, *47* (15), 7914–7928.
- (18) Mao, Z.; Hine, C.; Tian, X.; *et al.* SIRT6 promotes DNA repair under stress by activating PARP1. *Science* (80-). **2011**, 332 (6036), 1443–1446. (19) Onn, L.; Portillo, M.; Ilic, S.; *et al.* SIRT6 is a DNA double-strand break sensor. *eLife*. **2020**, 9, e51636.
- (20) Feldman, J. L.; Baeza, J.; Denu, J. M. Activation of the protein deacetylase SIRT6 by long-chain fatty acids and widespread deacylation by Mammalian Sirtuins. *J Biol Chem.* **2013**, *288* (43), 31350–31356.
- (21) Michishita, E.; McCord, R. A.; Berber, E.; *et al.* SIRT6 is a histone H3 lysine 9 deacetylase that modulates telomeric chromatin. *Nature.* **2008**, *452* (7186), 492–496.
- (22) Wang, W. W.; Zeng, Y.; Wu, B.; Deiters, A.; Liu, W. R. A Chemical Biology Approach to Reveal Sirt6-targeted Histone H3 Sites in Nucleosomes. *ACS Chem Biol.* **2016**, *11* (7), 1973–1981.
- (23) Pan, P. W.; Feldman, J. L.; Devries, M. K.; Dong, A.; Edwards, A. M.; Denu, J. M. Structure and biochemical functions of SIRT6. *J Biol Chem.* **2011**, 286 (16), 14575–14587.
- (24) Liu, W. H.; Zheng, J.; Feldman, J. L.; *et al.* Multivalent interactions drive nucleosome binding and efficient chromatin deacetylation by SIRT6. *Nat Commun.* **2020**, *11* (5244), 1–13.
- (25) Wang, Z. A.; Whedon, S. D.; Wu, M.; *et al.* Histone H2B Deacylation Selectivity: Exploring Chromatin's Dark Matter with an Engineered Sortase. *J Am Chem Soc.* **2022**, *144* (8), 3360–3364.
- (26) Dyer, P. N.; Raji, E. S.; White, C. L.; *et al.* Reconstitution of Nucleosome Core Particles from Recombinant Histones and DNA. *Methods Enzymol.* **2004**, *375*, 23–44.
- (27) Luger, K.; Rechsteiner, T. J.; Richmond, T. J. Preparation of Nucleosome Core Particle from Recombinant Histones. *Methods Enzymol.* **1999**, *304* (1997), 3–19.
- (28) Wang, Z. A.; Millard, C. J.; Lin, C.-L.; *et al.* Diverse nucleosome site-selectivity among histone deacetylase complexes. *eLife*. **2020**, *9*, e57663.
- (29) Madsen, A. S.; Andersen, C.; Daoud, M.; *et al.* Investigating the Sensitivity of NAD+-dependent Sirtuin Deacylation Activities to NADH. *J Biol Chem.* **2016**, *291* (13), 7128–7141.
- (30) Fiorentino, F.; Mai, A.; Rotili, D. Emerging Therapeutic Potential of SIRT6 Modulators. *J Med Chem.* **2021**, *64*, 9732–9758.
- (31) Feldman, J. L.; Dittenhafer-Reed, K. E.; Kudo, N.; *et al.* Kinetic and structural basis for Acyl-group selectivity and NAD+ dependence in sirtuin-catalyzed deacylation. *Biochemistry.* **2015**, *54* (19), 3037–3050.
- (32) Kugel, S.; Feldman, J. L.; Klein, M. A.; *et al.* Identification of and Molecular Basis for SIRT6 Loss-of-Function Point Mutations in Cancer. *Cell Rep.* **2015**, *13* (3), 479–488.
- (33) Gertz, M.; Fischer, F.; Nguyen, G. T. T.; *et al.* Ex-527 inhibits Sirtuins by exploiting their unique NAD+-dependent deacetylation mechanism. *Proc Natl Acad Sci U S A.* **2013**, *110* (30), E2772–E2781.
- (34) Zhou, Y.; Zhang, H.; He, B.; *et al.* The bicyclic intermediate structure provides insights into the desuccinylation mechanism of human sirtuin 5 (SIRT5). *J Biol Chem.* **2012**, *287* (34), 28307–28314.
- (35) Hoff, K. G.; Avalos, J. L.; Sens, K.; Wolberger, C. Insights into the Sirtuin Mechanism from Ternary Complexes Containing NAD+ and Acetylated Peptide. *Structure*. **2006**, *14* (8), 1231–1240.
- (36) Hirsch, B. M.; Hao, Y.; Li, X.; Wesdemiotis, C.; Wang, Z.; Zheng, W. A mechanism-based potent sirtuin inhibitor containing Nε- thiocarbamoyllysine (TuAcK). *Bioorganic Med Chem Lett.* **2011**, *21* (16), 4753–4757.
- (37) Piotukh, K.; Geltinger, B.; Heinrich, N.; et al. Directed evolution of sortase A mutants with altered substrate selectivity profiles. J Am Chem Soc. 2011, 133 (44), 17536–17539.
- (38) Fatkins, D. G.; Monnot, A. D.; Zheng, W. Nε-Thioacetyl-lysine: A

- multi-facet functional probe for enzymatic protein lysine Nε-deacetylation. *Bioorganic Med Chem Lett.* **2006**, *16* (14), 3651–3656.
- (39) Farooqi, A. S.; Hong, J. Y.; Cao, J.; *et al.* Novel Lysine-Based Thioureas as Mechanism-Based Inhibitors of Sirtuin 2 (SIRT2) with Anticancer Activity in a Colorectal Cancer Murine Model. *J Med Chem.* **2019**, *62* (8), 4131–4141.
- (40) Cole, P. A. Chemical probes for histone-modifying enzymes. *Nat Chem Biol.* **2008**, *4* (10), 590–597.
- (41) Hawse, W. F.; Hoff, K. G.; Fatkins, D. G.; *et al.* Structural Insights into Intermediate Steps in the Sir2 Deacetylation Reaction. *Structure.* **2008**, *16* (9), 1368–1377.
- (42) Vasudevan, D.; Chua, E. Y. D.; Davey, C. A. Crystal Structures of Nucleosome Core Particles Containing the "601" Strong Positioning Sequence. *J Mol Biol.* **2010**, *403* (1), 1–10.
- (43) Jumper, J.; Evans, R.; Pritzel, A.; et al. Highly accurate protein structure prediction with AlphaFold. *Nature*. **2021**, *596* (7873), 583–589.
- (44) Sanders, B. D.; Jackson, B.; Marmorstein, R. Structural basis for sirtuin function: What we know and what we don't. *Biochim Biophys Acta Proteins Proteomics*. **2010**, *1804* (8), 1604–1616.
- (45) McGinty, R. K.; Tan, S. Principles of nucleosome recognition by chromatin factors and enzymes. *Curr Opin Struct Biol.* **2021**, *71*, 16–26.
- (46) You, W.; Zheng, W.; Weiss, S.; Chua, K. F.; Steegborn, C. Structural basis for the activation and inhibition of Sirtuin 6 by quercetin and its derivatives. *Sci Rep.* **2019**, *9* (1), 1–11.
- (47) Wang, M.; Lin, H. Understanding the Function of Mammalian Sirtuins and Protein Lysine Acylation. *Annu Rev Biochem.* **2021**, *90* (1), 245–285. (48) Pastor, B. M.; Mostoslavsky, R. SIRT6: a new guardian of mitosis. *Nat Struct Mol Biol.* **2016**, *23* (5), 360–362.
- (49) Song, Y.; Dagil, L.; Fairall, L.; *et al.* Mechanism of Crosstalk between the LSD1 Demethylase and HDAC1 Deacetylase in the CoREST Complex. *Cell Rep.* **2020**, *30* (8), 2699–2711.
- (50) Worden, E. J.; Wolberger, C. Activation and regulation of H2B-Ubiquitin-dependent histone methyltransferases. *Curr Opin Struct Biol.* **2019**, *59*, 98–106.
- (51) Kim, S. A.; Zhu, J.; Yennawar, N.; Eek, P.; Tan, S. Crystal Structure of the LSD1/CoREST Histone Demethylase Bound to Its Nucleosome Substrate. *Mol Cell.* **2020**, *78* (5), 903-914.e4.
- (52) Skrajna, A.; Goldfarb, D.; Kedziora, K. M.; *et al.* Comprehensive nucleosome interactome screen establishes fundamental principles of nucleosome binding. *Nucleic Acids Res.* **2020**, *48* (17), 9415–9432.
- (53) McGinty, R. K.; Henrici, R. C.; Tan, S. Crystal structure of the PRC1 ubiquitylation module bound to the nucleosome. *Nature*. **2014**, *514* (7524), 591–596.
- (54) Hao, S.; Wang, Y.; Zhao, Y.; *et al.* Dynamic switching of crotonylation to ubiquitination of H2A at lysine 119 attenuates transcription-replication conflicts caused by replication stress. *Nucleic Acids Res.* **2022**, *50* (17), 9873–9892.
- (55) Worden, E. J.; Hoffmann, N. A.; Hicks, C. W.; Wolberger, C. Mechanism of Cross-talk between H2B Ubiquitination and H3 Methylation by Dot1L. *Cell.* **2019**, *176* (6), 1490-1501.e12.
- (56) Qu, K.; Chen, K.; Wang, H.; Li, X.; Chen, Z. Structure of the NuA4 acetyltransferase complex bound to the nucleosome. *Nature*. **2022**, *610* (7932), 569–574.
- (57) Zhang, X.; Khan, S.; Jiang, H.; *et al.* Identifying the functional contribution of the defatty-Acylase activity of SIRT6. *Nat Chem Biol.* **2016**, *12* (8), 614–620.
- (58) Marty, M. T.; Baldwin, A. J.; Marklund, E. G.; Hochberg, G. K. A.; Benesch, J. L. P.; Robinson, C. V. Bayesian deconvolution of mass and ion mobility spectra: From binary interactions to polydisperse ensembles. *Anal Chem.* **2015**, *87* (8), 4370–4376.
- (59) Emsley, P.; Cowtan, K. Coot: Model-building tools for molecular graphics. *Acta Crystallogr Sect D Biol Crystallogr.* **2004**, *60* (12 I), 2126–2132.
- (60) Adams, P. D.; Grosse-Kunstleve, R. W.; Hung, L. W.; et al. PHENIX: Building new software for automated crystallographic structure determination. Acta Crystallogr Sect D Biol Crystallogr. 2002, 58 (11), 1948–1954.

Authors are required to submit a graphic entry for the Table of Contents (TOC) that, in conjunction with the manuscript title, should give the reader a representative idea of one of the following: A key structure, reaction, equation, concept,

or theorem, etc., that is discussed in the manuscript. Consult the journal's Instructions for Authors for TOC graphic specifications.



Supporting Information

The Structural Basis of Sirtuin 6-Catalyzed Nucleosome Deacetylation

Zhipeng A. Wang,^{†,‡,#} Jonathan W. Markert,^{§,#} Samuel D. Whedon,^{†,‡,#} Maheeshi Yapa Abeywardana,^{†,‡} Kwangwoon Lee,^{†,‡} Hanjie Jiang,^{†,‡} Carolay Suarez,^{†,‡} Hening Lin,[^] Lucas Farnung,^{§,*} and Philip A. Cole.^{†,‡,*}

Equal contributors

[†] Division of Genetics, Department of Medicine, Brigham and Women's Hospital, Boston, MA, United States, 02115;

[‡] Department of Biological Chemistry and Molecular Pharmacology, Harvard Medical School, Boston, MA, United States, 02115;

[§] Department of Cell Biology, Blavatnik Institute, Harvard Medical School, Boston, MA 02115;

[^] Howard Hughes Medical Institute; Department of Chemistry and Chemical Biology, Cornell University, Ithaca, NY, United States, 14853;

^{*} Corresponding authors: Lucas Farnung@hms.harvard.edu; pacole@bwh.harvard.edu

Table of Contents

Design and cloning of Sirt6 mutants	3
Expression and purification of His-Sirt6, WT Sirt6 and Sirt6 mutants	5
Expression of TEV protease	6
Expression of sortase mutants	
General peptide synthesis methods	7
Incorporating depsipeptide Fmoc-Thr(OtBu)-glycolic acid (TOG) into peptides	7
Incorporating N-thioacetyl (Sac) into peptide	
Incorporating N-methyl thiourea (MTU) into peptide	8
Expression of histone H2A, H2B, H3, H4, gH3 and C-H2B	
F40 sortase-catalyzed histone H3 semisynthesis	9
W4 sortase-catalyzed histone H2B semisynthesis	. 10
147 and 185 bp DNA isolation	. 10
Octamer refolding and nucleosome reconstitution	. 11
Analysis of Sirt6 deacetylation of acetylated H3 and H2B nucleosomes and histones	. 12
Anti-H3K9ac antibody linearity test and antibody specificity test	. 13
Enzyme concentration-dependent Sirt6 mutant activity assay	. 13
Measuring NAD apparent Km for Sirt6 deacetylation of H3K9ac nucleosome-147	. 13
Measuring nucleosome apparent Km for Sirt6 deacetylation of H3K9ac nucleosome-147	. 13
Nucleosome Km measure of Sirt6 deacylation of H3K9ac nucleosome-185	. 13
NaCl effect of Sirt6 deacylation of H3K9ac nucleosome-147	. 14
MDL-800 inhibition assay of Sirt6 with H3K9ac nucleosome-147	. 14
Binding/activity assay with H3K9Sac nucleosome-185	. 14
Analysis of Sirt6 deacylation with H3K9Sac nucleosome	
Binding/activity assay with H3K9MTU nucleosome-185	. 14
Analysis of Sirt6 deacylation with H3K9MTU nucleosome	. 15
Sirt6 binding H3K9MTU nucleosome-185 complex sample preparation and grid preparation	. 15
Cryo-EM data collection and image processing	. 15
Model building and figure preparation	. 16
LC-MS analysis of Sirt6 binding/reacting with H3K9MTU nucleosome-185	. 16
Analysis of Sirt6 mutant deacetylation with H3K9ac nucleosome-147	. 16
EMSA of Sirt6 mutants with H3K9ac nucleosome-185	. 17
Figure SI 1-23	. 19
Table SI 1-3	. 48

Design and cloning of Sirt6 mutants

His-Sirt6 plasmid was donated by Hening Lin lab (Kanamycin resistant). A TEV cleavage site was inserted between the His-tag and Sirt6 sequence. A N-terminal Cys was left in case for further chemical biology handling.

His-TEV-Cys-Sirt6 1-355 sequence (TEV site are underlined)

CATCATCATCATCACAGCAGCGGCCTGGTGCCGCGCGCAGCCATgaaaacctgtattttcagtgcTC GGTGAATTACGCGGCGGGCTGTCGCCGTACGCGGACAAGGGCAAGTGCGGCCTCCCGGAG ATCTTCGACCCCCGGAGGAGCTGGAGCGGAAGGTGTGGGAACTGGCGAGGCTGGTCTGGC AGTCTTCCAGTGTGTTCCACACGGGTGCCGGCATCAGCACTGCCTCTGGCATCCCCGAC TTCAGGGGTCCCCACGGAGTCTGGACCATGGAGGAGGAGGTCTGGCCCCCAAGTTCGACA CCACCTTTGAGAGCGCGCGCCCACGCAGACCCACATGGCGCTGGTGCAGCTGGAGCGCGT GGGCCTCCTCGCTTCCTGGTCAGCCAGAACGTGGACGGGCTCCATGTGCGCTCAGGCTTCC CCAGGGACAAACTGGCAGAGCTCCACGGGAACATGTTTGTGGAAGAATGTGCCAAGTGTAA GACGCAGTACGTCCGAGACACAGTCGTGGGCACCATGGGCCTGAAGGCCACGGGCCGGCTC TGCACCGTGGCTAAGGCAAGGGGGCTGCGAGCCTGCAGGGGAGAGCTGAGGGACACCATCC TAGACTGGGAGGACTCCCTGCCCGACCGGGACCTGGCACTCGCCGATGAGGCCAGCAGGAA $\tt CGCCGACCTGTCCATCACGCTGGGTACATCGCTGCAGATCCGGCCCAGCGGGAACCTGCCGC$ TGGCTACCAAGCGCCGGGGAGGCCGCCTGGTCATCGTCAACCTGCAGCCCACCAAGCACGA $\tt CCGCCATGCTGACCTCCGCATCCATGGCTACGTTGACGAGGTCATGACCCGGCTCATGAAGC$ ACCTGGGGCTGGAGATCCCCGCCTGGGACGCCCCCGTGTGCTGGAGAGGGCGCTGCCACC CCTGCCCGCCCGCCCACCCCAAGCTGGAGCCCAAGGAGGAATCTCCCACCCGGATCAAC GGCTCTATCCCCGCCGGCCCCAAGCAGGAGCCCTGCGCCCAGCACAACGGCTCAGAGCCCG CCAGCCCAAACGGGAGCGCCCACCAGCCCTGCCCCCACAGACCCCCAAAAGGGTGAA GGCCAAGGCGGTCCCCAGCTG

Primers:

0. QC-TEVCysS6-F:

5'-TGGTGCCGCGCGCAGCCATGAAAACCTGTATTTTCAGTGCTCGGTGAATTACGCGGCGG QC-TEVCysS6-R:

5'-CCGCCGCGTAATTCACCGAGCACTGAAAATACAGGTTTTCATGGCTGCCGCGCGCACCA

1. Sirt6 R172A-F:

5'-gcgGGGCTGCGAGCCTGCAGGG

Sirt6 R172A-R:

5'-TGCCTTAGCCACGGTGCAGAGCC

2. Sirt6 R175A-F:

5'-gcgGCCTGCAGGGGAGAGCTGAGGG

Sirt6 R175A-R:

5'-CAGCCCCTTGCCTTAGCCACGG

3. Sirt6 acidic patch-binding tetra-mutant-F:

5'-agcggcctgtgcgGGAGAGCTGAGGGACACCATCCTAGACTGG

Sirt6 acidic patch-binding tetra-mutant-R:

5'-aaacetgeagetgeAGCCACGGTGCAGAGCCGGCCCG

4. Sirt6 R231A/R232A-F:

5'-gcgGGAGGCCGCCTGGTCATCGTCAACC

Sirt6 R231A/R232A-R:

5'-cgcCTTGGTAGCCAGCGGCAGGTTCCCGC

5. Sirt6 R248A-F:

5'-gcgCATGCTGACCTCCGCATCCATGGC Sirt6 R248A-R: 5'-GTCGTGCTTGGTGGGCTGCAGG

6. Sirt6 R205A-F:

5'-AACGCCGACCTGTCCATCACGCTGG Sirt6 R205A-R: 5'-TGCGCTGGCCTCATCGGCGAG

His-TEV-Cys-Sirt6 sequence (TEV site are underlined)

HHHHHHSSGLVPRGSH<u>ENLYFQC</u>SVNYAAGLSPYADKGKCGLPEIFDPPEELERKVWELARLV WQSSSVVFHTGAGISTASGIPDFRGPHGVWTMEERGLAPKFDTTFESARPTQTHMALVQLERVG LLRFLVSQNVDGLHVRSGFPRDKLAELHGNMFVEECAKCKTQYVRDTVVGTMGLKATGRLCT VAKARGLRACRGELRDTILDWEDSLPDRDLALADEASRNADLSITLGTSLQIRPSGNLPLATKRR GGRLVIVNLQPTKHDRHADLRIHGYVDEVMTRLMKHLGLEIPAWDGPRVLERALPPLPRPPTPK LEPKEESPTRINGSIPAGPKQEPCAQHNGSEPASPKRERPTSPAPHRPPKRVKAKAVPS

Other mutations were done by one or several rounds of quick-change site directed mutagenesis. Each of the PCR products was purified by PCR cleanup kit (Zymo), treated with DpnI (New England Biolabs), and then transformed into DH5 α *E. coli*. Single colonies were picked and let to grow overnight in 5 mL of Luria Bertani media (LB) supplemented with kanamycin (50 μ g / mL), then pelleted (5 minutes, 4500 rcf, 4 °C). Plasmids were obtained from cell pellets by mini-prep (Plasmid Miniprep Classic, Zymo) and Sanger sequenced.

Sirt6(1-355) M1C/R172A amino acid sequence (R172A) (mutations are <u>underlined</u>, TEV cut site is **bolded**, His tag is *italicized*)

HHHHHHSSGLVPRGSHENLYFQCSVNYAAGLSPYADKGKCGLPEIFDPPEELERKVWELARLV WQSSSVVFHTGAGISTASGIPDFRGPHGVWTMEERGLAPKFDTTFESARPTQTHMALVQLERVG LLRFLVSQNVDGLHVRSGFPRDKLAELHGNMFVEECAKCKTQYVRDTVVGTMGLKATGRLCT VAKAAGLRACRGELRDTILDWEDSLPDRDLALADEASRNADLSITLGTSLQIRPSGNLPLATKRR GGRLVIVNLQPTKHDRHADLRIHGYVDEVMTRLMKHLGLEIPAWDGPRVLERALPPLPRPPTPK LEPKEESPTRINGSIPAGPKOEPCAOHNGSEPASPKRERPTSPAPHRPPKRVKAKAVPS

Sirt6(1-355) M1C/R175A amino acid sequence (Sirt6 R175A) (mutations are <u>underlined</u>, TEV cut site is **bolded**, His tag is *italicized*)

HHHHHHSSGLVPRGSHENLYFQCSVNYAAGLSPYADKGKCGLPEIFDPPEELERKVWELARLV WQSSSVVFHTGAGISTASGIPDFRGPHGVWTMEERGLAPKFDTTFESARPTQTHMALVQLERVG LLRFLVSQNVDGLHVRSGFPRDKLAELHGNMFVEECAKCKTQYVRDTVVGTMGLKATGRLCT VAKARGLACRGELRDTILDWEDSLPDRDLALADEASRNADLSITLGTSLQIRPSGNLPLATKRR GGRLVIVNLQPTKHDRHADLRIHGYVDEVMTRLMKHLGLEIPAWDGPRVLERALPPLPRPPTPK LEPKEESPTRINGSIPAGPKQEPCAQHNGSEPASPKRERPTSPAPHRPPKRVKAKAVPS

Sirt6(1-355) M1C/K170A/R172A/R175A/R178A (Sirt6 acidic patch-binding tetra-mutant) amino acid sequence (mutations are <u>underlined</u>, TEV cut site is **bolded**, His tag is *italicized*) HHHHHHHSSGLVPRGSHENLYFQCSVNYAAGLSPYADKGKCGLPEIFDPPEELERKVWELARLV WQSSSVVFHTGAGISTASGIPDFRGPHGVWTMEERGLAPKFDTTFESARPTQTHMALVQLERVG LLRFLVSQNVDGLHVRSGFPRDKLAELHGNMFVEECAKCKTQYVRDTVVGTMGLKATGRLCT VAAAAGLAACAGELRDTILDWEDSLPDRDLALADEASRNADLSITLGTSLQIRPSGNLPLATKRR

GGRLVIVNLQPTKHDRHADLRIHGYVDEVMTRLMKHLGLEIPAWDGPRVLERALPPLPRPPTPK LEPKEESPTRINGSIPAGPKQEPCAQHNGSEPASPKRERPTSPAPHRPPKRVKAKAVPS

Sirt6(1-355) M1C/R231A/R232A amino acid sequence (Sirt6 R2312232A) (mutations are <u>underlined</u>, TEV cut site is **bolded**, His tag is *italicized*)

HHHHHHSSGLVPRGSHENLYFQCSVNYAAGLSPYADKGKCGLPEIFDPPEELERKVWELARLV WQSSSVVFHTGAGISTASGIPDFRGPHGVWTMEERGLAPKFDTTFESARPTQTHMALVQLERVG LLRFLVSQNVDGLHVRSGFPRDKLAELHGNMFVEECAKCKTQYVRDTVVGTMGLKATGRLCT VAKARGLRACRGELRDTILDWEDSLPDRDLALADEASRNADLSITLGTSLQIRPSGNLPLATK<u>AA</u> GGRLVIVNLQPTKHDRHADLRIHGYVDEVMTRLMKHLGLEIPAWDGPRVLERALPPLPRPPTPK LEPKEESPTRINGSIPAGPKQEPCAQHNGSEPASPKRERPTSPAPHRPPKRVKAKAVPS

Sirt6(1-355) M1C/R248A amino acid sequence (Sirt6 R248A) (mutations are <u>underlined</u>, TEV cut site is **bolded**, His tag is *italicized*)

HHHHHHSGLVPRGSHENLYFQCSVNYAAGLSPYADKGKCGLPEIFDPPEELERKVWELARLV WQSSSVVFHTGAGISTASGIPDFRGPHGVWTMEERGLAPKFDTTFESARPTQTHMALVQLERVG LLRFLVSQNVDGLHVRSGFPRDKLAELHGNMFVEECAKCKTQYVRDTVVGTMGLKATGRLCT VAKARGLRACRGELRDTILDWEDSLPDRDLALADEASRNADLSITLGTSLQIRPSGNLPLATKRR GGRLVIVNLQPTKHDAHADLRIHGYVDEVMTRLMKHLGLEIPAWDGPRVLERALPPLPRPPTPK LEPKEESPTRINGSIPAGPKQEPCAQHNGSEPASPKRERPTSPAPHRPPKRVKAKAVPS

Sirt6(1-355) M1C/R205A/ R231A/R232A/R248A (Sirt6 DNA-binding tetra-mutant) amino acid sequence (mutations are <u>underlined</u>, TEV cut site is **bolded**, His tag is *italicized*) HHHHHHHSSGLVPRGSHENLYFQCSVNYAAGLSPYADKGKCGLPEIFDPPEELERKVWELARLV WQSSSVVFHTGAGISTASGIPDFRGPHGVWTMEERGLAPKFDTTFESARPTQTHMALVQLERVG LLRFLVSQNVDGLHVRSGFPRDKLAELHGNMFVEECAKCKTQYVRDTVVGTMGLKATGRLCT VAKARGLRACRGELRDTILDWEDSLPDRDLALADEASANADLSITLGTSLQIRPSGNLPLATKAA GGRLVIVNLQPTKHDAHADLRIHGYVDEVMTRLMKHLGLEIPAWDGPRVLERALPPLPRPPTPK LEPKEESPTRINGSIPAGPKQEPCAQHNGSEPASPKRERPTSPAPHRPPKRVKAKAVPS

Expression and purification of His-Sirt6, WT Sirt6 and Sirt6 mutants

All Sirt6 constructs were transformed into LOBSTR E. coli strain derived from Rosetta (DE3). Single colony was picked to let to grow in 5 mL Luria Bertani (LB) seed culture for overnight (12-16 hr) with constant shaking (200 rpm). Then 1 L of LB media supplemented with 50 mg/L kanamycin was inoculated with 10 mL from a starter culture. The 1 L LB culture was grown at 37 °C, 200 rpm for about 3.5 h to an OD₆₀₀ of 0.6, and the overexpression was induced with the addition of IPTG to 0.5 mM. Then the temperature was brought down to 25 °C, and the culture grew for a further 18 hr at 25 °C, 200 rpm. The culture was pelleted by centrifugation at 4,000 × g, 4 °C, and the supernatant was removed. Cell pellets were stored at -80 °C overnight before being processed. The cell pellet was resuspended in 30 mL ice cold lysis buffer (20 mM Tris, 500 mM NaCl, 20 mM imidazole, pH 7.5) and then lysed by passing through a French pressure cell three times. Lysate was centrifuged at 13,000 × g, 4 °C, and the lysate supernatant was applied to pre-equilibrated Ni-NTA resin (2 mL resin bed volume / 1 L culture). After incubating for 1 h at 4 °C, the flow-through was removed by passing the column by gravity at a moderate drip rate. The resin bed was first washed with 10 column volumes of wash buffer (20 mM Tris, 500 mM NaCl, 50 mM imidazole, 0.5 mM TCEP, pH 7.5), and then washed with 25 column volumes of high-salt wash buffer (20 mM Tris, 2 M NaCl, 20 mM imidazole, pH 7.5), followed by 10 column volumes of elution buffer (20 mM Tris, 500 mM NaCl, 200 mM imidazole, 0.5 mM TCEP, pH 7.5). The elution was concentrated by spin concentrator (Amicon, 10 kDa MWCO, 4,000 rpm, 4 °C), before overnight dialysis at 4 °C (dialysis buffer: 20 mM Tris, 150 mM NaCl, 20 mM imidazole, 0.5 mM TCEP, pH 7.5). For WT-Sirt6 and all Sirt6 mutants, ~ 1 mL TEV protease (~ 1 mg/mL) was mixed with the elution before dialysis. The dialyzed sample was re-applied to pre-equilibrated Ni-NTA resin. After incubating for 1 h at 4 °C, the flow-through was collected

by gravity at a moderate drip rate. After diluting with 10 mL Heparin buffer A (50 mM Tris, 150 mM NaCl, 5 % glycerol, 0.5 mM TCEP, pH 7.5), the flow-through was concentrated by spin concentrator (Amicon, 10 kDa MWCO, 4,000 rpm, 4 °C), and then applied to Heparin column (1 mL, Cytiva, #17040601), and eluted with a linear gradient from 0-50 % Heparin buffer B (50 mM Tris, 2000 mM NaCl, 5 % glycerol, 0.5 mM TCEP, pH 7.5) over 20 column volumn (CV) at a flow rate of 0.6 mL/min (Figure S3A). Elution fractions were checked by SDS-PAGE (6-20 %, Biorad), and the pure fractions were collected and concentrated. This was further purified by size exclusion using a Superdex200 column (GE, #28-9909-44) with Superdex running buffer (50 mM Tris, 150 mM NaCl, 0.5 mM TCEP, pH 7.5) (Figure S3B). Elution fractions were checked by SDS-PAGE, and the pure fractions were combined and concentrated to ~200 μ L, or a final concentration of ~40 μ M. (Figure S3C). SDS-PAGE was used for densitometry and quality check for WT Sirt6 and all the Sirt6 mutants. WT Sirt6 was characterized by ESI-MS (Q Exactive, Thermo Scientific) and deconvoluted using UniDec¹ (Figure S1). WT Sirt6 and all Sirt6 mutants were aliquoted and flash-frozen in liquid nitrogen, then stored at -80 °C.

WT Sirt6 calculated average mass for C₁₇₁₈H₂₇₇₀N₅₁₄O₅₀₃S₁₃ [M]+: 39090.82 Da; Observed: 39089.0 Da

Expression of TEV protease

The pET-6xHis-TEV plasmid was transformed into Rosetta (DE3) pLysS Codon Plus $E.\ coli$ competent cells for recombinant protein expression. The transformed cells were cultured from fresh LB plates into 2xYT medium to optimal cell density at OD₆₀₀ = 0.6. Then 0.5 mM isopropyl thiogalactoside (IPTG) was added to induce protein expression at 20 °C for 20 h. After french press lysis, Ni-NTA resin was used for the purification in a buffer containing 25 mM HEPES, pH 7.8, 500 mM NaCl, 25 mM imidazole, and 1mM TCEP. After washing and gradually increasing the imidazole concentration for elution, the eluted fractions were analyzed by Coomassie Blue–stained SDS-PAGE and fractions containing high purity protein were combined. Then the combined fractions were dialyzed against a buffer containing 25 mM HEPES, pH 7.8, 500 mM NaCl, and 1 mM TCEP at 4 °C to gradually remove imidazole. After dialysis, glycerol was added to 20 % (v/v) to the protein and the protein was concentrated to 1mg/mL, determined by SDS-PAGE gel with BSA standards. The purified proteins were aliquoted, flash-frozen, and stored at -80 °C.

Expression of sortase mutants

Sortase mutants were derived from *S. aureus* sortase A (Srt A). The previously reported F40 sortase has altered sorting motif preference for APXTG, while W4 recognizes the sequence HPXTG. DNA encoding S. aureus Srt A (60-206) (from Dirk Schwarzer lab) was cloned into pET21 vector (Ampicillin resistant). W4 was derived from F40 by sequential site-directed mutagenesis, as previously described.

F40 amino acid sequence (mutations distinguishing F40 from Srt A are <u>underlined</u>, His tag is *italicized*) MQAKPQIPKDKSKVAGYIEIPDADIKEPVYPGPATPEQLNRGVSFAEENESLDDQNISIAGHTFIDR PNYQFTNLKAAK<u>M</u>GSMVYFKVGNETRKYKMTSIRDVKPQDVG<u>MHLAE</u>KGKDKQLTLITCDDY NEKTGVWEKRKIFVATEVKLE*HHHHHHH*

W4 amino acid sequence (mutations distinguishing W4 from Srt A are <u>underlined</u>, His tag is <u>italicized</u>) MQAKPQIPKDKSKVAGYIEIPDADIKEPVYPGPAT<u>S</u>EQLNRGVSFA<u>K</u>ENQSLDDQNISIAGHTFI<u>G</u> RPNYQFTNLKAAK<u>M</u>GSMVYFKVGNETRKYKMTSIR<u>N</u>VKPQDVG<u>MHLAE</u>KGKDKQLTLITCDD <u>LNRE</u>TGVWE<u>T</u>RKIFVATEVKLE*HHHHHH*

Constructs were transformed into BL21-CodonPlus (DE3) RIPL *E. coli*. Starter cultures were grown overnight (12-16 hr, 37 °C, 200 rpm) in 50 mL of Luria Bertani (LB) media supplemented with 100 mg/L ampicillin from scrapings of a frozen cell stock. Subsequently 1 L LB cultures with 100 mg/L ampicillin were inoculated with 10 mL of starter culture and grown to an OD₆₀₀ of 0.3-0.5 (37 °C, 200 rpm). Prior to induction the temperature was reduced to 25-30 °C. At an OD₆₀₀ of 0.5-0.8 overexpression was induced with the addition of IPTG to 0.3 mM. Cells were grown for a further 3 hr, then cultures were pelleted by centrifugation (5,000 \times g, 4 °C). Cell pellets were either stored at -80 °C, or immediately processed. Cell

pellets were resuspended in 5 pellet volumes ice cold lysis buffer (20 mM Tris, pH 7.5, 0.1% Triton X-100), made uniform by dounce homogenizer, and lysed by three passages through a microfluidizer. Lysates were clarified by centrifugation (13,000 x g, 4 °C), and lysate supernatants were applied to Ni-NTA resin (2.5 mL resin bed volume / 1 L culture) pre-equilibrated with cold lysis buffer. Resin was washed with 10 column volumes of lysis buffer, then 20 volumes of wash buffer (20 mM Tris, pH 7.5, 500 mM NaCl), and then 10 volumes of lysis buffer supplemented with 5% elution buffer (20 mM Tris, pH 7.5, 400 mM imidazole). Protein was eluted in five to ten fractions of elution buffer, each of 2 column volumes. Elution fractions were checked by SDS-PAGE (15%) and pooled. Purified protein was dialyzed three times against 40 volumes of 50 mM Tris, pH 7.5, 150 mM NaCl, 5 mM CaCl₂ at 4 °C. Protein was then concentrated by spin concentrator (Amicon, 10 kDa MWCO, 4,000 rpm, 4 °C) to 1-3 mM by the absorbance at 280 nm measured by nanodrop (Thales).

General peptide synthesis methods

All peptides were synthesized by Fmoc-based solid phase peptide synthesis with Rink Amide AM resin (EMD Millipore). Syntheses were performed using a Prelude automated peptide synthesizer (Gyros Protein Technologies) using the following deprotection & coupling cycle for a 0.2 mmol scale synthesis: 5 mL of 20% piperidine in DMF was added to the reaction vessel and mixed for 10 min, the vessel was drained, and a second identical deprotection followed; 4 mL of DMF was added to the reaction vessel and mixed for 30 sec, the vessel was drained, and five more washes followed alternating solvent delivery from the top and bottom of the reaction vessel; 0.8 mmol (4 eq) Fmoc-amino acid in 4 mL DMF, and 0.75 mmol (3.75 eq) HATU and 1.6 mmol (8 eq) N-methylmorpholine (NMM) in 4 mL DMF were sequentially added to the reaction vessel and mixed for 90 min, followed one wash with 4 mL DMF (as before), and a second identical coupling. After the final amino acid coupling peptides were N-terminally deprotected, as described above, and the resin was sequentially washed with DMF and dichloromethane (DCM), then dried under vacuum. Cleavage of the peptide from the resin and removal of the side chain protecting groups was accomplished by addition of Reagent B (5 % water, 5 % phenol, 2.5 % triisopropyl silane (TIPS), 87.5 % trifluoroacetic acid (TFA)) and 90-180 minutes of agitation. Resin was removed by filtration, and crude peptide was preciptated by adding 10 volumes of ice-cold diethyl ether. The precipitate was washed a further two times with ice-cold diethyl ether before drying under a stream of nitrogen. Crude peptides were purified by reverse-phase HPLC with either a C18 semi-preparative column (Varian Dynamax Microsorb 100, 250×21.4 mm) or a C8 semi-prep column (Varian Dynamax Microsorb 100, 250×21.4mm). H3(1-34) peptides were purified using the C18 column and a linear gradient from 7 % CH₃CN/0.05 % TFA to 30 % CH₃CN/0.05 % TFA over 30 min at a flow rate of 10 mL/min. H2B(4-52) TOG peptides were purified using the C8 column and a linear gradient from 25 % CH₃CN/0.05 % TFA to 55 % CH₃CN/0.05 % TFA over 30 min, at a flow rate of 10 mL/min. Pure fractions were determined by MALDI-TOF MS (Dana Farber Cancer Institute Molecular Biology Core Facilities, 4800 MALDI TOF/TOF, Applied Biosystems/MDS Sciex) or ESI-MS (Q Exactive, Thermo Scientific), then combined, lyophilized and stored at -80 °C as dry powders, or concentrated stock solutions. Pooled, purified materials were characterized by ESI-MS (O Exactive, Thermo Scientific) and deconvoluted using UniDec.¹

Incorporating depsipeptide Fmoc-Thr(OtBu)-glycolic acid (TOG) into peptides

The synthesis of TOG was done as described before². After the coupling of the first Gly, the second amino acid coupled in each H3 and H2B peptide was the depsipeptide TOG, which was hand coupled overnight with 0.4 mmol (2 eq) TOG, 0.36 mmol (1.8 eq) HATU, and 0.8 mmol (4 eq) DIPEA. No capping step was used, and subsequent couplings followed the general protocol.

Incorporating N-thioacetyl (Sac) into peptide

Fmoc-Lys(alloc)-OH was installed using the standard conditions described above into H3K9 site as H3K9alloc 1-34 TOG. To facilitate side-chain derivatization, Boc-Ala was used instead of Fmoc-Ala at the 1 position in the H3 peptide. Side chain deprotection was conducted as previously reported². Briefly,

vacuum dried Pd(PPh₃)₄ (0.35 eq relative to resin; Strem Chemicals cat# 46-2150) was dissolved in anhydrous dichloromethane (Sigma-Aldrich cat# 270997), and combined with phenylsilane (20 eq relative to resin; Chem-Impex cat# 31483). This solution was added to the peptide resin and mixed by bubbling with nitrogen for 60 minutes. The reaction solution was drained, and the deprotection was repeated once more. The resin was then extensively washed with dichloromethane and DMF, however it unavoidably retained a darker color after Pd deprotection.

Thioacetylation of the the free amino group of K9 was accomplished with ethyl dithioacetate. To the resin was added ethyl dithioacetate (20 eq relative to resin; Sigma-Aldrich #358851-1ML) and *N,N*-diisopropylethylamine (DIPEA, 40 eq; Sigma-Aldrich cat# 125806). This mixture was placed on an endover-end rotator for 8 h, after which the reagent was removed by vacuum and fresh reagent was added. The reaction was repeated for a total of 3 times. After carefully washing, Fmoc-Cl (10 eq, Sigma-Aldrich #23186-1G) was added together with DIPEA (20 eq) to cap unreacted lysine, and the mixture was placed on an end-over-end rotator for 18 h. Peptide cleavage, precipitation and purification followed the general protocol. Pooled, purified materials were characterized by ESI-MS (Q Exactive, Thermo Scientific) and deconvoluted using UniDec¹ (Figure S2A).

Sequence: ARTKQTARK(Sac)STGGKAPRKQLATKAARKSAPA-TOG-G

H3K9Sac 1-34 TOG [M]⁺ calculated for C₁₄₆H₂₆₃N₅₅O₄₄S as 3507.96 Da; Observed: 3508.8 Da

Incorporating N-methyl thiourea (MTU) into peptide

N-terminal Boc protection and alloc deprotection was performed as described in the above N-thioacetyl incorporation protocol. Methyl isothiocyanate (1 eq relative to resin; Sigma-Aldrich # 112771) in dry dichloromethane was added to the peptide resin. DIPEA was dried by passing over a silica plug column, and then added to the peptide resin (1 eq relative to resin). This mixture was placed on an end-over-end rotator. After 60 hours the reaction was judged to have stopped at ~60% conversion (RP-HPLC peak area). Peptide cleavage, precipitation and purification followed the general protocol. Pooled, purified materials were characterized by ESI-MS (Q Exactive, Thermo Scientific) and deconvoluted using UniDec¹ (Figure S2B).

Sequence: ARTKQTARK(MTU)STGGKAPRKQLATKAARKSAPA-TOG-G H3K9MTU 1-314 TOG $[M]^+$ calculated for $C_{146}H_{263}N_{55}O_{44}S$ as 3522.98 Da, observed at 3521.9 Da

Expression of histone H2A, H2B, H3, H4, gH3 and C-H2B

Wild type (WT) Xenopus laevis core histones H2A, H2B, H3, and H4,³ together with gH3 (aa33-135) and C-H2B (aa53-125) were expressed and purified as previously reported. Both H3 and gH3 constructs carry a C110A mutation, which is widely used in both nucleosome chemical biology and nucleosome structural studies. Generally, histone expression was freshly transformed E. coli Rosetta (DE3) pLysS, which were plated on LB agar plates supplemented with ampicillin (100 μg/mL). After 12-16 h at 37 °C, a single colony was used to inoculate a 50 mL starter culture of LB media supplemented with 100 mg/L ampicillin, and grown at 37 °C (200 rpm). After a further 12-16 hours 10 mL of starter culture was used to inoculate 1 L of LB media supplemented with 100 mg/L ampicillin. This culture was grown at 37 °C (200 rpm) until the OD₆₀₀ was 0.6. Expression was induced with 0.5 mM IPTG at 37 °C for 2-4 hr. Cells were harvested by centrifugation at 4,000 rpm for 15 min. Cell pellets were resuspended in histone lysis buffer (50 mM Tris-HCl at pH 7.5, 100 mM NaCl, 1 mM EDTA, 5 mM 2-mercaptoethanol (BME), with 1% Triton X-100). Resuspended cell pellets were made uniform by dounce homogenizer and lysed by three passages through a microfluidizer. Lysed cells were centrifuged for 30 min at 15,000 g, 4 °C, and the supernatant was discarded. The pellet (inclusion bodies) was then washed by resuspending and vortexing five times with histone wash buffer (50 mM Tris-HCl at pH 7.5, 100 mM NaCl, 1 mM EDTA). After the removal of all the supernatants, the pellets were resuspended in ion exchange (IEX) buffer A (7 M urea, 10 mM Tris pH 7.8, 1 mM EDTA, and 5 mM BME) with vortexing, stirring and sonication to maximize protein solublization (Note: these resuspended samples are not completely soluble, and generally contain translucent amber particulate). The resuspension is centrifuged for 30 min at 15,000 g, 4 °C, and the supernatant is loaded onto passed over connected, pre-packed Q and SP columns (5 mL HiTrap Q HP and 5 mL HiTrap SP HP,

GE healthcare). IEX buffer A containing 100 mM NaCl was used to equilibrate and wash both Q and SP columns. After the Q column is washed with 5-10 column volumes of IEX A it is detached from the SP column, and the histone is isolated by gradient wash and elution of SP column (100 mM - 500 mM NaCl in IEX A). All fractions are evaluated by SDS-PAGE (15%), and those containing histone are combined and dialyzed three times against pre-chilled, ice-cold water with 0.05% TFA, then concentrated (Amicon Ultra 15 mL, 10 kDa MWCO, EMD Millipore), aliquoted in 3 mg portions, flash-frozen, lyophilized to dryness and stored at -80 °C until usage. C-H2B samples were re-dissolved in denaturant and further purified by reverse-phase HPLC with a C8 semi-preparative column (Varian Dynamax Microsorb 100, 250×21.4 mm). A linear gradient from 30 % CH₃CN/0.05 % TFA to 50 % CH₃CN/0.05 % TFA over 30 min at a flow rate of 10 mL/min was used for C-H2B purification to reach a final > 95 % purity by Coomassie stained SDS-PAGE. The combined C-H2B solution was then lyophilized to dryness and stored at -80 °C until usage.

H2A:

SGRGKQGGKTRAKAKTRSSRAGLQFPVGRVHRLLRKGNYAERVGAGAPVYLAAVLEYLTAEIL ELAGNAARDNKKTRIIPRHLQLAVRNDEELNKLLGRVTIAQGGVLPNIQSVLLPKKTESSKSAKS K

H2B:

AKSAPAPKKGSKKAVTKTQKKDGKKRRKTRKESYAIYVYKVLKQVHPDTGISSKAMSIMNSFV NDVFERIAGEASRLAHYNKRSTITSREIQTAVRLLLPGELAKHAVSEGTKAVTKYTSAK H3·

ARTKQTARKSTGGKAPRKQLATKAARKSAPATGGVKKPHRYRPGTVALREIRRYQKSTELLIRK LPFQRLVREIAQDFKTDLRFQSSAVMALQEASEAYLVALFEDTNLAAIHAKRVTIMPKDIQLARR IRGERA

H4:

SGRGKGGKGLGKGGAKRHRKVLRDNIQGITKPAIRRLARRGGVKRISGLIYEETRGVLKVFLEN VIRDAVTYTEHAKRKTVTAMDVVYALKRQGRTLYGFGG

F40 sortase-catalyzed histone H3 semisynthesis

Histone H3 semisynthesis with F40 followed a previously reported protocol.⁵ Briefly, dried gH3 is resuspended in ice cold water with gentle pipetting, and used for ligation within 72 hours, after which aggregation limits ligation efficiency. Lyophilized peptide is resuspended to 20 mM in ice cold water. Peptide (2 mM) and gH3 (0.2 mM) are combined in ligation buffer (40 mM PIPES pH 7.0, 5 mM CaC12, 1 mM DTT) and the pH is adjusted to 7.0 with concentrated PIPES (400 mM PIPES pH 7.5), then F40 sortase is added (0.2 mM), and the reaction is placed in a 37 °C incubator overnight. The insoluble fraction contains the bulk of the product, and as such is separated from soluble peptide and sortase by centrifugation (3 min at 21,100 rcf). The pelleted solid is dissolved in ion exchange (IEX) buffer A (7 M urea, 10 mM Tris pH 7.8, 1 mM EDTA, and 5 mM BME) with vortexing and sonication, then loaded on a pre-equilibrated SP column (1 mL HiTrap SP HP, Cytiva) at 1 mL / min using a peristaltic pump (Pharmacia Biotech). The column is washed with 120 mM NaCl in IEX A for >20 column volumes, followed by sequential 5 column volume washes in which the concentration of NaCl is stepped up by 10 mM per wash (130 mM, 140 mM, 150 mM, etc.) until 200 mM NaCl is reached. The bulk of the product can be eluted in 250 mM and 300 mM NaCl fractions of 5-10 column volumes each. Washes and fractions are checked by SDS-PAGE (15%), and pure fractions are combined and dialyzed three times against pre-chilled, ice-cold water with 0.05% TFA, then lyophilized. Pooled, purified materials were characterized by ESI-MS (Q Exactive, Thermo Scientific) and deconvoluted using UniDec (Figure S2C,D, some data were shown before⁵).

WT-H3: [M]⁺ calculated as m/z 15238.8, observed as m/z 15238.0;

gH3: [M]⁺ calculated as m/z 11918. 8, observed as m/z 11918.0;

H3K9ac: [M]⁺ calculated as m/z 15280.6, observed as m/z 15280.1;

H3K9Sac: [M]⁺ calculated as m/z 15296.71 Da; Observed: 15296.5;

H3K9MTU: [M]⁺ calculated as m/z 15311.7, observed as m/z 15311.2;

H3K14ac: [M]⁺ calculated as m/z 15280.6, observed as m/z 15280.2;

```
H3K18ac: [M]<sup>+</sup> calculated as m/z 15280.6, observed as m/z 15280.1; H3K23ac: [M]<sup>+</sup> calculated as m/z 15280.6, observed as m/z 15280.0; H3K27ac: [M]<sup>+</sup> calculated as m/z 15280.6, observed as m/z 15279.8;
```

W4 sortase-catalyzed histone H2B semisynthesis

H2B semisynthesis by W4 sortase was done following a similar protocol as reported for F40 sortase catalyzed H3 semisynthesis. ⁵ The modified histone H2B N-terminal peptide (H2B 4-52 TOG) was prepared as a 5 mM stock solution, and the C-H2B (53-125) was prepared as a 1 mM stock solution. If necessary, both solutions were centrifuged to remove any precipitate. With the optimized condition tested by small scale (20 µL), large scale (~5 mL) W4 sortase-catalyzed H2B semisynthesis reaction was then carried out. H2B 4-52 TOG (~1 mM) and C-H2B (~0.1 mM) were added to a sortase reaction buffer (20 mM PIPES at pH 7.5, 1 mM DTT, without the addition of 5 mM CaCl₂), and mixed well. After being initiated by the addition of W4 sortase (to final ~500 mM), the ligation reaction was incubated at 37 °C for 12 hr. The reaction produces substantial precipitate, which contains most of the H2B product, C-H2B with some W4 sortase, and could be isolated from the supernatant by centrifugation. The precipitate was then dissolved in 1 mL IEX buffer A (7 M urea, 10 mM Tris at pH 7.8, 1 mM EDTA and 5 mM BME). The combined solution was purified by reverse-phase HPLC with a C8 semi-prep column. These product fractions containing some C-H2B were carefully pooled and lyophilized until dry. The dry powder was then dissolved in 10 % CH₃CN/ 0.05% TFA in H2O/0.05 % TFA, and repurified by reverse-phase HPLC with a C18 analytic column (Agilent, Eclipse XDB-C18, 4.6×250 mm) with a linear gradient from 30 % CH₃CN/0.05 % TFA to 50 % CH₃CN/0.05 % TFA over 30 min at a flow rate of 1 mL/min. The collected fractions were then characterized by MALDI-TOF MS and pooled, lyophilized to powder, and stored at -80 °C. H2BK20ac and H2BK46ac were characterized by ESI-MS (LTQ Orbitrap, Thermo Q Exactive), while C-H2B, H2BK11ac, H2BK12ac, were characterized by MALDI-TOF (Dana Farber Cancer Institute Molecular Biology Core Facilities, 4800 MALDI TOF/TOF, Applied Biosystems/MDS Sciex) (data were shown before²).

C-H2B: $[M + H]^+$ calculated as m/z 7940.1, observed as m/z 7939.5; H2BK11ac: $[M + H]^+$ calculated as m/z 13536.7, observed as m/z 13541.2; H2BK12ac: $[M + H]^+$ calculated as m/z 13536.7, observed as m/z 13538.6;

H2BK20ac: [M]⁺ calculated as m/z 13535.7, deconvolution as m/z 13537.8;

H2BK46ac: [M]⁺ calculated as m/z 13535.7, deconvolution as m/z 13537.9;

147 and 185 bp DNA isolation

Preparation of 146 and 185 bp Widom 601 DNA was as previously reported⁶. Briefly, scrapings from a frozen cell stock were used to inoculate a 50 mL starter culture of LB media supplemented with 50 mg/L kanamycin, and grown at 37 °C (200 rpm) for 12-16 h. From this starter culture 10 mL was used to inoculate 1 L of CircleGrow media supplemented with 50 mg/L kanamycin. The 1 L culture was grown for a 24-30 h at 37 °C (200 rpm). Cells were harvested by centrifugation at 4,000 rpm for 15 min. Cell pellets were resuspended in 10 mM Tris pH 7.5, 10 mM EDTA (10 mL/g wet cell pellet mass) with vigorous mixing. Cells were lysed with lysozyme powder (10 mg powder / 1 mL lysozyme solution, Sigma-Aldrich cat# 62971) dissolved in 10 mM Tris pH 7.5, 10 mM EDTA (5 mL lysis solution / g wet cell pellet mass) and vigorously shaken, but not vortexed. The suspension became very viscous, taking on an appearance like wet dough. To this suspension was added 0.2 M sodium hydroxide (Chem-Impex cat# 30056) with 1% sodium dodecyl sulfate (Amresco cat# M107) (15 mL / g wet cell pellet weight), followed by vigorous shaking, but not vortexing. After 5 minutes of lysis the mixture was neutralized for a further 5 minutes with 1.5 M potassium acetate in 1.5 M acetic acid (12 mL/g wet cell pellet weight), followed by vigorous shaking. Insoluble material was pelleted by centrifugation at 4,000 rpm for 20 min. Any remaining insoluble material was removed by filtering over a glass fritted column. The solution was combined with 0.6 volumes of isopropanol, mixed by inverting, and allowed to stand for 5 minutes. The samples were pelleted by centrifugation at 4,000 rpm for 15 min, and the supernatant was discarded. The pellets were resuspended by pipetting in 10 mM Tris pH 7.5, 10 mM EDTA (15 mL/g wet cell pellet weight), then combined with

1 volume ice cold 5 M lithium chloride and kept for 5 minutes on ice. Insoluble material was removed by centrifugation at 4,000 rpm for 15 min, and the pellet was discarded. The supernatant was combined with 0.6 volumes of isopropanol, mixed by inverting and allowed to stand for 5 minutes. The samples were pelleted by centrifugation at 4,000 rpm for 15 min, and the supernatant was discarded. The pellets were resuspended by pipetting in 10 mM Tris pH 7.5, 1 mM EDTA (10 mL/g wet cell pellet weight), and heat treated RNAse A was added (0.005 volumes of 10 mg/mL stock) and the solution was incubated for 15 min at room temperature. The solution was combined with 3 volumes of isopropanol, mixed by inverting, allowed to stand for 5 minutes, and plasmid DNA was pelleted by centrifugation at 4,000 rpm for 10 min. Pellets were air dried and dissolved in 50 mM Tris pH 8.0, 1 mM EDTA (~40 mg plasmid DNA / 1 L culture). Dissolved plasmid DNA was combined with 10× rCutSmart buffer (NEB) and EcoRV (45 units / 1 mg plasmid DNA, NEB), and the pH was confirmed to be > 7.8 before incubating overnight at 37 °C with constant mixing. Digestion was checked by 1.5% Agarose TAE gel, and judged to have reached completion when the only observed bands were vector backbone (2.5-kbp) and single copy Widom 601 fragments (100-200 bp). The crude digest was diluted 10-fold with 10 mM Tris pH 7.5, 1 mM EDTA and loaded onto a 5 mL Q column (Cytiva) at a flow rate of 1 mL / min. The absorbance at 260 nm and 280 nm were monitored during column washing and elution. Washes with 200 mM NaCl in 10 mM Tris pH 7.5, 1 mM EDTA, then 600 mM NaCl in 10 mM Tris pH 7.5, 1 mM EDTA remove protein components. The product elutes at 700 mM NaCl in 10 mM Tris pH 7.5, 1 mM EDTA, while the vector backbone elutes at 800 mM NaCl in 10 mM Tris pH 7.5, 1 mM EDTA. The elution fractions were concentrated to 1 mg/mL by 260 nm absorbance and checked by 1.5% agarose/TAE gel before storing at -20 °C (data not shown).

DNA sequence:

185 bp DNA:

5'-

ATCGCTGTTCAATACATGCACAGGATGTATATATCTGACACGTGCCTGGAGACTAGGGAGTA ATCCCCTTGGCGGTTAAAACGCGGGGGACAGCGCGTACGTGCGTTTAAGCGGTGCTAGAGCT GTCTACGACCAATTGAGCGGCCTCGGCACCGGGATTCTCCAGGGCGGCCGCGTATAGGGAT-3'

147 bp DNA:

5'-

CTGGAGAATCCCGGTGCCGAGGCCGCTCAATTGGTCGTAGACAGCTCTAGCACCGCTTAAACGCACGTACGCGCTGTCCCCCGCGTTTTAACCGCCAAGGGGATTACTCCCTAGTCTCCAGGCACGTGTCAGATATATACATCCTGT-3'

Octamer refolding and nucleosome reconstitution

In vitro octamer refolding and nucleosome assembly were carried out as previously reported. Briefly, all four histone proteins (H2A, H2B, H3 and H4) were dissolved in denaturing buffer (7 M guanidine, 20 mM Tris-HCl at pH 7.5 and 10 mM DTT) with gentle mixing, then allowed to stand for ~30 min and quantified by 280 nm absorbance (nanodrop). Octamer preparations containing acylated H3 were mixed in a 1.2:1.2: 1: 1.1 ratio of H2A:H2B:H3ac:H4, such that the final protein concentration was ~1 mg/mL. Octamer preparations containing acylated H2B were mixed in a 1.1:1:0.9:0.9 ratio of H2A:H2Bac:H3:H4, such that the final protein concentration was ~1 mg/mL. The histone solution was then dialyzed (10 kDa molecular weight cutoff (MWCO) cassette, Slide-a-lyzer) against high salt octamer refolding buffer (20 mM Tris at pH 7.5, 2.0 M NaCl, 1 mM EDTA and 5 mM BME) three times at 4 °C. Crude octamers were concentrated (10 kDa MWCO, Amicon Ultra 0.5 mL, EMD Millipore) at 4 °C and purified by size exclusion FPLC (AKTApurifier, GE Healthcare) using a Superdex 200 10/300 GL column (GE Healthcare) with octamer refolding buffer as the mobile phase. Purified octamer was mixed with 147 bp Widom 601 DNA in 1:1 molar ratio, or with 185 bp Widom 601 DNA in a 1.2:1 molar ratio (octamer:DNA) in high salt buffer (10 mM Tris at pH 7.5, 2.0 M KCl, 1 mM EDTA and 1 mM DTT) with a final concentration of 6 µM octamer. A Minipuls two channel peristaltic pump (Gilson) was used to continuously add low salt buffer (10 mM Tris at pH 7.5, 250 mM KCl, 1 mM EDTA and 1 mM DTT) to the dialysis chamber, while

simultaneously removing buffer from the chamber. Buffers were transferred at a rate of ~1 mL/min over a period of 33-48 hours. The crude nucleosomes were purified by HPLC (Waters, 1525 binary pump, 2489 UV-Vis detector) with a TSKgel DEAE-5PW ion exchange column (TOSOH Bioscience, #83W-00096C) to remove free DNA. Mobile phase buffers were A TES250 (10 mM Tris pH 7.5, 250 mM KCl, 0.5 mM EDTA) and B TES600 (10 mM Tris pH 7.5, 600 mM KCl, 0.5 mM EDTA). The purification gradient was 0 % B for 4 min, followed by a linear gradient from 25 % to 75 % B over 30 min at 1 mL/ min flow rate. The fractions containing nucleosome products were immediately diluted with one volume of TCS Buffer (20 mM Tris at pH 7.5 and 1 mM DTT), then concentrated (10 kDa MWCO Amicon Ultra 4 mL, EMD Millipore) at 4 °C, and dialyzed three times against TCS buffer. Nucleosome samples intended for long-term storage were dialyzed against storage buffer (10 mM Tris pH 7.5, 25 mM NaCl, 1 mM DTT, 20% glycerol). Dialyzed nucleosomes were concentrated to 1-5 mM (Amicon Ultra 4 mL, 10 kDa MWCO, EMD Millipore), and analyzed by native 4-20 % TBE gels (NovexTM, Thermo Fisher Scientific EC62252BOX) at 120-125 V for 40-90 minutes on ice (Typical native gel results can be referred to Figure S5).

Analysis of Sirt6 deacetylation of acetylated H3 and H2B nucleosomes and histones

For all the deacetylation assays with WT Sirt6 and mutants, each of the semi-synthetic free histone proteins (H3K9ac, H3K14ac, H3K18ac, H3K23ac, H3K27ac, H2BK11ac, H2BK12ac, H2BK20ac, H2B46ac, H2BK11lac, and H2BK11bhb) (final 1.0 μM) or the corresponding nucleosomes (H3K9ac, H3K14ac, H3K18ac, H3K23ac, H3K27ac, H2BK11ac, H2BK12ac, H2BK20ac, H2B46ac, H2BK11lac, and H2BK11bhb) (final 100 nM) were diluted into Sirt6 reaction buffer (50 mM HEPES at pH 7.5, 1 mM DTT, 0.2 mg/mL BSA, and 1 mM NAD).8 The reaction solution was kept on ice until the addition of Sirt6 and then incubated at 37 °C. At different time points, multiple reaction samples from the same reaction tubes were taken. In a typical sample, 6.5 µL aliquots of the reaction were first taken and quenched with Dual quenching buffer (6.5 µL 4 × Laemmli sample buffer 1:1 diluted with 40 mM EDTA) to a final quenched solution with 1 × Laemmli sample buffer with 10 mM EDTA. For typical nucleosome assay, the time points contain 0, 30, 60, 90, 120 min. For typical free H3 protein assay, the time points contain 0, 5, 10, 20, 30 min, while for typical free H2B histone protein assay, the time points contain 0, 2, 4, 6, 8, 20 min. Each sample was then boiled for 3-5 min at 95 °C and resolved on a 4-20 % gradient SDS-PAGE gel (TGXTM, Bio-Rad, 4561096) at 180 Volts for ~25 min. Gels were then transferred to nitrocellulose membrane (Transfer Stack, Invitrogen, IB301031) for western blot analysis (WB) by iBlot (Invitrogen) with P3 (20 V) for 5.0 min. Site-specific antibodies for acetylated H3 and acylated H2B, such as for anti-H3K9ac, anti-H3K14ac, anti-H3K18ac, anti-H3K23ac, anti-H3K27ac, anti-H2BK11ac (Invitrogen, #PA5-112479), anti-H2BK12ac (ActiveMotif, #39669), anti-H2BK20ac (Revmab Biosciences #31-1113-00), and anti-H2BK46ac (ActiveMotif, #39571) were used to blot the corresponding membranes. Meanwhile, anti-H3 or anti-H2B (Abcam, #ab1791, Abcam, #ab134211, or Abcam, #ab52484) was used to visualize total H3 or H2B, respectively. The affinities and specificities of the primary antibodies anti-H3K9ac, anti-H3K14ac, anti-H3K18ac, anti-H3K23ac, and anti-H3K27ac have been confirmed previously⁵, while the affinities and specificities of the primary H2B antibodies were also tested and validated². After secondary antibody Anti-Rabbit IgG, HRP linked antibody (Cell signaling #7074S) blotting for 1 h at room temperature, the membranes were treated with the ECL substrate reagent (Bio-Rad, #170-5061), and visualized by the G:BOX mini gel imager (Syngene). The bands on the membrane were then quantified by ImageJ (Download from imagej.nih.gov/ij/). All intensity values were divided by the intensity value at t=0 to get relative intensity, and then fit to a single-phase exponential decay curve with constrain Y0=1, Plateau=0 (GraphPad Prism 9). Each plotted point represents at least 2 replicates (Figure S5,6). The kinetic parameter V/[E] was calculated using GraphPad Prism 9. For the free histone protein assays with H3 (Figure S7) and H2B (Figure S8), a decrease in each histone loading control was observed over time (Figure 1B, Figure S7ABCE, and Figure S8ABCD), which we speculate may be due to aggregation/precipitation of these histones under the conditions of the assay. To account for this we normalized the PTM signal relative to the corresponding total histone signal at each time point. This is indicated in the Figure S7F and Figure S8E as "normalized relative intensity". Normalization was applied before plotting and fitting to get the kinetic data for V/[E] calculation. Normalized V/[E] were calculated for histone assays (V/[E] divided by a factor of 5) given that each nucleosome contains two H3 molecules and the final histone protein substrate (1.0 μ M) is ten times more than nucleosome substrate (100 nM). The velocity data for the histone protein assays are within statistical error, and thus indistinguishable from zero rate, which we indicate as normalized V/[E] of <0.01 (Figure S7,8). The remaining nucleosome samples after assay were loaded onto a native 4-20 % TBE gels (NovexTM, Thermo Fisher Scientific EC62252BOX) at 130 Volts for 110 min to compare with the samples before assay to confirm the stability of nucleosome throughout the assay (Figure S5,6). Note that in the Coomassie staining of the TBE gels the presence of extra bands is attributed to BSA multimers due to temperature of and buffer conditions of the temperature of the temp

Anti-H3K9ac antibody linearity test and antibody specificity test

A calibration curve was measured out to confirm that the substrate recognition by the anti-H3K9ac site-specific antibody was in the linear range. Different concentrations of H3K9ac nucleosome-147 were loaded followed by the primary and secondary antibody blotting as described above to get band intensity. The intensity shows good linearity with the amount of H3K9ac nucleosome-147 input (Figure S4). The antibody specificity test has been done as before.²

Enzyme concentration-dependent Sirt6 mutant activity assay

For all the Sirt6 mutants, an enzyme concentration-dependent assay was carried out for both acetylated H3 and H2B nucleosomes. For WT Sirt6 nucleosome deacetylation assay on H3K9ac nucleosome as an example, two different final concentrations of the Sirt6 (10 nM, 30 nM) were mixed with H3K9ac nucleosomes (Figure S3D). The rate "V" showed a linear relationship with enzyme concentration, while the V/[E] remained relatively constant (Figure S3E). Similarly, enzyme concentration-dependent assays were also carried out for all the other H3 and H2B nucleosomes. In each of these cases, the V measurements generally showed a linear relationship with enzyme concentration. For different Sirt6 mutants mean \pm SD was plotted as a bar graph, in which all the V/[E] from different enzyme concentrations were taken into account for the p-value calculation (Figure S5-8).

Measuring NAD apparent Km for Sirt6 deacetylation of H3K9ac nucleosome-147

It has been reported that sirtuin family members can have different apparent affinities 11 for NAD under different acyl-Lys substrate conditions 12 . Several similar deacetylation activity assays were set up with 56.95, 227.8, 1000, or 1139 μM NAD under 10 nM WT Sirt6 and 100 nM nucleosome unchanged condition. The kinetic parameter V/[E] \pm SD under each NAD concentration was calculated using GraphPad Prism 9, and then fit into Michaelis–Menten equation to calculate $K_{m(NAD)}$ and (V/[E]) $_{max(NAD)}$ (Figure S9).

Measuring nucleosome apparent Km for Sirt6 deacetylation of H3K9ac nucleosome-147

A concern for measuring apparent nucleosome Km values is the uncertain nucleosome stability at low concentrations. A series of nucleosome stability tests have been carried out showing that as low as 10 nM our nucleosomes appear stable under the deacetylation activity assay conditions (data not shown). Based on this, deacetylation activity assays were performed with 10, 20, 50, 100, 200, and 400 nM nucleosomes with fixed 1000 μ M NAD. In these experiments, the WT Sirt6 concentration was varied with different nucleosome concentrations so that we could accurately measure the rates of deacetylation. The kinetic parameter V/[E] \pm SD under each nucleosome concentration was calculated using GraphPad Prism 9, and then fit into Michaelis–Menten equation to calculate $K_{m(Nucleosome-147)}$ and $(V/[E])_{max(Nucleosome-147)}$ (Figure S10).

Nucleosome Km measure of Sirt6 deacylation of H3K9ac nucleosome-185

Since Sirt6 has been wildly believed to prefer to bind with DNA, one possible outcome is the nucleosome with longer DNA will favor Sirt6 binding than the nucleosome with traditional 147 "601" sequence. Based on the Km measurement of H3K9ac nucleosome-147, several similar deacetylation activity assays were set up with 10, 20, 50, 100, and 200 nM H3K9ac nucleosome-185 under 1000 μ M NAD unchanged condition. But the WT Sirt6 varies under different nucleosome concentration conditions to get proper and calculatable

rate constants. The kinetic parameter $V/[E] \pm SD$ under each nucleosome concentration was calculated using GraphPad Prism 9, and then fit into Michaelis–Menten equation to calculate $K_{m(Nucleosome-185)}$ and $(V/[E])_{max(Nucleosome-185)}$ (Figure S11).

NaCl effect of Sirt6 deacylation of H3K9ac nucleosome-147

Under our standard Sirt6 deacetylation activity assay conditions no NaCl was added (beyond that present in enzyme and nucleosome storage buffers). However, while testing EMSA/binding assays, we observed that at high concentrations of Sirt6 a precipitate formed, while the addition of supplemental NaCl prevented this (data not shown). This suggested NaCl concentration may affect Sirt6 stability and/or deacetylation activity, and even oligomerization state (suggested by a high molecular weight peak observed in Superdex200 purification of His-Sirt6, data not shown). We thus measured deacetylation activity with different salt concentrations including 25, 50, 100, and 250 nM NaCl using 100 nM nucleosome and 1000 μ M NAD. The WT Sirt6 varies under different nucleosome concentration conditions to get proper and calculatable rate constants. The kinetic parameter V/[E] \pm SD was calculated using GraphPad Prism 9 (Figure S12).

MDL-800 inhibition assay of Sirt6 with H3K9ac nucleosome-147

MDL-800 (Sigma-Aldrich #SML2529-5MG) was first prepared as stock solution in DMSO with the stock concentration of 10 mM, followed by the serial dilution from 20 μ M down to 20 nM in DMSO. In each of the reaction, 2 nM WT Sirt6 was mixed with buffer containing 100, 10, 1, 0.1, 0.01 μ M MDL-800 and preincubated at room temperature for 5 min. Buffer containing 10 % DMSO was used as a vehicle control, while buffer without DMSO was used as a positive control. After cooling on ice for 3 min, 20 nM final H3K9ac nucleosome-147 was added to initiate the deacetylation reaction. At different time points as 0, 30, 60, 120 min, multiple reaction samples from the same reaction tubes were taken, before processing as described above. The final (V/[E] \pm SD)_{MDL-800=100, 10, 1, 0.1, 0.01 μ M under each MDL-800 condition was calculated as described above, and then divided by the control (V/[E] \pm SD)_{MDL-800=0, DMSO}, providing the SD for each measurement (Figure S13).}

Binding/activity assay with H3K9Sac nucleosome-185

To assess the binding between WT Sirt6 and H3K9Sac nucleosome-185, different nucleosome types, different WT Sirt6 concentrations, different H3K9Sac nucleosome-185 concentrations, different salt concentrations, different buffer contents have been screened (data not shown). Sirt6 binding buffer (HEPES 50 mM, NaCl 100 mM, DTT 1 mM, BSA 0.2 mg/mL, 150 μ M NAD, pH=7.45) was discovered to allow both WT Sirt6 and nucleosome to be stable in solution. In a typical binding screening experiment, 400 nM H3K9Sac nucleosome-185 was mixed with 1 μ M WT Sirt6 (NCP:Sirt6=1:2.5 ratio) in Sirt6 binding buffer, and was incubated on ice, room temperature, or 37 °C for 2h. The solution was applied to a native 4-20 % TBE gel (Figure S14A), SDS-PAGE, and WB analysis. SDS-PAGE showed no significant precipitation (data not shown), while WB analysis showed a significant decrease signal with anti-H3K9ac antibody (data not shown).

Analysis of Sirt6 deacylation with H3K9Sac nucleosome

To explain why the binding between WT Sirt6 and H3K9Sac nucleosome-185 was not as strong as expected, a typical deacetylation activity assay was set up under 10 and 30 nM WT Sirt6 condition, before processing as described above (Figure S15).

Binding/activity assay with H3K9MTU nucleosome-185

The binding assay between WT Sirt6 and H3K9MTU nucleosome-185 was done similarly to H3K9Sac. 0.2 and 1 μ M WT Sirt6 were incubated with 400 nM H3K9MTU nucleosome-185 (NCP:Sir6=1:0.5 ratio and NCP:Sirt6=1:2.5 ratio) using Sirt6 binding buffer with or without 150 μ M NAD. The solution was then incubated at 37 °C for 2h before being applied to a native 4-20 % TBE gel (Figure S14B), SDS-PAGE, and

WB analysis. SDS-PAGE showed no significant precipitation from the solution (data not shown), while WB analysis showed no significant decrease in signal by anti-H3K9ac antibody (data not shown).

Analysis of Sirt6 deacylation with H3K9MTU nucleosome

To confirm that WT Sirt6 and H3K9MTU nucleosome-185 bind without the removal of MTU, a typical deacetylation activity assay was set up under 10 and 30 nM WT Sirt6 condition, before processing as described above. Although signal is pretty weak with anti-H3K9ac antibody, there is no significant decrease after 2 h (data not shown).

Sirt6 binding H3K9MTU nucleosome-185 complex sample preparation and grid preparation

A 200 μ L large-scale binding assay was set up with WT Sirt6 and H3K9MTU nucleosome-185 in Sirt6 binding buffer (400 nM NCP: 1 μ M Sirt6 = 1:2.5 ratio). After incubation at 37 °C for 2h, the sample was centrifuged for 10 minutes at 21,300g at 4°C and loaded onto a Superose 6 Increase 3.2/300 (Cytiva) column, equilibrated in buffer (50 mM HEPES (pH 7.5) at 25°C, 1 mM TCEP, 100 mM NaCl). Absorbance was measured at 260 nm and 280 nm. Corresponding sample was collected in 50 μ L fractions and analyzed by SDS-PAGE (Figure S16A-C). Fractions containing the complex were crosslinked with 0.1% (v/v) glutaraldehyde for 10 minutes on ice followed by quenching with 2.4 mM aspartate and 2 mM lysine for 10 minutes on ice. Samples were dialyzed for three hours in buffer (50 mM HEPES (pH 7.5), 1 mM TCEP 100 mM NaCl).

Quantifoil R2/1 on 200 Mesh copper grids were glow discharged for 30 s at 15 mA using a Pelco Easiglow plasma discharge system. 4 μ L of dialyzed sample was applied to grids for 8 s, blotted for 5.5 s with a blot force of 8 and vitrified by plunging into liquid ethane using a Vitrobot Mark IV (FEI) at 5 °C and 100 % humidity.

Cryo-EM data collection and image processing

Cryo-EM data were collected on a ThermoFisher Titan Krios at 300 keV equipped with a Gatan K3 direct electron detector and a BioOuantum GIF energy filter. Data collection was automated using SerialEM¹³ software. Two datasets were collected at a pixel size of 0.83 Å. The first data set, collected with 0° tilt and a defocus range of 0.7 to 1.7 µm, yielded 15,192 micrographs. The second data set, collected with 30° tilt and a defocus range of 0.9 to 1.9 µM, yielded 6,922 micrographs. The first dataset was collected with 44 movie frames at an exposure time of 2.802 s with an electron flux of 18.0055 e⁻ Å⁻² s⁻¹ for a total exposure of 50.45 e⁻ Å⁻². The second dataset was collected with 44 movie frames at an exposure time of 2.871 s with an electron flux of 17.8487 e⁻ Å⁻² s⁻¹ for a total exposure of 51.24 e⁻ Å⁻². Initial image processing was conducted in cryoSPARC (v3.2.0)¹⁴. Movies were aligned using cryoSPARC Live Patch Motion Correction followed by CTF estimation. The cryoSPARC Blob picker was used to pick 2,507,720 particles from the first dataset and 1,556,859 particles from the second dataset. The combined 4,064,579 particles were extracted at a box size of 350 pixels. An ab initio reconstruction was performed with select particles. Subsequently, three ab initio classes were placed into a heterogenous refinement job with all particles. After multiple rounds of classification and subsequent removal of junk particles, one class with a clear intact nuclesome was present. This class consisted of 595,268 particles and was further processed with global and local CTF refinements to produce a 2.9 Å reconstruction after non-uniform refinement. This was further classified using heterogenous refinement into 4 classes to enrich for Sirt6. Particles with Sirt6 bound were refined to 3.0 Å after non-uniform refinement with 251,037 particles. The resulting map had high resolution features for histones but lacked high resolution information for Sirt6 (Figure S18). Therefore, a mask encompassing Sirt6 and the extranucleosomal DNA was created in Relion, and masked classification without image alignment was performed. Upon multiple rounds of masked classifications, a resulting class with 95,205 particles was refined to 3.1 Å after non-uniform refinement in cryoSPARC (map A). To enhance local Sirt6 features and the H3 tail density, a new mask was created encompassing Sirt6 and the H3 tail was created in RELION, and masked classification without image alignment was performed. After two rounds of this, a resulting class with 81,315 particles was refined to 3.3 Å after homogenous refinement (map B). The resulting map had subsequent details required for the N-terminus of the H3 tail. Maps were

post-processed with Noise2map (map A) and cryoSPARC (map B) and local resolution was determined using cryoSPARC. Angular distribution plots were generated using the available software in WARP (Table S2).¹⁵

Model building and figure preparation

Initial structures of the nucleosome (PDB 3LZ0)¹⁶, H3 tail (PDB 5Y2F), Sirt6 (PDB 5Y2F)¹⁷, and Sirt6 N-terminal residues 2-16 (AlphaFold2)¹⁸ were rigid body docked into the electron density (map A and B). Residues 17 to 83 of Sirt6 are partially less well-resolved and were rigid body docked according to the available crystal structures (PDB 5Y2F). We observe additional density for the acidic patch binding region of Sirt6 on the opposite site of the nucleosomal disk as well. Additional H3 tail residues were manually built with Coot¹⁹. Extranucleosomal DNA on the Sirt6 binding side was built in ChimeraX²⁰ and further locally adjusted in Coot. DNA on the other side of the nucleosome (opposite of Sirt6 binding side) was only partially visible in the region from ~SHL 4 to SHL 7. However, the DNA is visible upon low pass filtering, therefore the DNA from PDB 3LZ0 was maintained in the final model. The ADP-ribose analog was built in PyMol with restraints obtained from ELBOW in PHENIX²¹ and docked into corresponding density based on NAD (PDB 5Y2F). The resulting structure was locally real-space refined using Coot. Final models were real space refined in PHENIX using map A, secondary restraints from PDB 5Y2F (Sirt6) and 3LZ0 (nucleosome) with global minimization, local rotamer fitting, adp refinement and restraints generated from the ELBOW job (Table S3).

All figures with cryo-EM maps and structural models were prepared using ChimeraX. Graphs were plotted in GraphPad Prism, and final figures were assembled in Adobe Illustrator.

LC-MS analysis of Sirt6 binding/reacting with H3K9MTU nucleosome-185

The purest fractions from the micro gel filtration were combined and repurified by HPLC using a TSKgel DEAE-5PW ion exchange column (TOSOH Bioscience, #83W-00096C). Nucleosomes were separated by the apparent number of bound Sirt6 molecules (2, 1 or 0) using buffers A TES150 (10 mM Tris pH 7.5, 150 mM KCl, 0.5 mM EDTA) and B TES600 (10 mM Tris pH 7.5, 600 mM KCl, 0.5 mM EDTA) with the following gradient: 22% B for 3 minutes, 22-54% B for 1 minute, 54-75% B for 21 minutes, 75-100% B for 1 minute. Fractions containing nucleosome modified with two Sirt6 were immediately diluted with one volume of TCS Buffer (20 mM Tris at pH 7.5 and 1 mM DTT), then concentrated (30 kDa MWCO Amicon Ultra 4 mL, EMD Millipore) at 4 °C. Concentration was assessed using the absorbance at 260 nm, and samples were diluted to a DNA concentration of 10 ng/μL in 6 M guanidine, 1.6 M sodium chloride. This sample was analyzed by RP-HPLC (Vanquish HPLC, Thermo Scientific; MAbPac 2.1 x 100 mm, 4 μm Ph, Thermo Scientific) coupled to ESI-MS (Q Exactive, Thermo Scientific). Using water with 0.1% formic acid and acetonitrile with 0.1% formic acid as mobile phases A and B respectively, sample (3 uL) was separated over a 17 minute 25-40% B gradient following an initial 2 minute wash at 0% B. Mass spectra were deconvoluted using UniDec. (Figure S20)

Sirt6(1-355) M1C [M]⁺: calculated as m/z 39090.82, observed as m/z 39087.1;

H4 [M]⁺: calculated as m/z 11236.15, observed as m/z 11235.4;

H2B [M]⁺: calculated as m/z 13493.68, observed as m/z: 13493.1;

H2A [M]⁺: calculated as m/z 13950.20, observed as m/z 13949.4;

WT-H3: [M]⁺ calculated as m/z 15238.8, observed as m/z 15238.0;

H3K9MTU: [M]⁺ calculated as m/z 15311.7, observed as m/z 15311.2;

H3K9 N ϵ -1,3-oxathiolan-2-ylidene amine intermediate analog [M]⁺: calculated as m/z 15821.97, observed as m/z 15821.4.

Analysis of Sirt6 mutant deacetylation with H3K9ac nucleosome-147

All six Sirt6 mutants were expressed and purified as described above. Densitometry based on Coomassie staining with BSA as standard was used to measure each concentration and to confirm the purity (data not shown). Deacetylation activity assays were set up (as described above) with 100 nM H3K9ac nucleosome-147 and 1000 μ M NAD with each Sirt6 mutant, before processing as described above (Figure S21,22).

EMSA of Sirt6 mutants with H3K9ac nucleosome-185

To assess WT Sirt6 and Sirt6 mutants to nucleosome, EMSA assays with WT Sirt6 and each Sirt6 mutant were performed. The Sirt6 proteins were diluted to a working stock solution of 9.6 μ M, followed by serial dilution to 4800, 2400, 1200, 600, 300, 150, 75, 0 nM in each tube. A final concentration of 20 nM solution of H3K9ac nucleosome-185 in Sirt6 binding buffer without 150 μ M NAD was added and mixed to each tube to reach final Sirt6 concentration as 960, 480, 240, 120, 60, 30, 15, 0 nM. The solution was incubated for 30 min on ice, followed by being applied to a native 4-20 % TBE gel. The whole assay has been conducted for at least 2 times (Figure S23).

Supplemental References

- (1) Marty, M. T.; Baldwin, A. J.; Marklund, E. G.; Hochberg, G. K. A.; Benesch, J. L. P.; Robinson, C. V. Bayesian deconvolution of mass and ion mobility spectra: From binary interactions to polydisperse ensembles. *Anal Chem.* **2015**, *87* (8), 4370–4376.
- (2) Wang, Z. A.; Whedon, S. D.; Wu, M.; *et al.* Histone H2B Deacylation Selectivity: Exploring Chromatin's Dark Matter with an Engineered Sortase. *J Am Chem Soc.* **2022**, *144* (8), 3360–3364.
- (3) Luger, K.; Rechsteiner, T. J.; Richmond, T. J. Preparation of Nucleosome Core Particle from Recombinant Histones. *Methods Enzymol.* **1999**, *304* (1997), 3–19.
- (4) Gatchalian, J.; Wang, X.; Ikebe, J.; *et al.* Accessibility of the histone H3 tail in the nucleosome for binding of paired readers. *Nat Commun.* **2017**, δ (1), .
- (5) Wang, Z. A.; Millard, C. J.; Lin, C.-L.; *et al.* Diverse nucleosome site-selectivity among histone deacetylase complexes. *eLife*. **2020**, *9*, e57663.
- (6) Wu, M.; Hayward, D.; Kalin, J. H.; Song, Y.; Schwabe, J. W.; Cole, P. A. Lysine-14 acetylation of histone H3 in chromatin confers resistance to the deacetylase and demethylase activities of an epigenetic silencing complex. *eLife*. **2018**, *7*, e37231.
- (7) Dyer, P. N.; Raji, E. S.; White, C. L.; *et al.* Reconstitution of Nucleosome Core Particles from Recombinant Histones and DNA. *Methods Enzymol.* **2004**, *375*, 23–44.
- (8) Watson, P. J.; Millard, C. J.; Riley, A. M.; *et al.* Insights into the activation mechanism of class i HDAC complexes by inositol phosphates. *Nat Commun.* **2016**, *7* (11262), 1–13.
- (9) Madeira, P. P.; Rocha, I. L. D.; Rosa, M. E.; Freire, M. G.; Coutinho, J. A. P. On the aggregation of bovine serum albumin. *J Mol Liq.* **2022**, *349*, 118183.
- (10) Holm, N. K.; Jespersen, S. K.; Thomassen, L. V.; *et al.* Aggregation and fibrillation of bovine serum albumin. *Biochim Biophys Acta Proteins Proteomics.* **2007**, *1774* (9), 1128–1138.
- (11) Madsen, A. S.; Andersen, C.; Daoud, M.; *et al.* Investigating the Sensitivity of NAD+-dependent Sirtuin Deacylation Activities to NADH. *J Biol Chem.* **2016**, *291* (13), 7128–7141.
- (12) Feldman, J. L.; Dittenhafer-Reed, K. E.; Kudo, N.; *et al.* Kinetic and structural basis for Acylgroup selectivity and NAD+ dependence in sirtuin-catalyzed deacylation. *Biochemistry.* **2015**, *54* (19), 3037–3050.
- (13) Mastronarde, D. N. Automated electron microscope tomography using robust prediction of specimen movements. *J Struct Biol.* **2005**, *152* (1), 36–51.
- (14) Punjani, A.; Rubinstein, J. L.; Fleet, D. J.; Brubaker, M. A. CryoSPARC: Algorithms for rapid unsupervised cryo-EM structure determination. *Nat Methods.* **2017**, *14* (3), 290–296.
- (15) Tegunov, D.; Cramer, P. Real-time cryo-electron microscopy data preprocessing with Warp. *Nat Methods.* **2019**, *16* (11), 1146–1152.

- (16) Vasudevan, D.; Chua, E. Y. D.; Davey, C. A. Crystal Structures of Nucleosome Core Particles Containing the "601" Strong Positioning Sequence. *J Mol Biol.* **2010**, *403* (1), 1–10.
- (17) Huang, Z.; Zhao, J.; Deng, W.; *et al.* Identification of a cellularly active SIRT6 allosteric activator. *Nat Chem Biol.* **2018**, *14* (12), 1118–1126.
- (18) Jumper, J.; Evans, R.; Pritzel, A.; *et al.* Highly accurate protein structure prediction with AlphaFold. *Nature*. **2021**, *596* (7873), 583–589.
- (19) Emsley, P.; Cowtan, K. Coot: Model-building tools for molecular graphics. *Acta Crystallogr Sect D Biol Crystallogr.* **2004**, *60* (12 I), 2126–2132.
- (20) Pettersen, E. F.; Goddard, T. D.; Huang, C. C.; *et al.* UCSF ChimeraX: Structure visualization for researchers, educators, and developers. *Protein Sci.* **2021**, *30* (1), 70–82.
- (21) Adams, P. D.; Grosse-Kunstleve, R. W.; Hung, L. W.; *et al.* PHENIX: Building new software for automated crystallographic structure determination. *Acta Crystallogr Sect D Biol Crystallogr.* **2002**, *58* (11), 1948–1954.

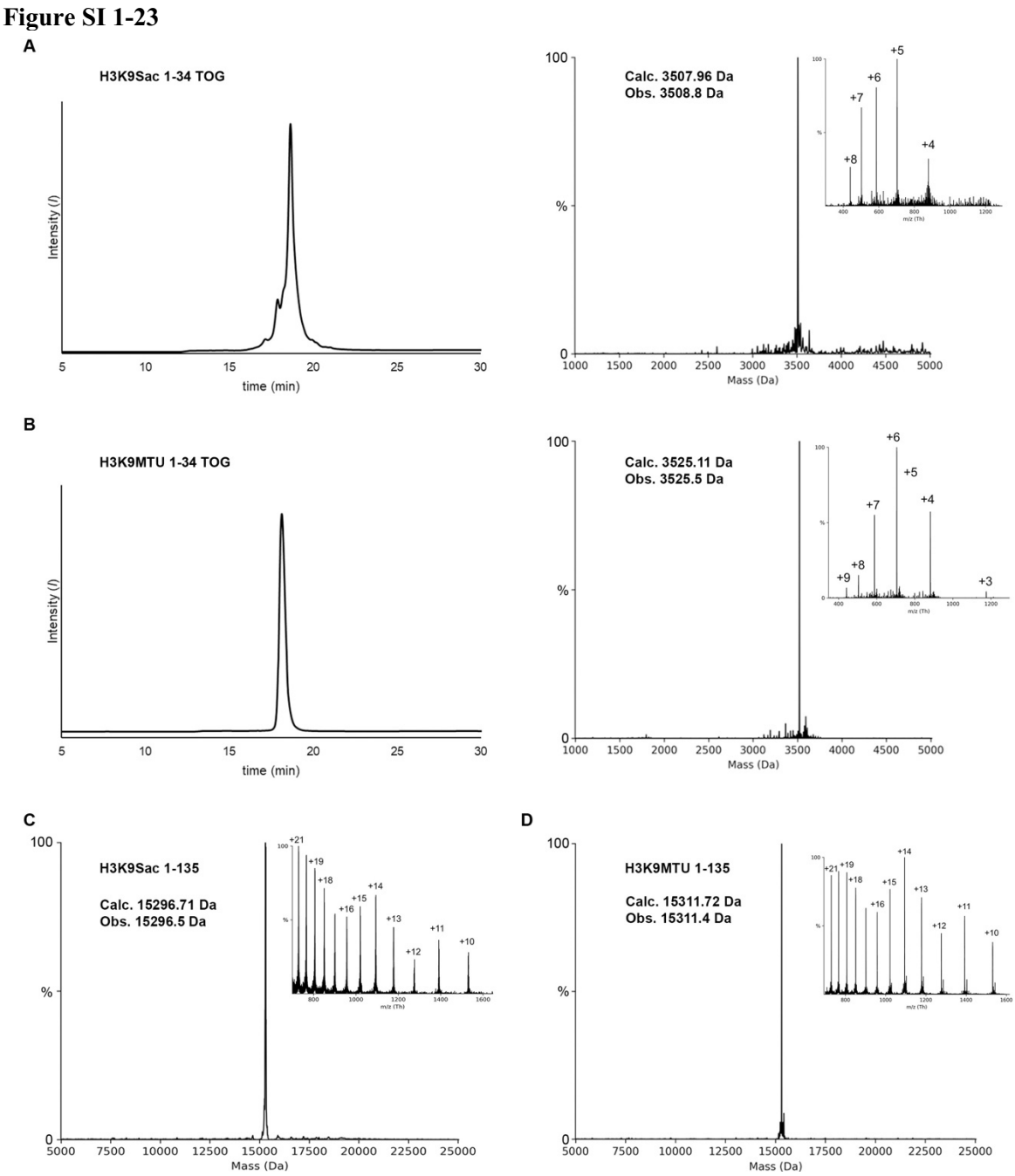


Figure S1. H3 peptides and semisynthetic H3 protein characterization. (A) Analytical RP-HPLC chromatogram (C18, 7-30% B, 30 min), intact peptide ESI-MS (inset), and deconvoluted peptide ESI-MS for H3K9Sac 1-34 TOG (Calculated exact mass for C₁₄₆H₂₆₂N₅₄O₄₄S [M]⁺: 3507.96 Da; Observed: 3508.8 Da). (B) Analytical RP-HPLC chromatogram (C18, 7-30% B, 30 min), intact peptide ESI-MS (inset), and deconvoluted peptide ESI-MS for H3K9MTU 1-34 TOG (Calculated exact mass for C₁₄₆H₂₆₃N₅₅O₄₄S [M]⁺: 3525.11 Da; Observed: 3525.5 Da). (C) Intact protein ESI-MS (inset) and deconvoluted protein ESI-MS for H3K9Sac 1-135 protein (Calculated average mass for C₆₇₂H₁₁₃₃N₂₁₅O₁₈₆S₃ [M]⁺: 15296.71 Da; Observed: 15296.5 Da). (D) Intact protein ESI-MS (inset) and deconvoluted protein ESI-MS for H3K9MTU 1-135 protein (Calculated average mass for C₆₇₂H₁₁₃₄N₂₁₆O₁₈₆S₃ [M]⁺: 15311.72 Da; Observed: 15311.4 Da).

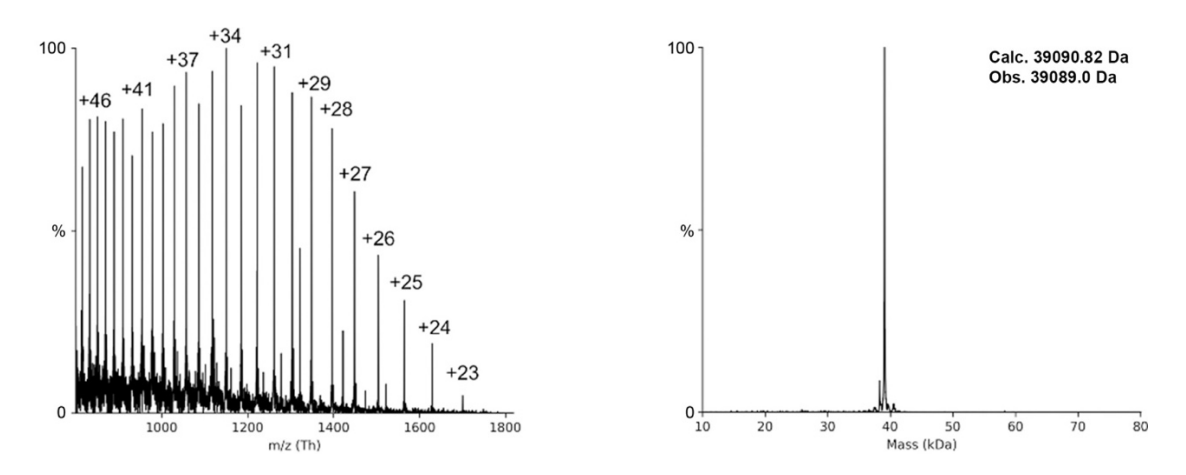


Figure S2. ESI for WT Sirt6. Intact protein ESI-MS and deconvoluted protein ESI-MS for WT Sirt6. Calculated average mass for $C_{1718}H_{2770}N_{514}O_{503}S_{13}$ [M]+: 39090.82 Da; Observed: 39089.0 Da.

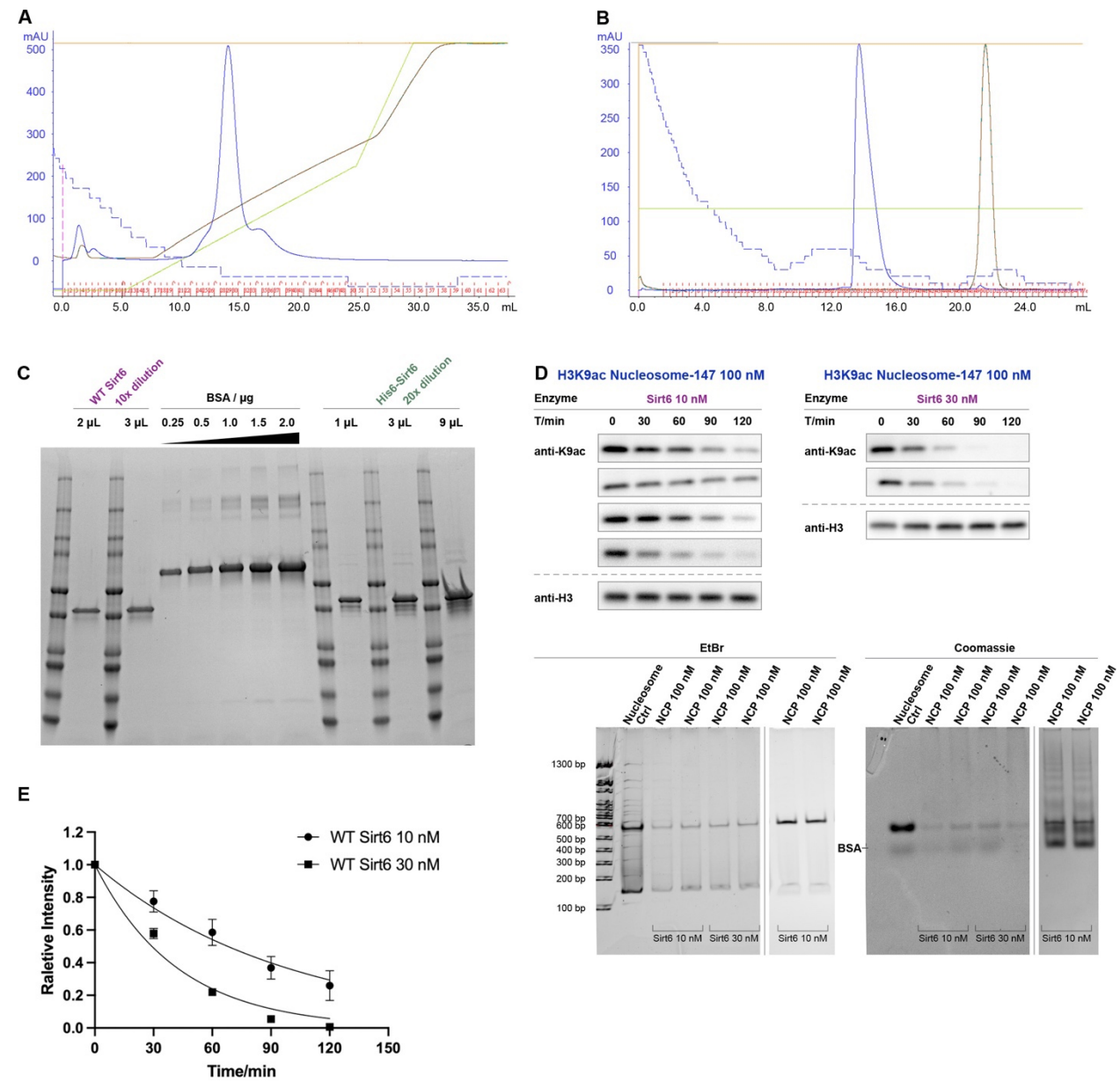


Figure S3. WT Sirt6 purification and activity measurement. (A) Heparin column FPLC chromatography for WT Sirt6 purification. (B) Superdex200 column FPLC chromatography for WT Sirt6 purification. (C) SDS-PAGE and Coomassie staining of final WT Sirt6 before and after TEV cleavage. (D) Western blot of WT Sirt6 (10 nM, 30 nM) deacetylation assay on H3K9ac nucleosome. (E) Curve fitting for nucleosome kinetics with 10, 30 nM WT Sirt6.

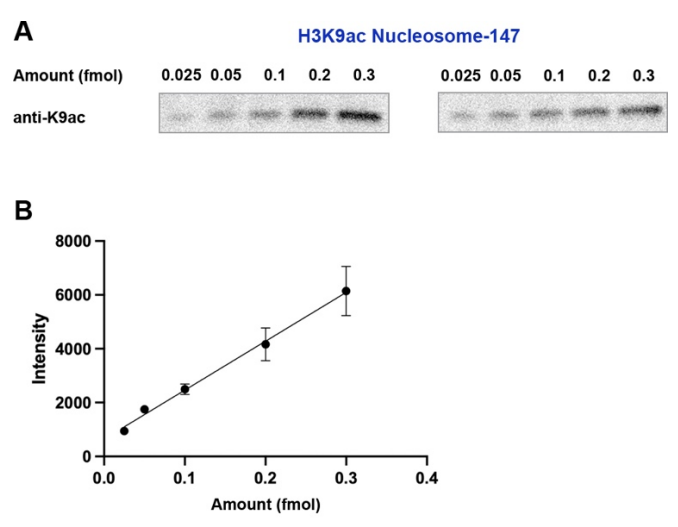


Figure S4. Anti-H3K9ac antibody linearity test. A series of 0.025, 0.05, 0.1, 0.2, and 0.3 fmol of H3K9ac nucleosome-147 were resolved by SDS-PAGE, transferred, blocked and blotted with primary anti-H3K9ac antibody, followed by HRP secondary antibody, and ECL to get band intensity. The intensity was then plotted with H3K9ac nucleosome-147 amount to determine the linear detection range.

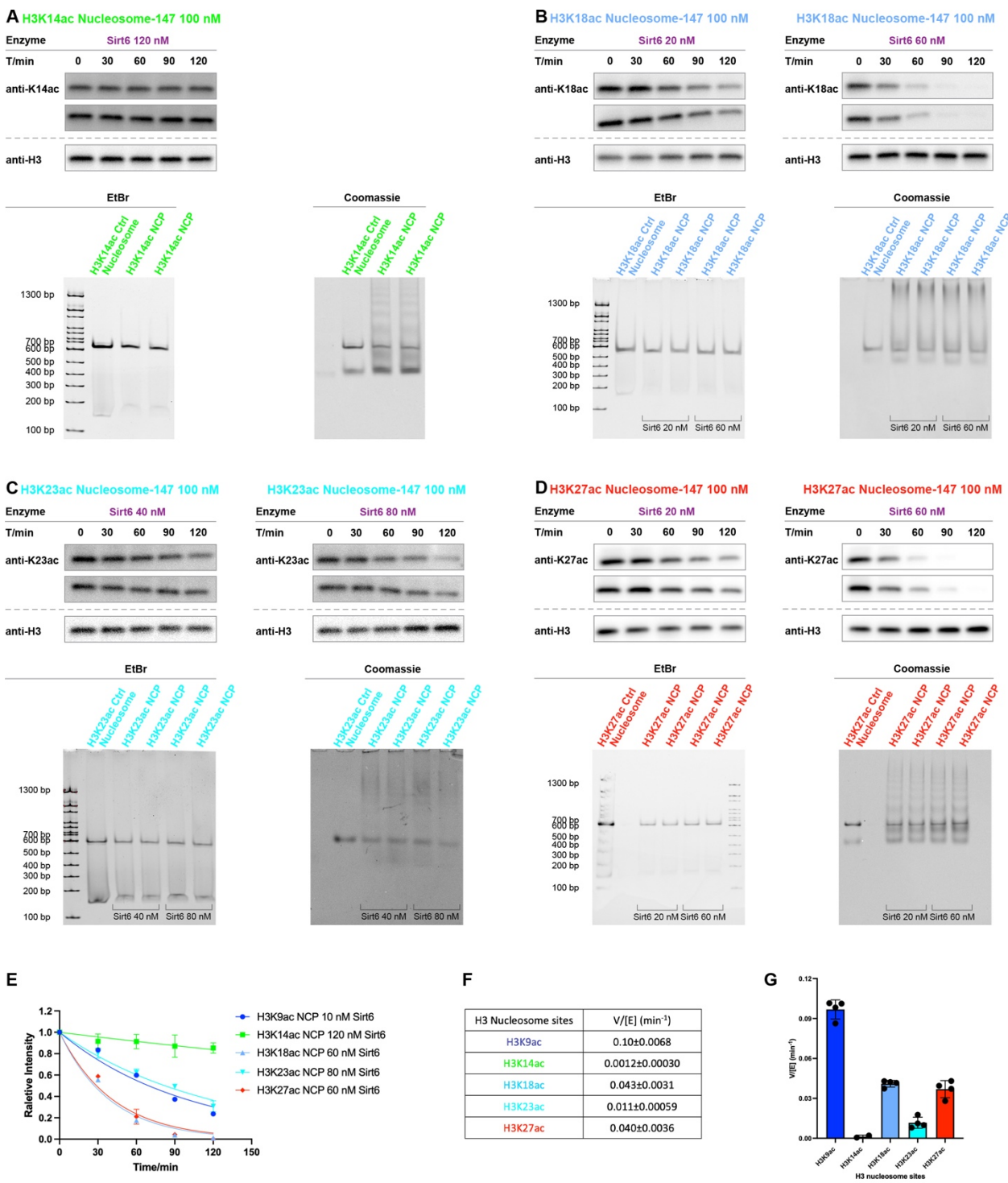


Figure S5. WT Sirt6 deacetylation on different H3 nucleosome sites. Western blot of WT Sirt6 (1 or 2 different concentrations) deacetylation assay on (A) H3K14ac, (B) H3K18ac, (C) H3K23ac, (D) H3K27ac; (E) Curve fitting for H3 nucleosome kinetics with different concentration of WT Sirt6. (F) Table for H3 nucleosome kinetics. (G) Bar graph for H3 nucleosome kinetics.

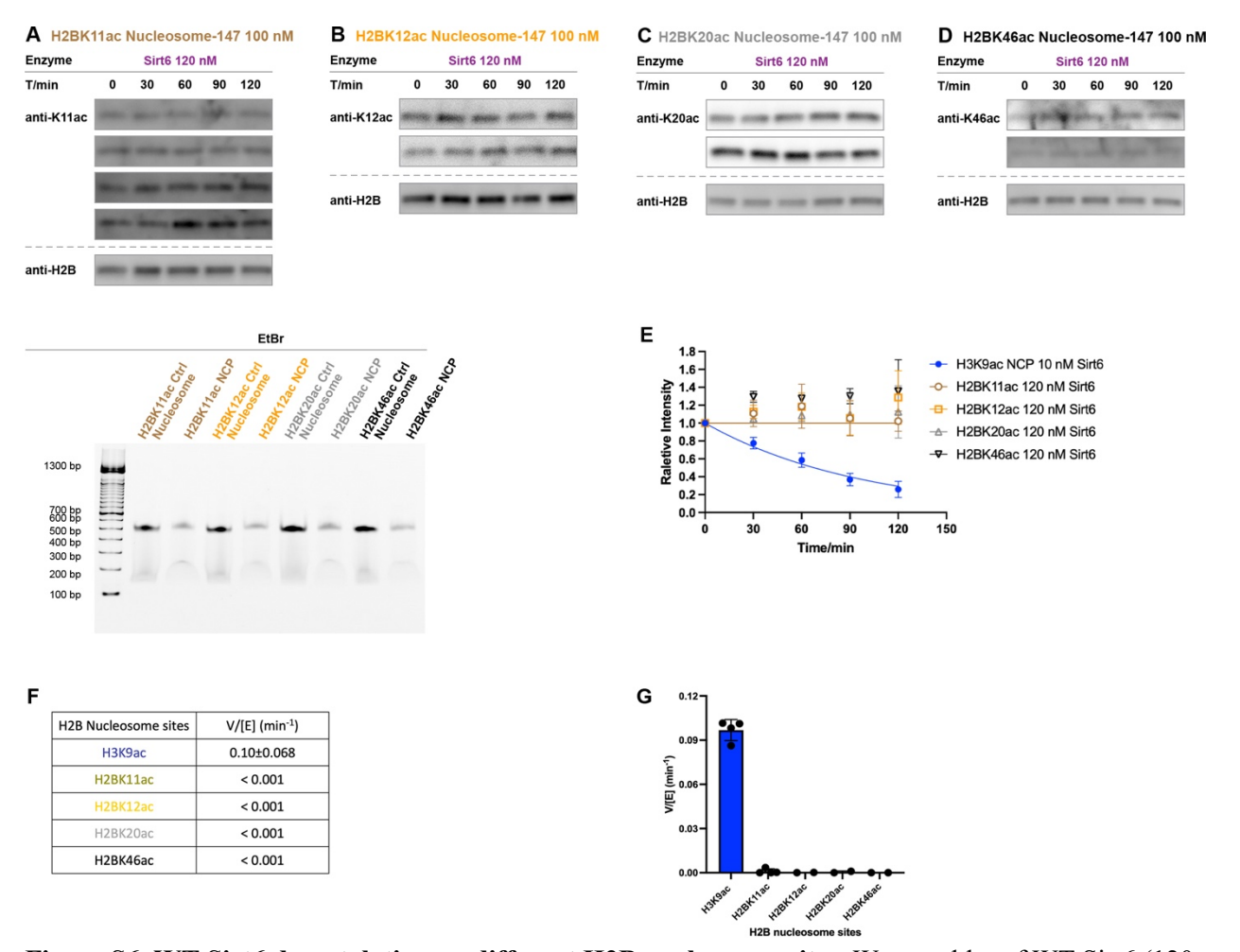


Figure S6. WT Sirt6 deacetylation on different H2B nucleosome sites. Western blot of WT Sirt6 (120 nM) deacetylation assay on (A) H2BK11ac, (B) H2BK12ac, (C) H2BK20ac, (D) H2BK46ac; (E) Curve fitting for H2B nucleosome kinetics with different concentration of WT Sirt6. (F) Table for H2B nucleosome kinetics. (G) Bar graph for H2B nucleosome kinetics.

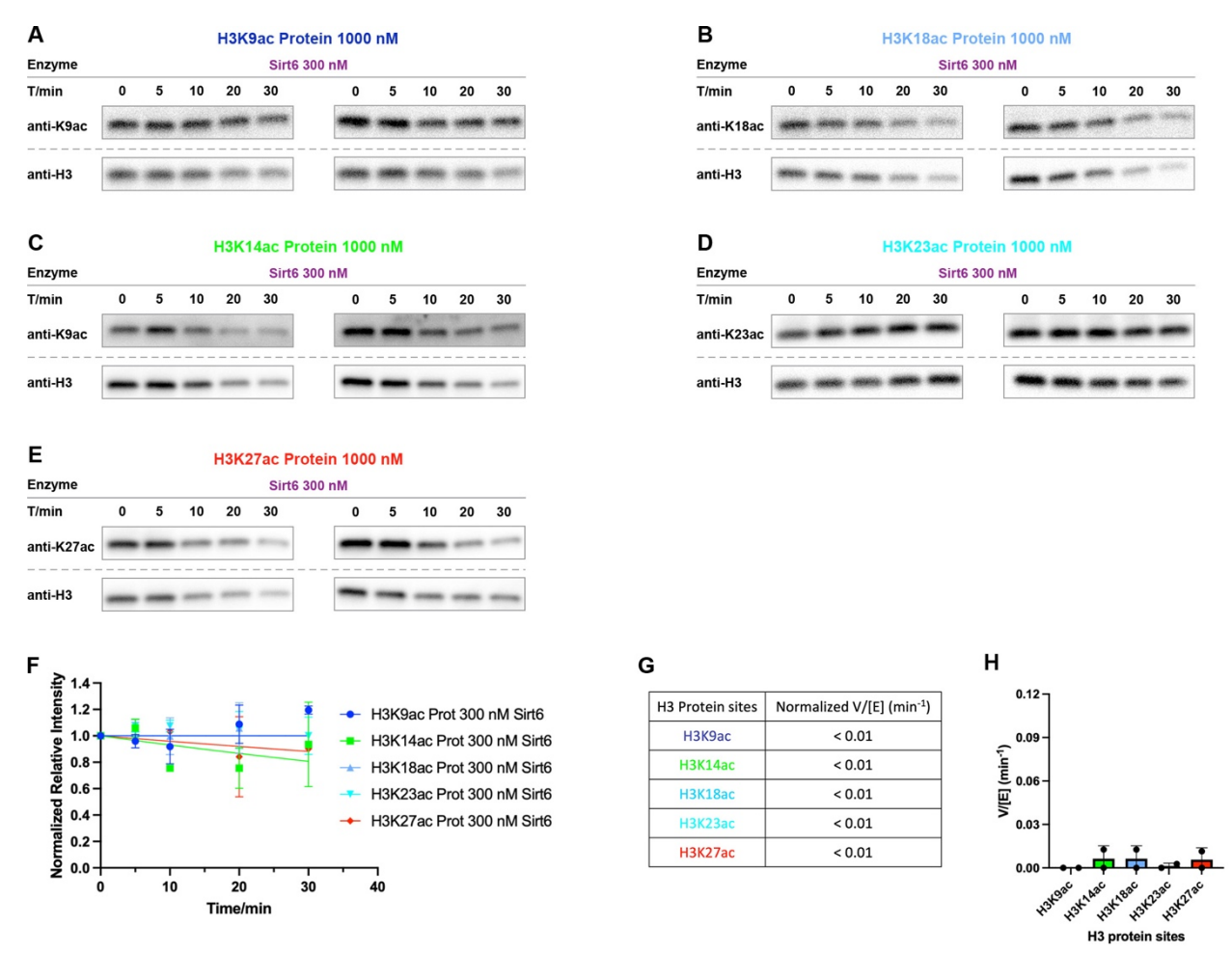


Figure S7. WT Sirt6 deacetylation on different free H3 protein sites. Western blot of WT Sirt6 (300 nM) deacetylation assay on (A) H3K9ac, (B) H3K14ac, (C) H3K18ac, (D) H3K23ac, (E) H3K27ac. (F) Curve fitting for free H3 protein kinetics with different concentration of WT Sirt6. To account for the decrease of anti-H3 signal, we normalized the PTM signal relative to the corresponding total histone signal at each time point. (G) Table for free H3 protein kinetic parameters. (H) Bar graph for free H3 protein kinetic parameters.

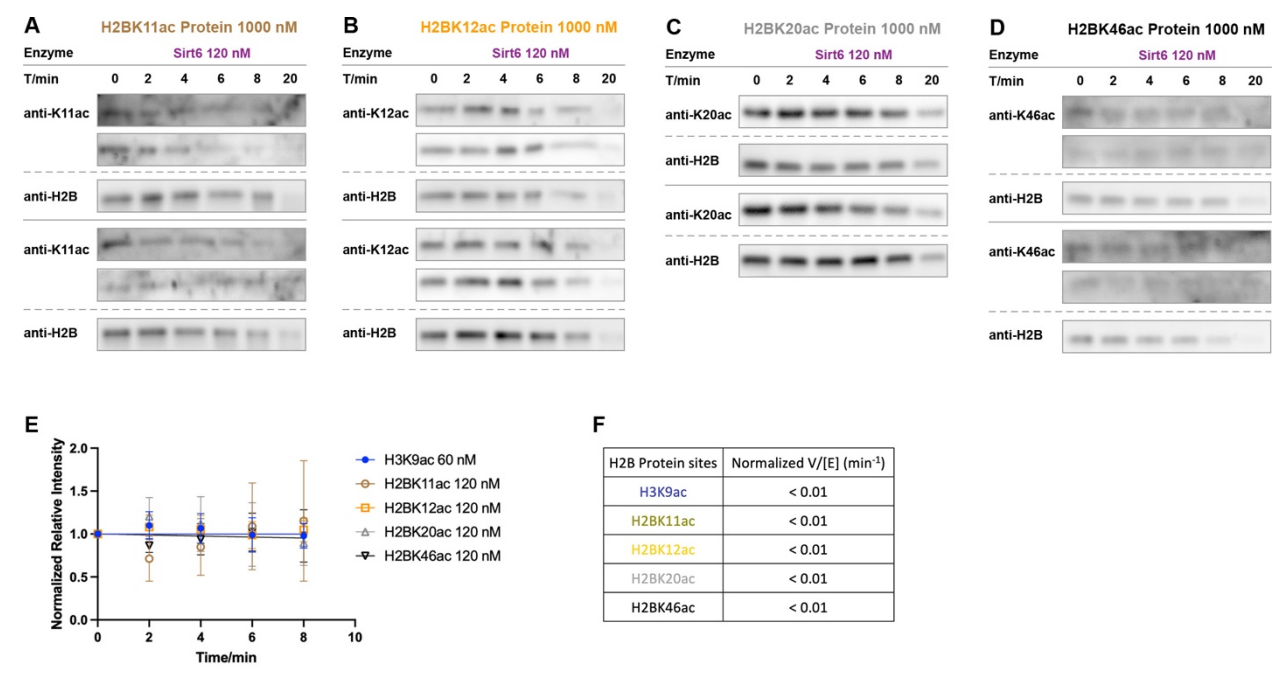


Figure S8. WT Sirt6 deacetylation on different free H2B protein sites. Western blot of WT Sirt6 (300 nM) deacetylation assay on (A) H2BK11ac, (B) H2BK12ac, (C) H2BK20ac, (D) H2BK46ac; (E) Curve fitting for free H2B histone kinetics with different concentration of WT Sirt6. To account for the decrease of anti-H2B signal, we normalized the PTM signal relative to the corresponding total histone signal at each time point. (F) Table for free H2B protein kinetic parameters.

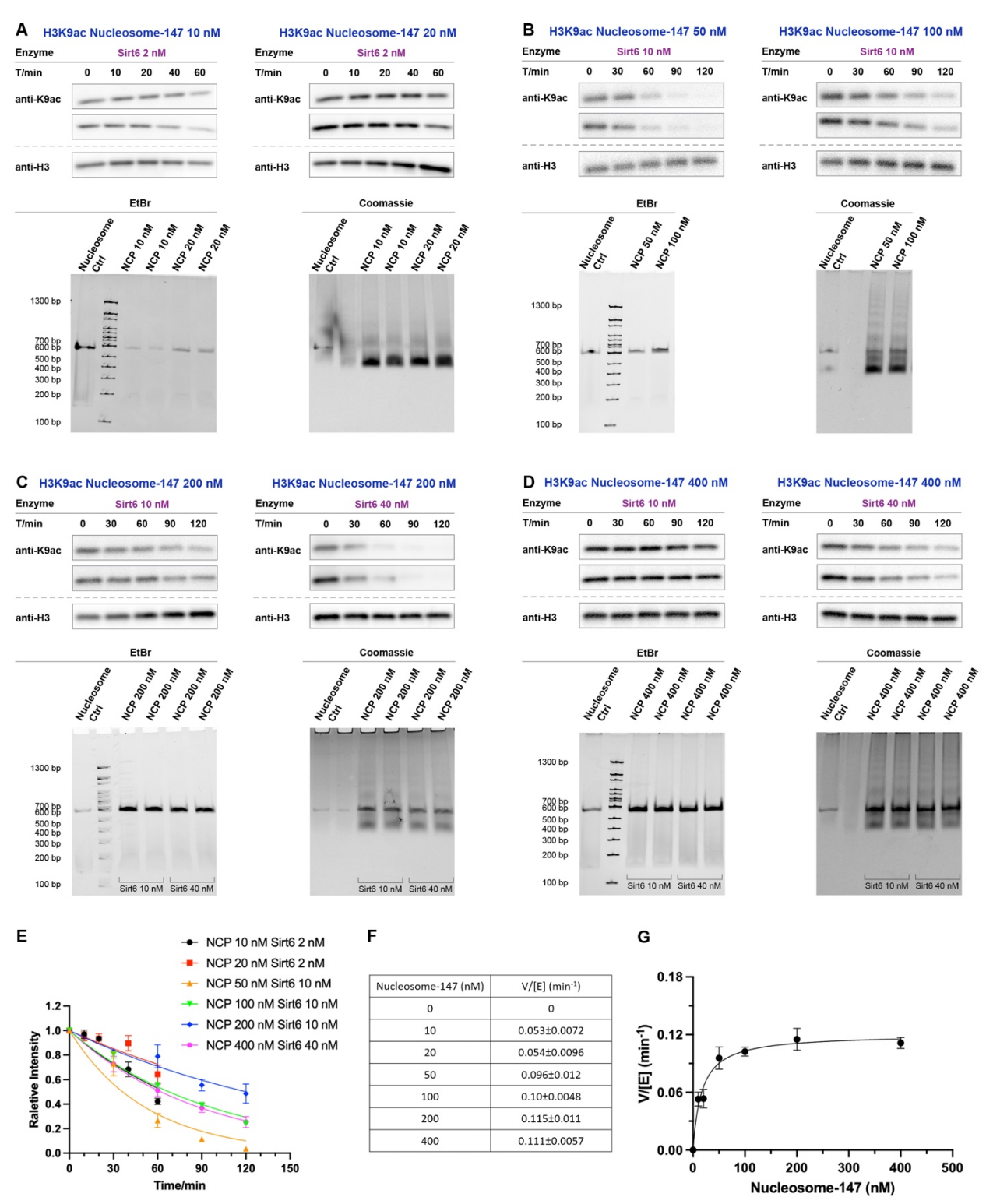


Figure S9. Km of WT Sirt6 for H3K9ac nucleosome-147. Western blot of WT Sirt6 (1 or 2 different concentrations) deacetylation assay on H3K9ac nucleosome-147 with nucleosome final concentration as (A) 10 & 20 nM, (B) 50 & 100 nM, (C) 200 nM, (D) 400 nM. (E) Curve fitting for H3K9ac nucleosome kinetics with different nucleosome final concentration. (F) Table for H3K9ac nucleosome kinetics with different nucleosome final concentration. (F) Michaelis–Menten curve fitting for V/[E] at different nucleosome concentrations.

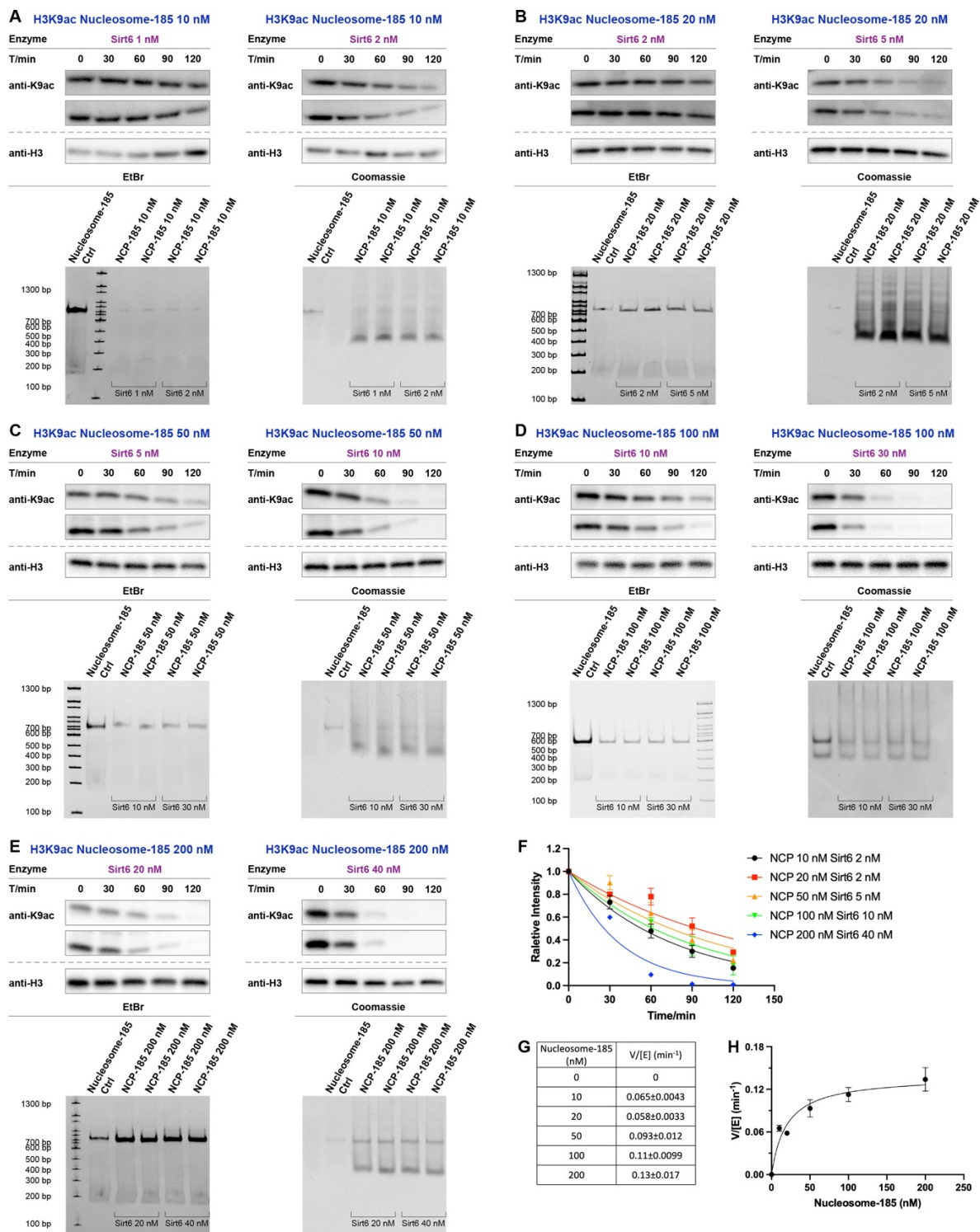


Figure S10. Km of WT Sirt6 for H3K9ac nucleosome-185. Western blot of WT Sirt6 (1 or 2 different concentrations) deacetylation assay on H3K9ac nucleosome-185 with nucleosome final concentration as (A) 10 nM, (B) 20 nM, (C) 50 nM, (D) 100 nM. (E) 200 nM. (F) Curve fitting for H3K9ac nucleosome kinetics with different nucleosome final concentration. (G) Table for H3K9ac nucleosome kinetics with different nucleosome final concentration. (H) Michaelis–Menten curve fitting for V/[E] at different nucleosome concentrations.

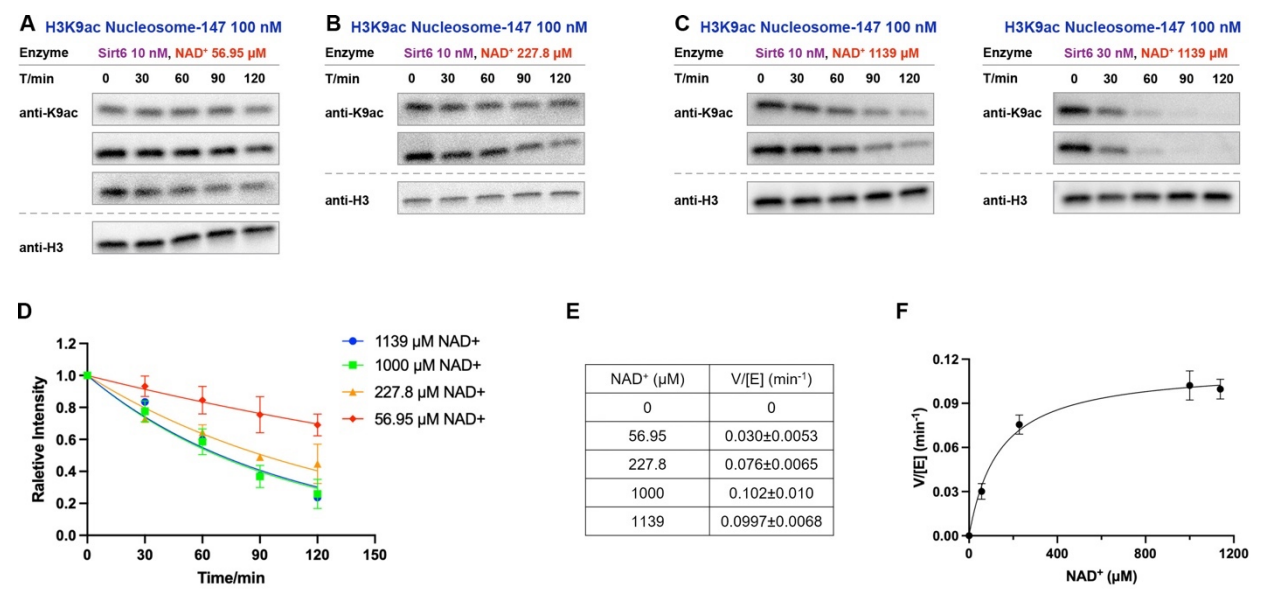


Figure S11. Km of WT Sirt6 for NAD. Western blot of WT Sirt6 (10 nM and 30 nM) deacetylation assay on H3K9ac nucleosome-147 with (A) 56.95, (B) 227.8, (C) 1139 μ M NAD. (D) Curve fitting for H3K9ac nucleosome kinetics with different concentration of NAD. (E) Table for H3K9ac nucleosome kinetic parameters with different concentration of NAD. (F) Michaelis–Menten curve fitting for V/[E] with different concentration of NAD.

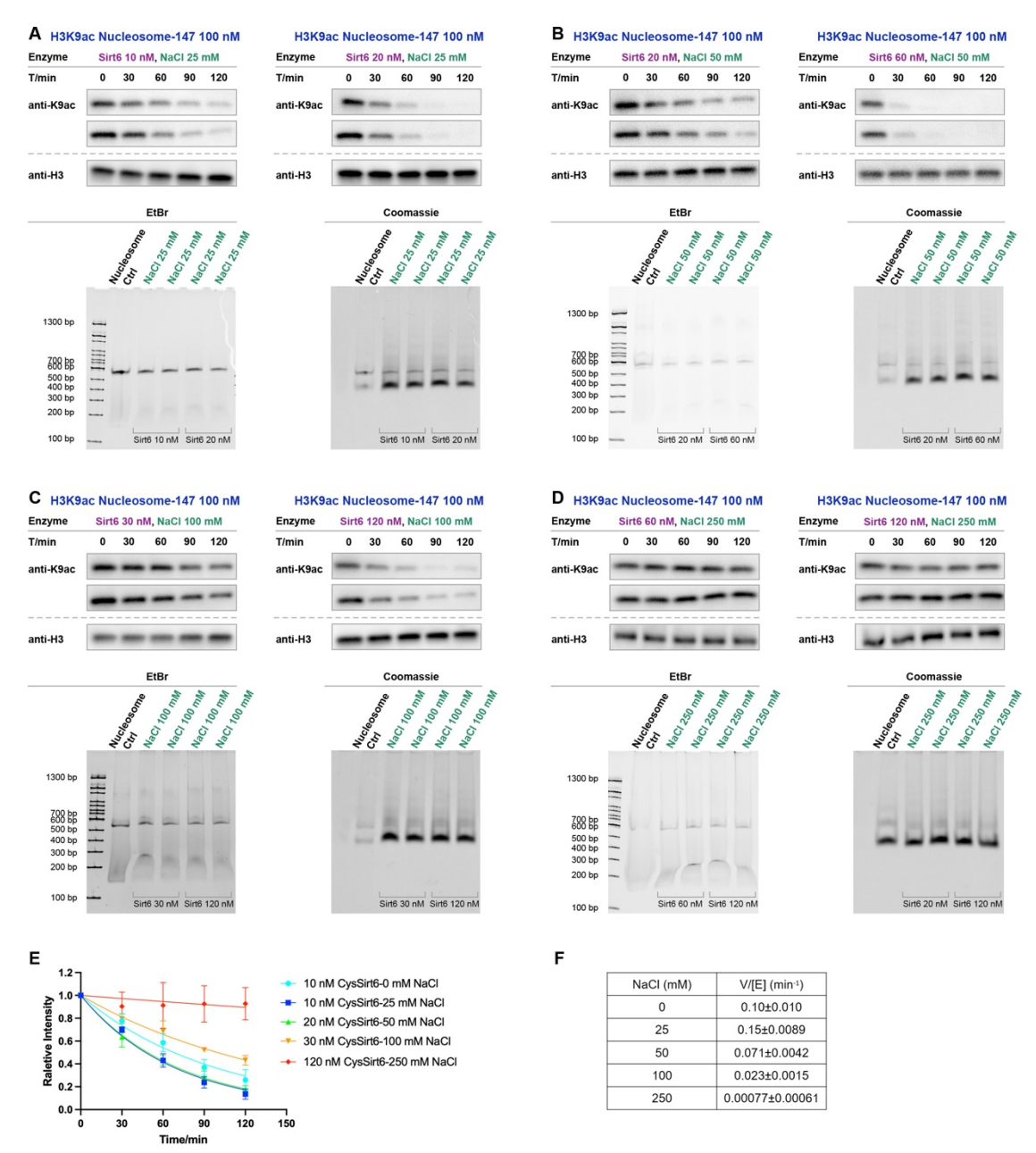


Figure S12. Effect of NaCl on WT Sirt6 activity toward H3K9ac nucleosome-147. Western blot of WT Sirt6 (1 or 2 different concentrations) deacetylation assay on H3K9ac nucleosome-147 with different buffer NaCl concentration as (A) 25 nM, (B) 50 nM, (C) 100 nM, (D) 250 nM. (E) Curve fitting for H3K9ac nucleosome kinetics with different buffer NaCl concentration. (F) Table for H3K9ac nucleosome kinetics with different buffer NaCl concentration.

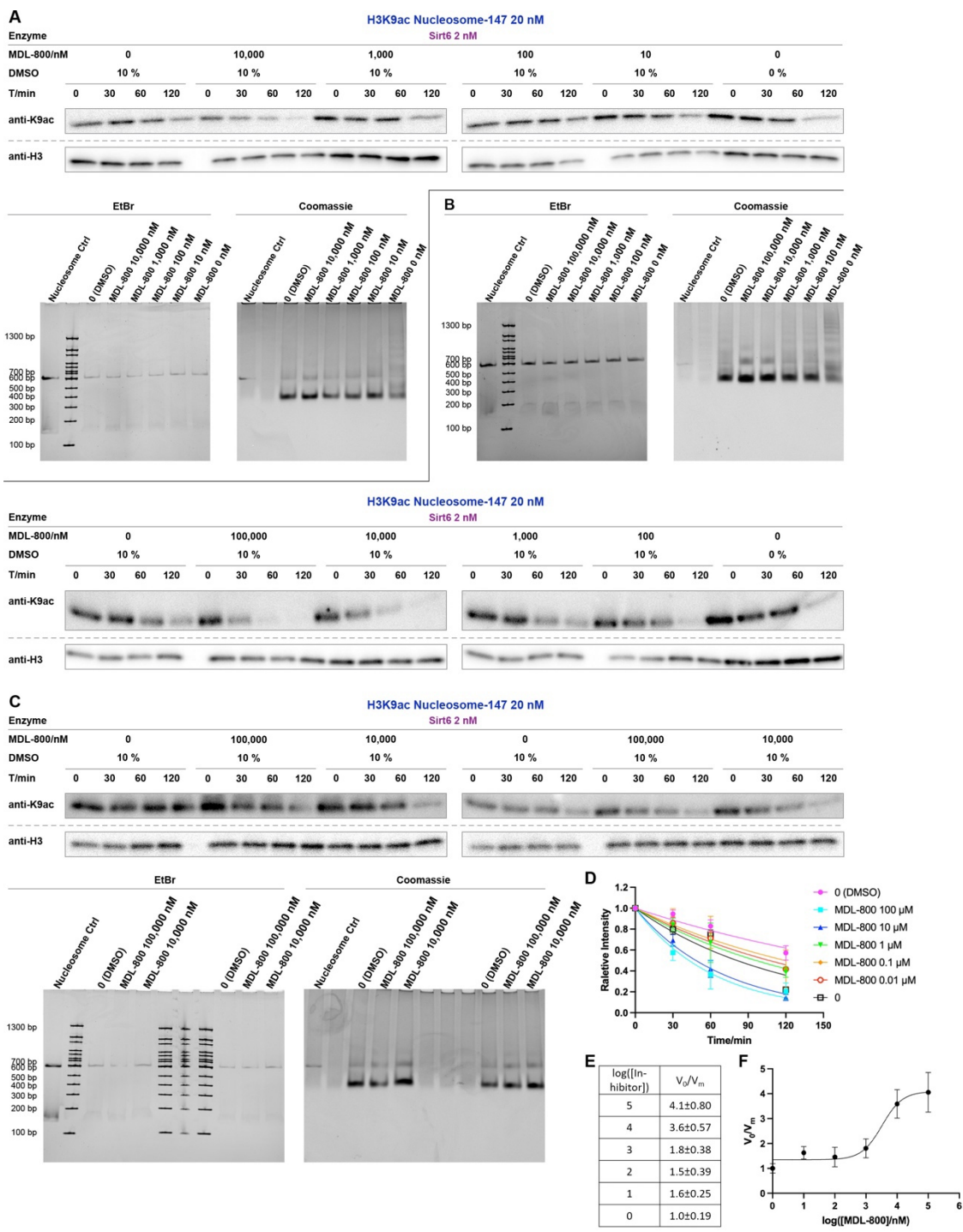


Figure S13. MDL-800 activation assay on H3K9ac nucleosome-147. Western blot of 2 nM WT Sirt6 deacetylation assay on 20 nM H3K9ac nucleosome-147 with (A-C) different concentration of MDL-800 in 10 % DMSO, DMSO vehicle alone, or no DMSO. (D) Curve fitting for H3K9ac nucleosome kinetics with different MDL-800 concentration. (E) Table of H3K9ac nucleosome kinetic parameters at different MDL-800 concentrations. (F) Curve fitting of "log(activator) vs. response -- Variable slope (four parameters)" with logEC50(nM) = 3.5 ± 0.25 (EC50 = $\sim3.3\pm2.0$ μ M), Hill slope = 1.3.

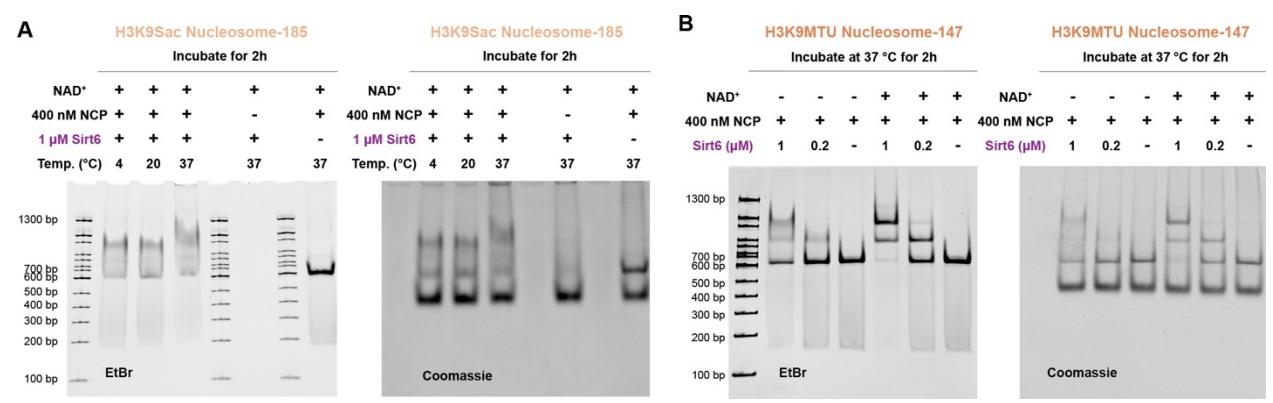


Figure S14. EMSA for H3K9Sac and H3K9MTU nucleosome-185. (A) EMSA of WT Sirt6 binding with H3K9Sac nucleosome-185 at different temperatures. (B) EMSA of WT Sirt6 binding with H3K9MTU nucleosome-185 with or without NAD.

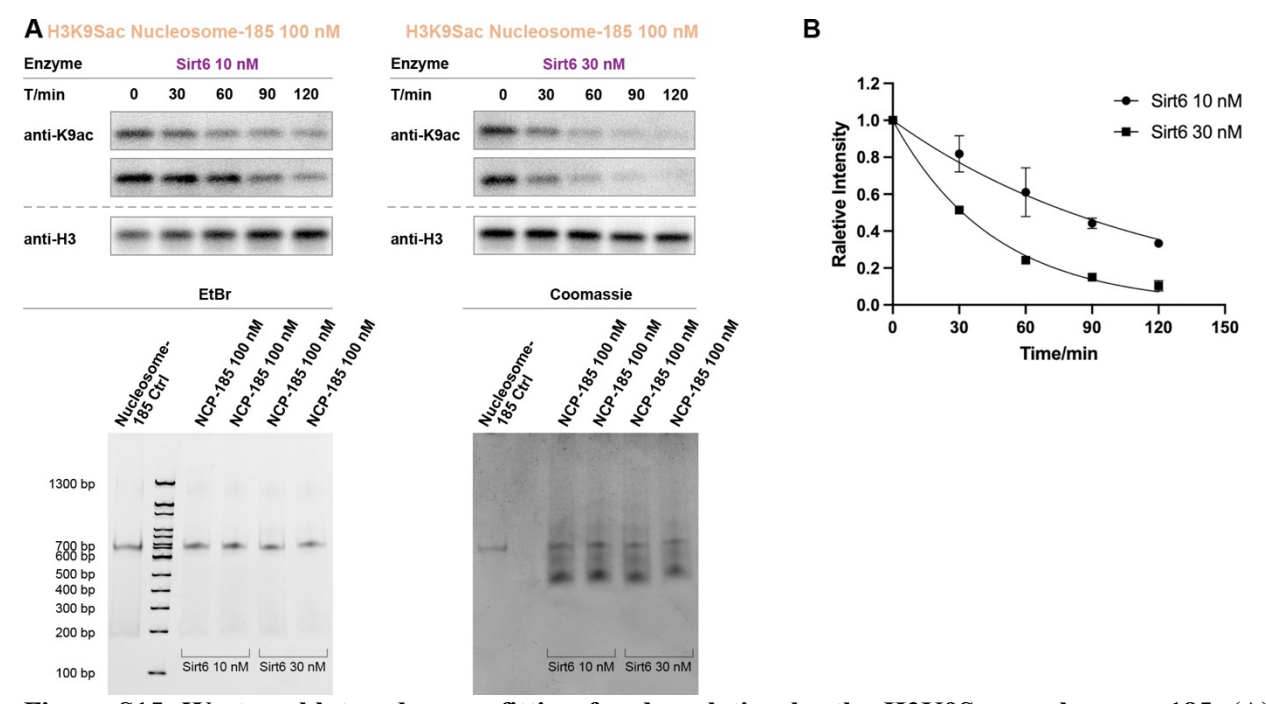


Figure S15. Western blot and curve fitting for deacylation by the H3K9Sac nucleosome-185. (A) Western blot of WT Sirt6 (10 or 30 nM) deacetylation assay on H3K9Sac nucleosome-185. (B) Curve fitting for H3K9Sac nucleosome kinetics at different concentrations of WT Sirt6.

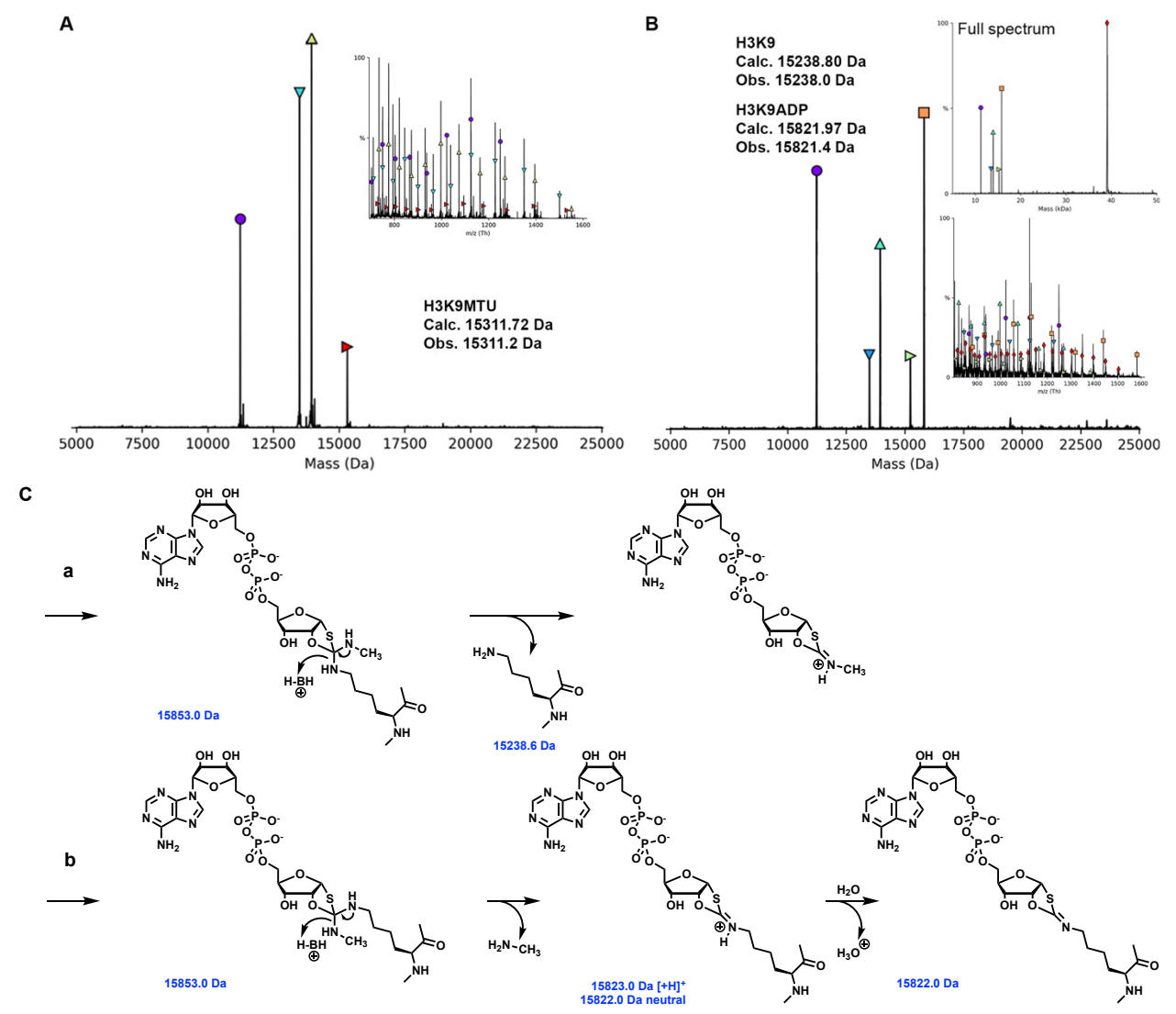


Figure S16. ESI and mechanism of WT Sirt6 binding with H3K9MTU nucleosome-185. (A) Intact ESI-MS (inset) and deconvoluted mass spectrum of H3K9MTU nucleosome-185 before binding to WT Sirt6; H4 (purple circle), H2B (downward-pointed cyan triangle), H2A (upward-pointed yellow-green triangle) and H3K9MTU (rightward-pointed red triangle). (B) Intact ESI-MS (lower inset) and deconvoluted mass spectrum of H3K9MTU nucleosome-185 after binding to WT Sirt6 (upper inset); H4 (purple circle), H2B (downward-pointed blue triangle), H2A (upward-pointed cyan triangle), unmodified H3 (rightward-pointed yellow-green triangle), H3K9 Nε-1,3-oxathiolan-2-ylidene amine intermediate (orange square), and Sirt6 (red diamond). (C) Scheme for catalytic activity of WT Sirt6 on H3K9MTU nucleosome-185 with intermediate analog and product masses listed in blue. Pathway a to remove the thiourea group to generate unmodified H3; Pathway b to generate the intermediate analog.

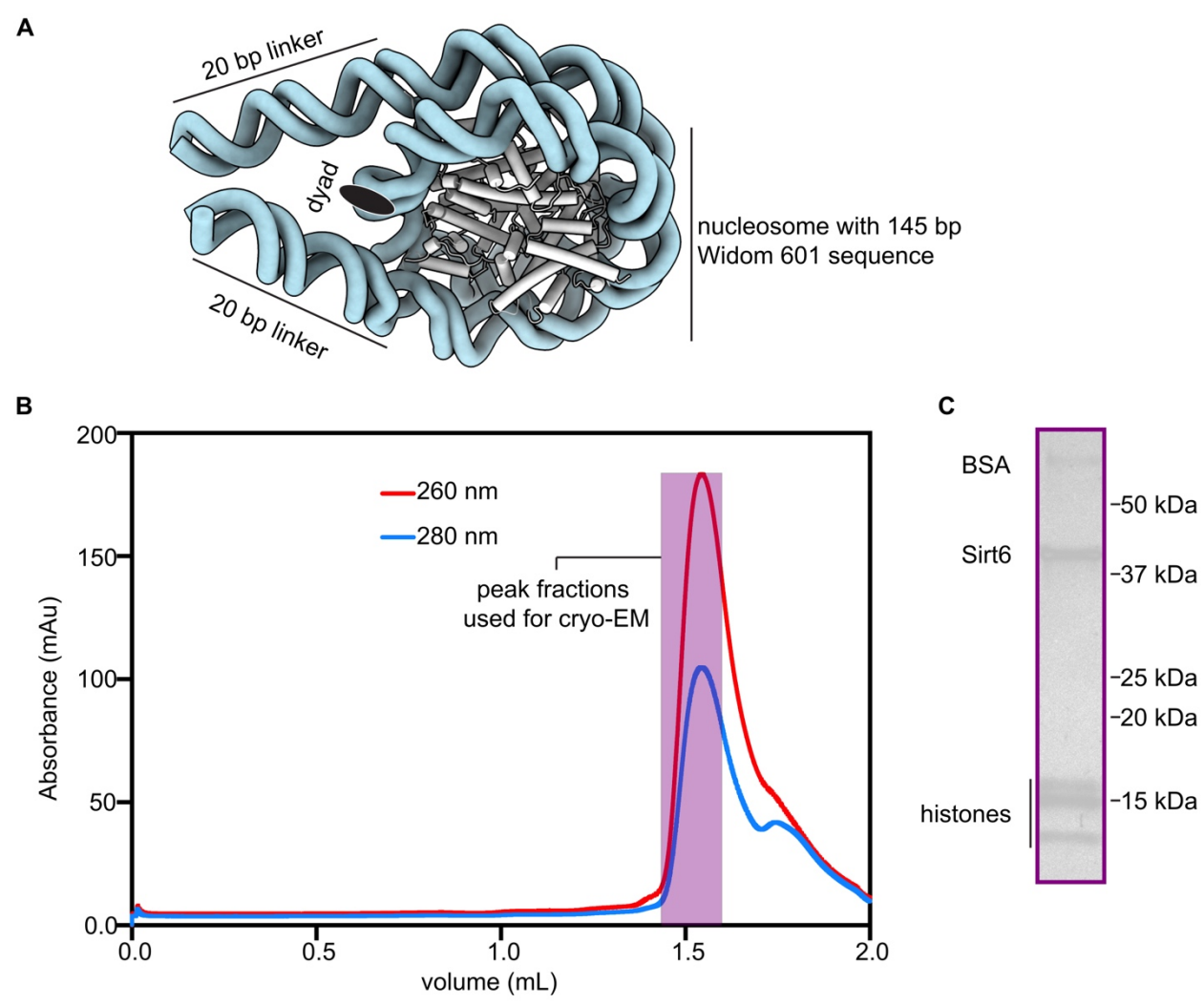


Figure S17. Formation of H3K9MTU nucleosome-Sirt6 complex. (A) Nucleosome structure (B) Chromatogram of nucleosome-Sirt6 complex formation. (C) SDS-PAGE gel of nucleosome-Sirt6 complex.

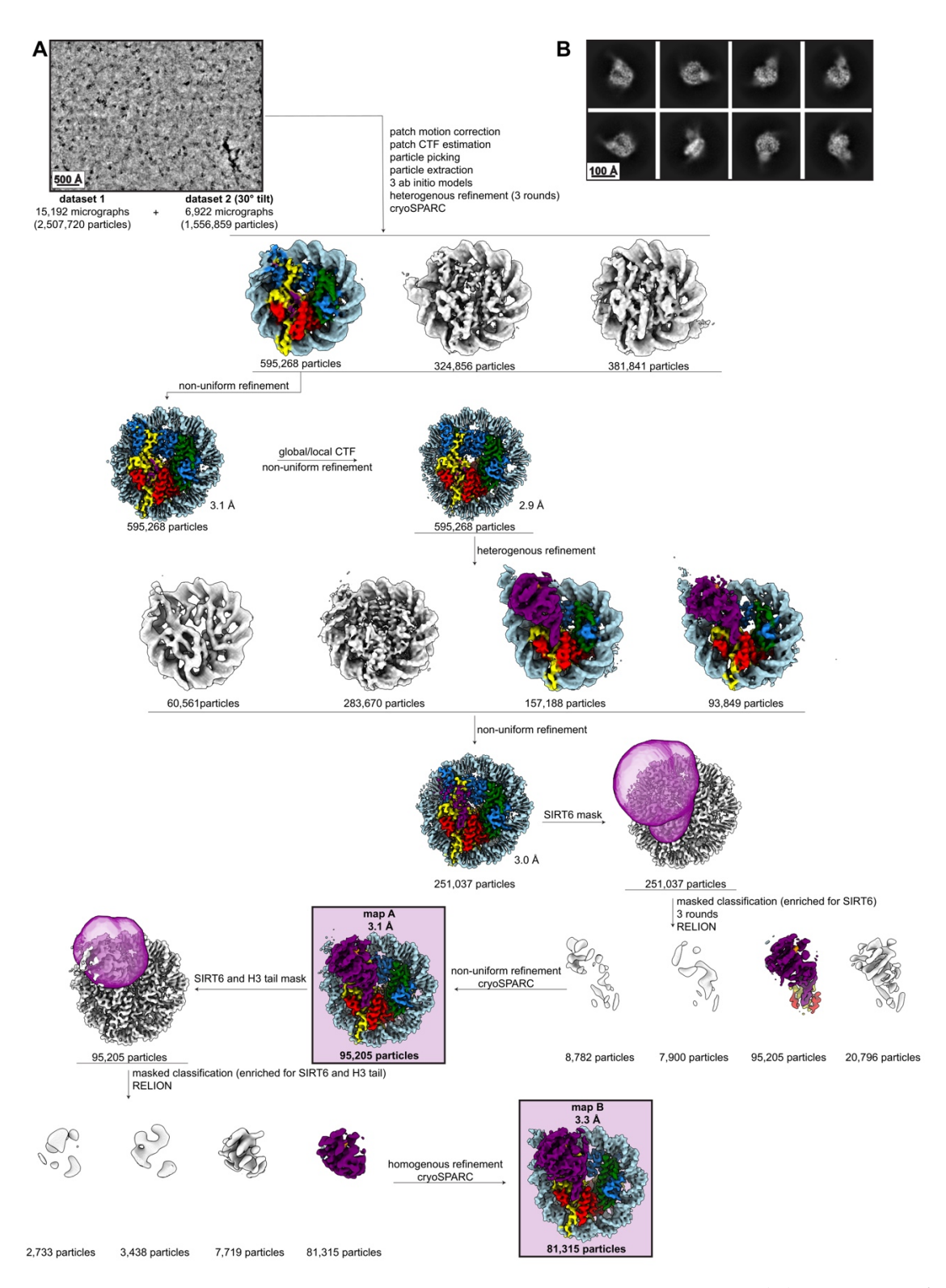


Figure S18. Data acquisition and processing of the nucleosome-Sirt6 complex. (A) Representative low-pass filtered micrograph of data collection with scale bar (500 Å) and sorting and classification tree of nucleosome-Sirt6 complex dataset. Final maps (map A and B) are indicated. (B) 2D classes of final refinement show Sirt6, and nucleosome-like shape with scale bar of 100 Å.

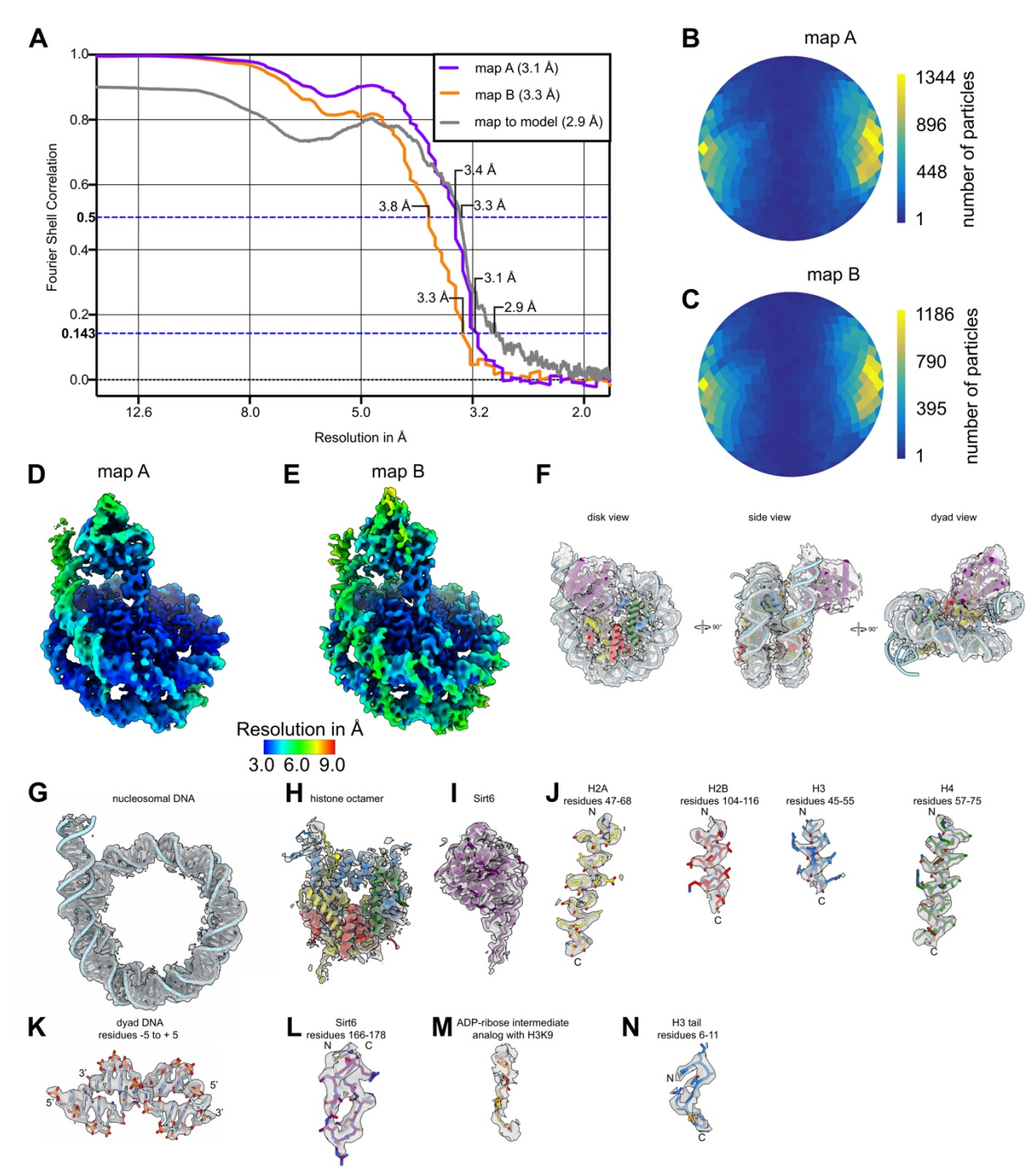


Figure S19. Data quality metrics and densities of the nucleosome-Sirt6 complex. (A) FSC curves of overall maps (map A and B) and map-to-model. Resolutions at FSC threshold criterions 0.143 and 0.5 are indicated. (B,C) Angular distribution of particles employed to reconstruct nucleosome-Sirt6 complex maps A and B. (D,E) Local resolutions of nucleosome-Sirt6 complex maps A and B. (F) Three views of nucleosome-Sirt6 atomic model with corresponding cryo-EM map (map A). Cryo-EM map is shown in grey. (G) DNA with corresponding density from nucleosome-Sirt6 complex (map A). (H) Histone octamer with corresponding density from nucleosome-Sirt6 complex (map A). (I) Sirt6 with corresponding density from nucleosome-Sirt6 complex (map A). Residue numbers are indicated. (K) DNA around the dyad (base pairs -5 to +5) with corresponding density from nucleosome-

Sirt6 complex (map A). N- and C-terminus are indicated. (L) Zn binding insertion loop from Sirt6 with corresponding density from nucleosome-Sirt6 complex (map A). Residue numbers are indicated. N- and C-terminus are indicated. (M) NAD transition state analog and H3K9 with corresponding density from nucleosome-Sirt6 complex (map A). (N) H3 tail residues (residues 6-11) with corresponding density from nucleosome-Sirt6 complex (map A). N- and C-terminus are indicated.



Figure S20. Multiple sequence alignment of *H. sapiens* Sirt1-7 small zinc binding domains. Beta sheets 4 and 5 of the small zinc binding domain are indicated above. Zinc-binding cysteine residues are indicated below. The basic loop involved in Sirt6 binding to the H2A/H2B acidic patch, indicated on the lower right, is unique to Sirt6 among human sirtuins. Basic loop residues are numbered on the top right.

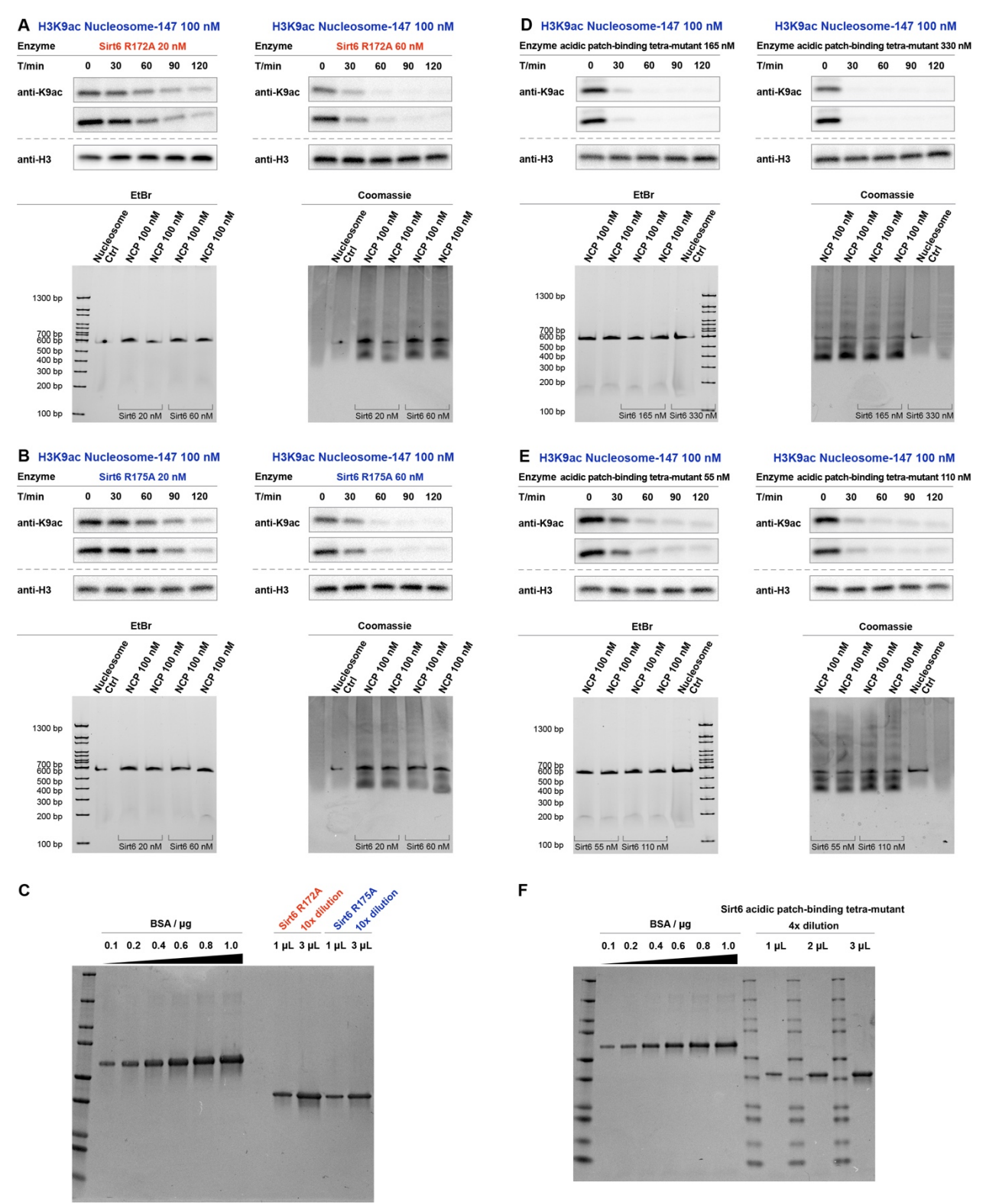


Figure S21. Western blot and curve fitting for deacylation by 3 acidic-patch binding mutants. Western blot of deacetylation assay on H3K9ac nucleosome-147 with (A) Sirt6 R172A (20 nM and 60 nM). (B) Sirt6 R175A (20 nM and 60 nM). (D)(E) Sirt6 acidic patch-binding tetra-mutant (55, 110, 165, and 330 nM). SDS-PAGE densitometry for (C) Sirt6 R172A and Sirt6 R175A; (F) Sirt6 acidic patch-binding tetramutant.

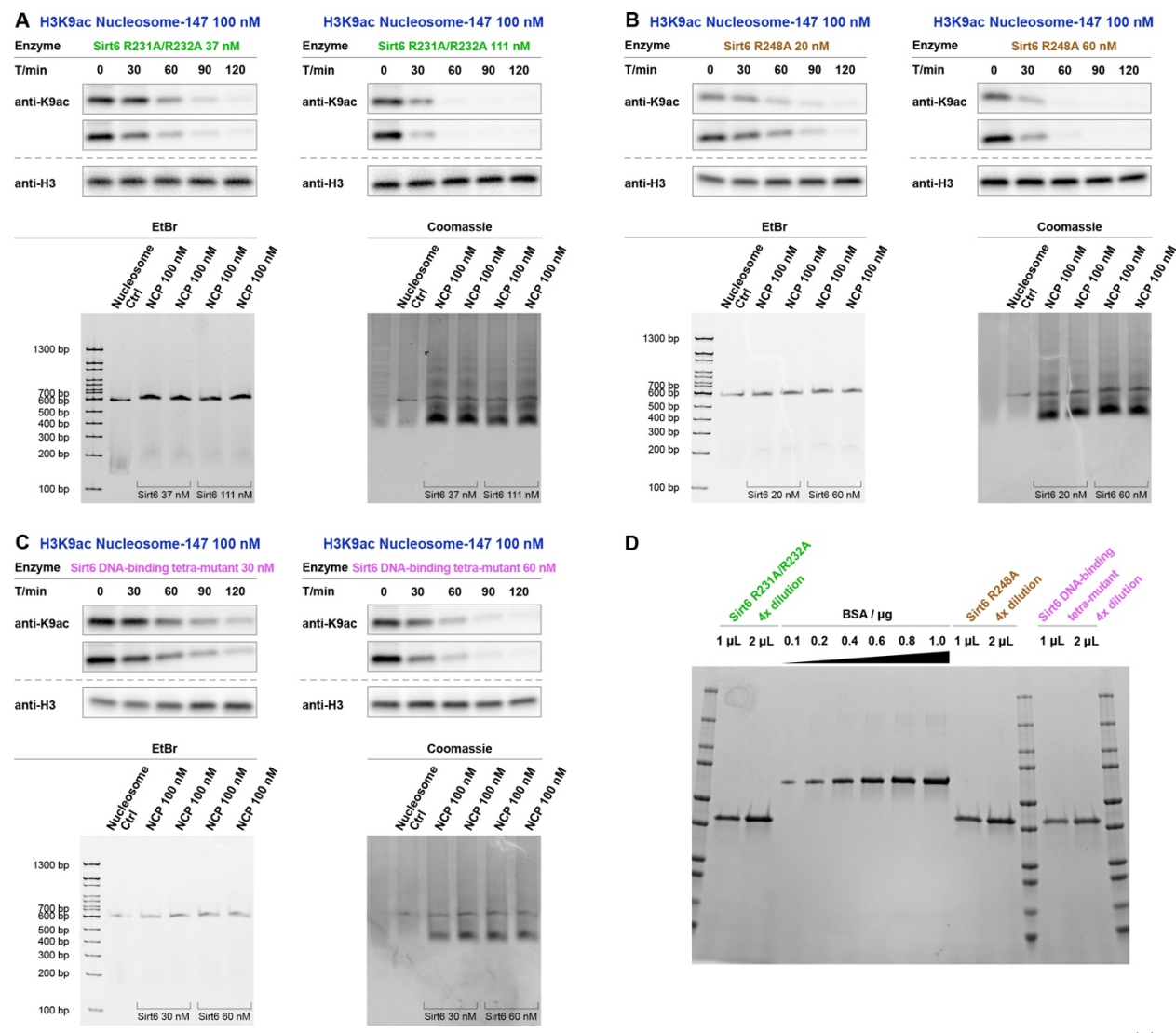
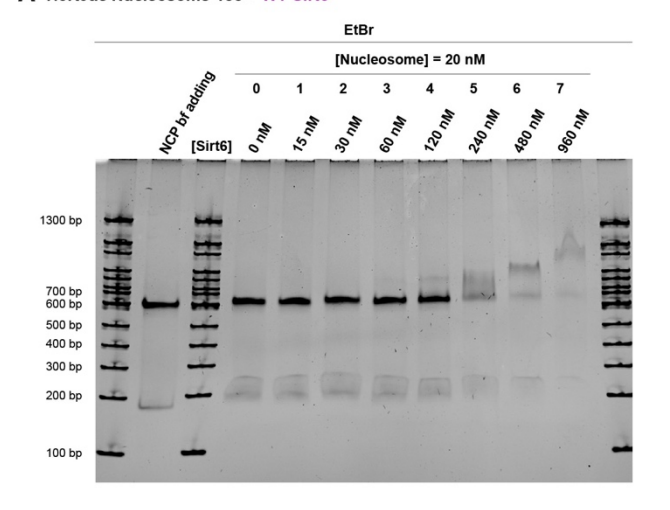
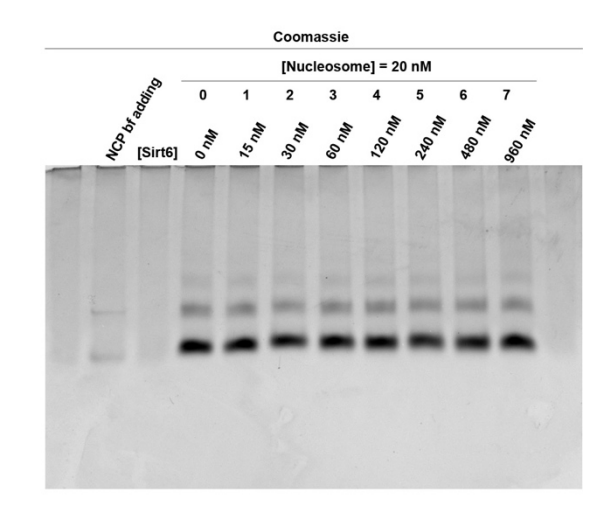


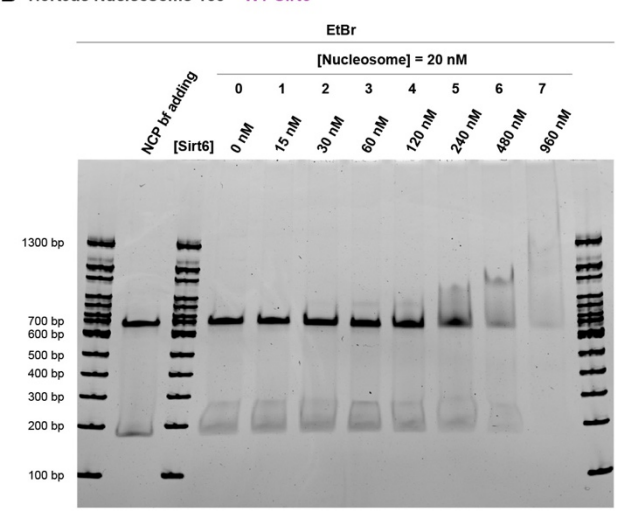
Figure S22. Western blot and curve fitting for deacylation by 3 DNA binding mutants. Western blot of deacetylation assay on H3K9ac nucleosome-147 with (A) Sirt6 R231A/R232A (37 nM and 111 nM). (B) Sirt6 R248A (20 nM and 60 nM). (C) Sirt6 DNA-binding tetra-mutant (30 nM and 60 nM). SDS-PAGE densitometry for (D) Sirt6 R231A/R232A, Sirt6 R248A, and Sirt6 DNA-binding tetra-mutant.

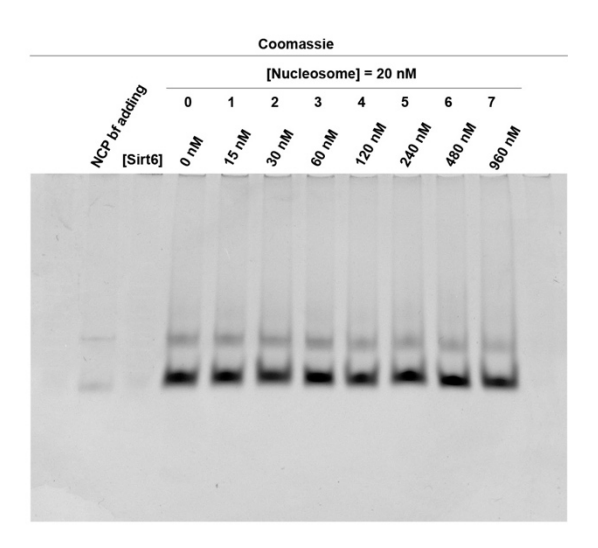
A H3K9ac Nucleosome-185 + WT Sirt6



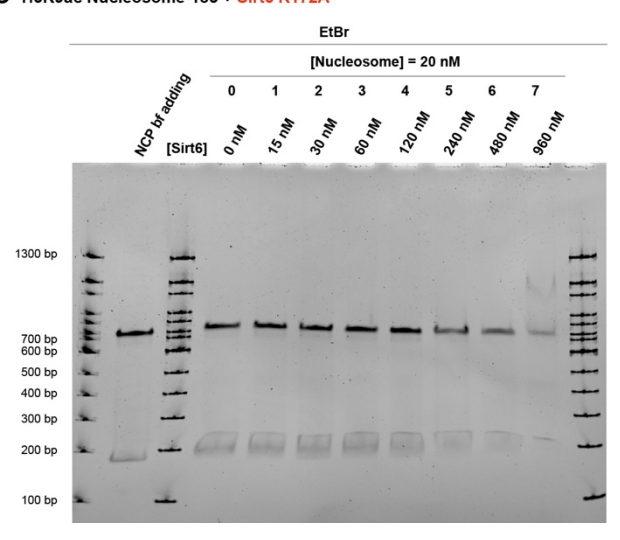


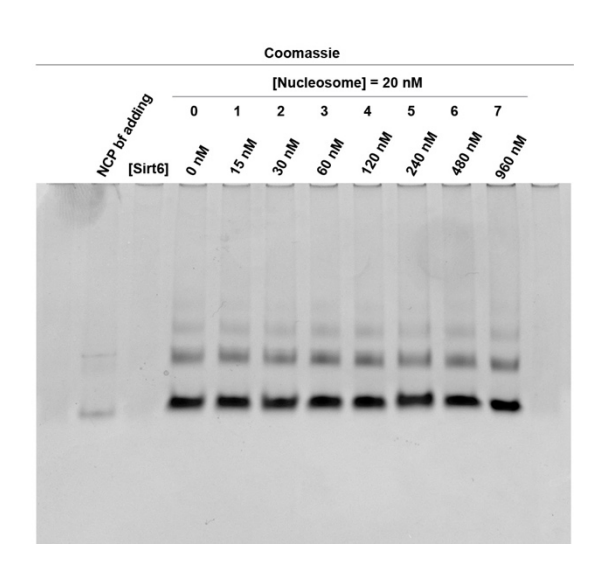
B H3K9ac Nucleosome-185 + WT Sirt6



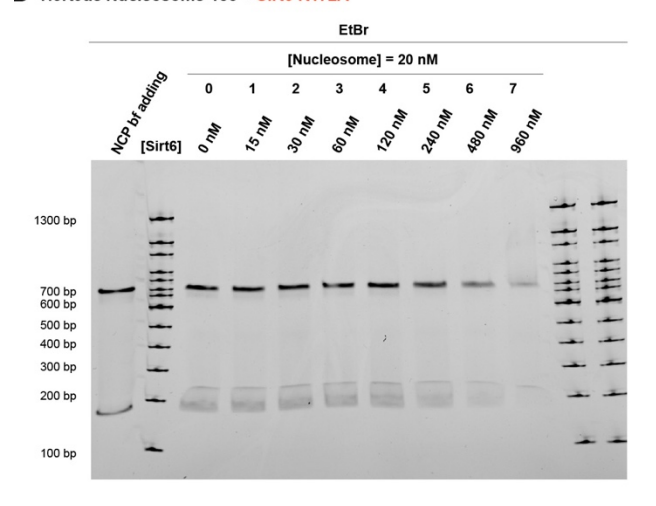


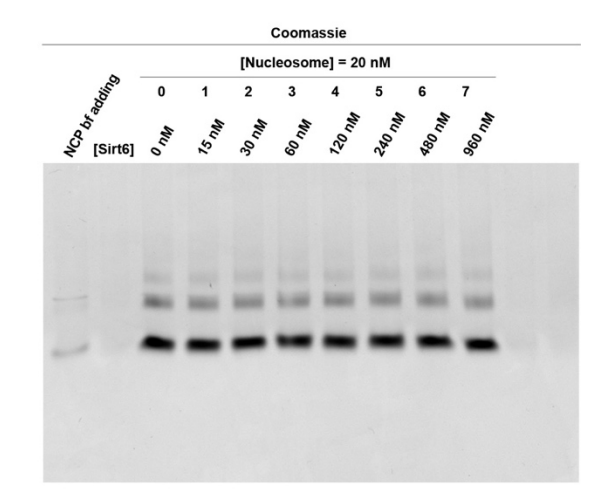
C H3K9ac Nucleosome-185 + Sirt6 R172A



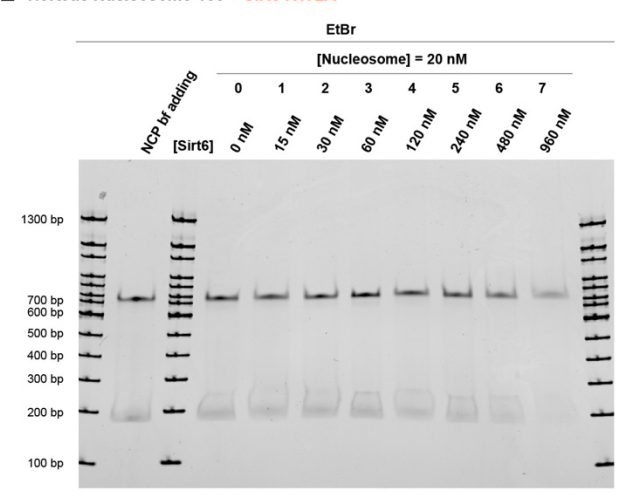


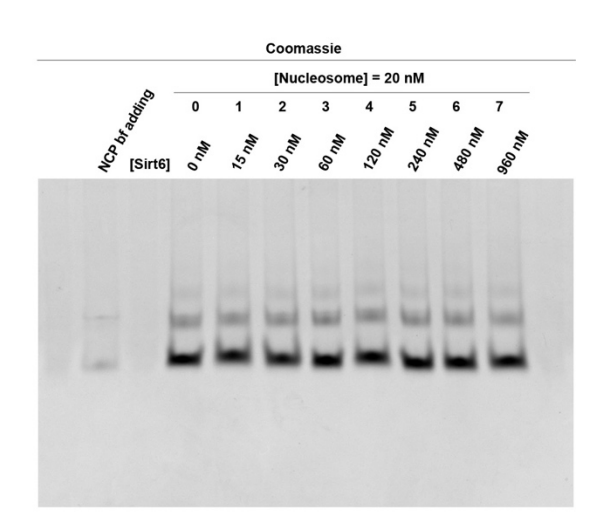
D H3K9ac Nucleosome-185 + Sirt6 R172A



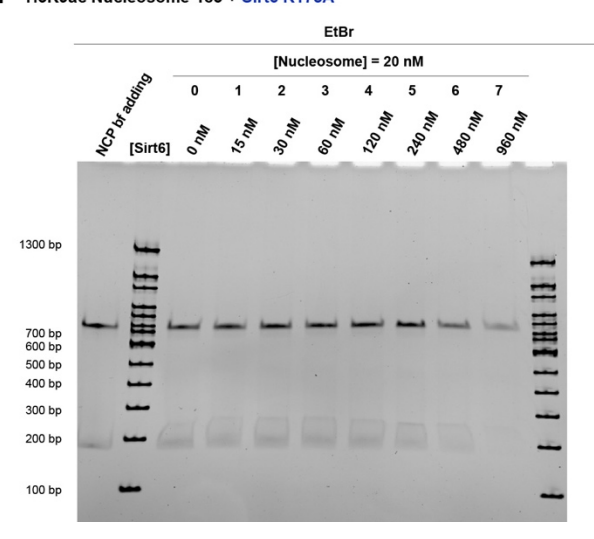


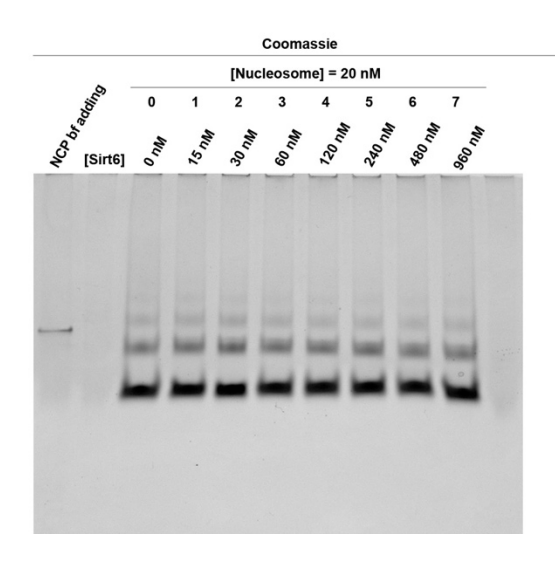
E H3K9ac Nucleosome-185 + Sirt6 R172A



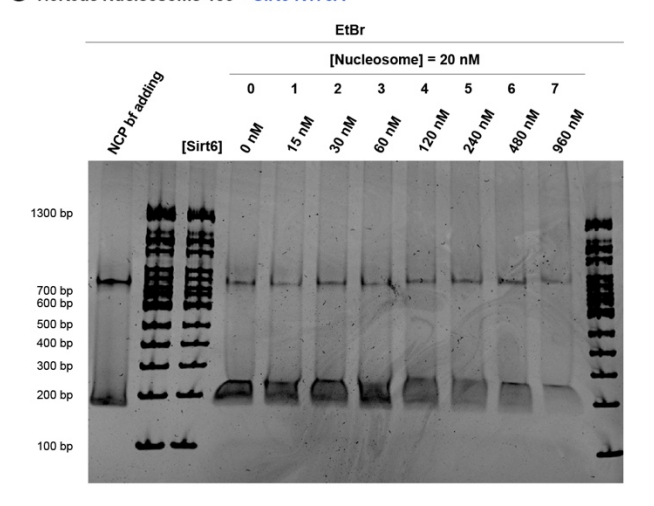


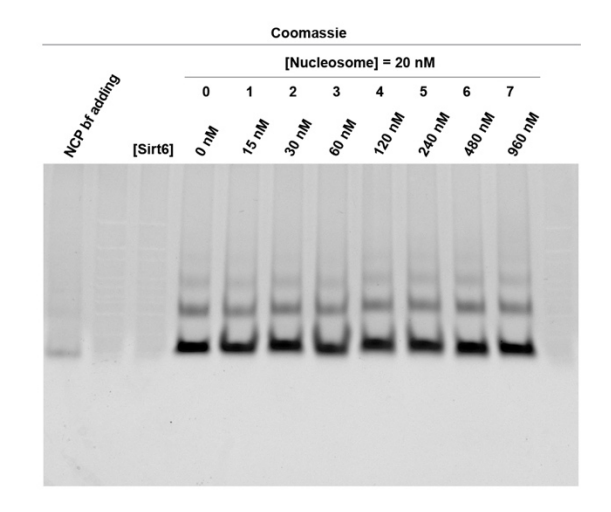
F H3K9ac Nucleosome-185 + Sirt6 R175A



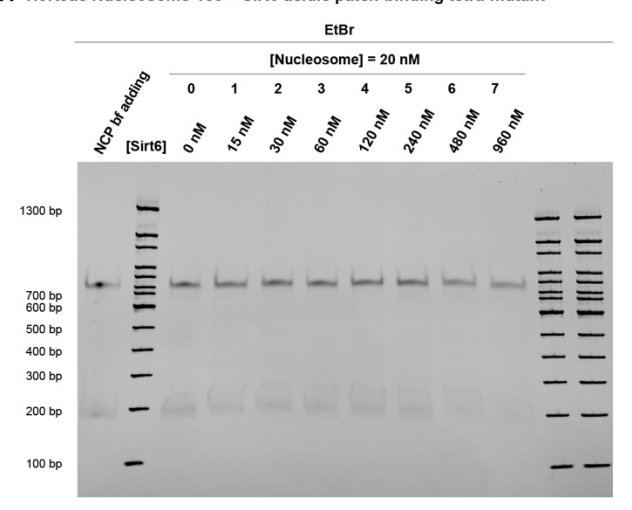


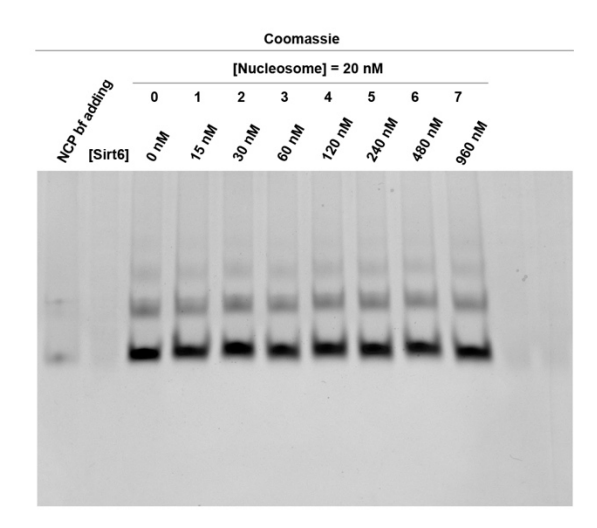
G H3K9ac Nucleosome-185 + Sirt6 R175A



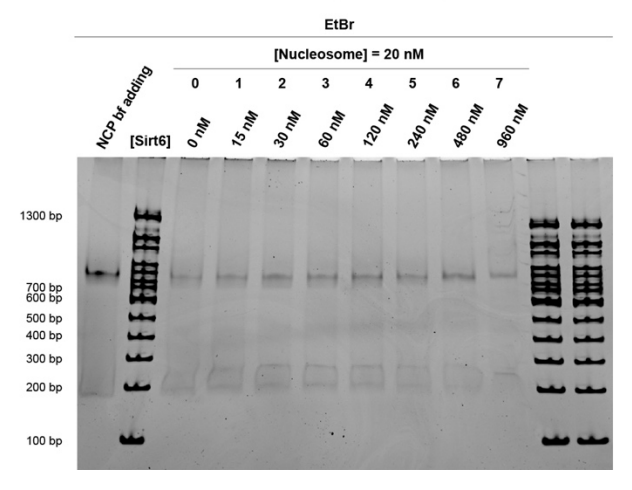


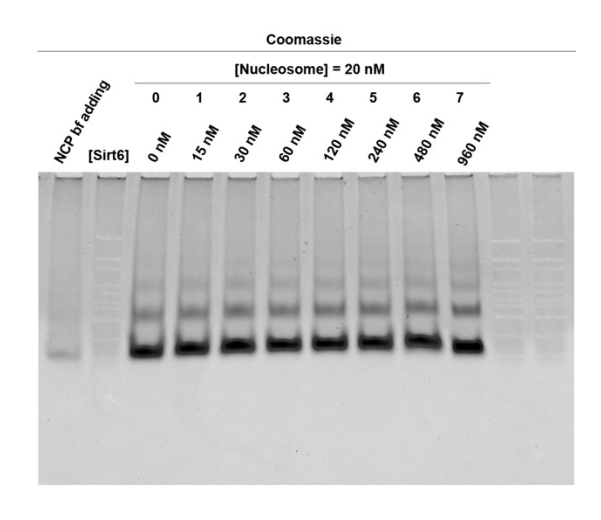
H H3K9ac Nucleosome-185 + Sirt6 acidic patch-binding tetra-mutant



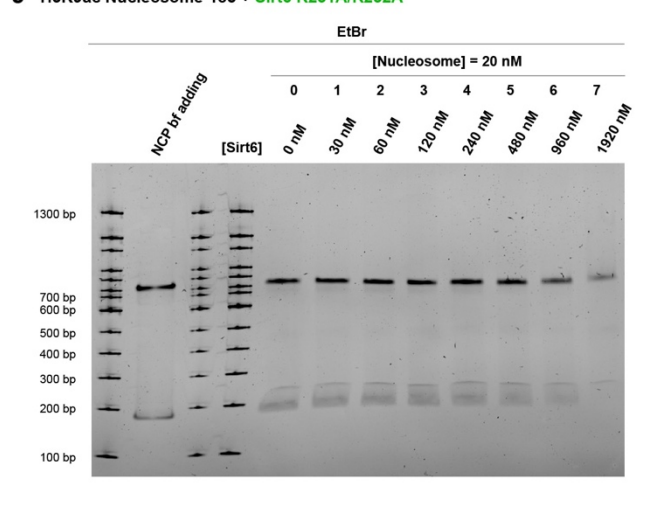


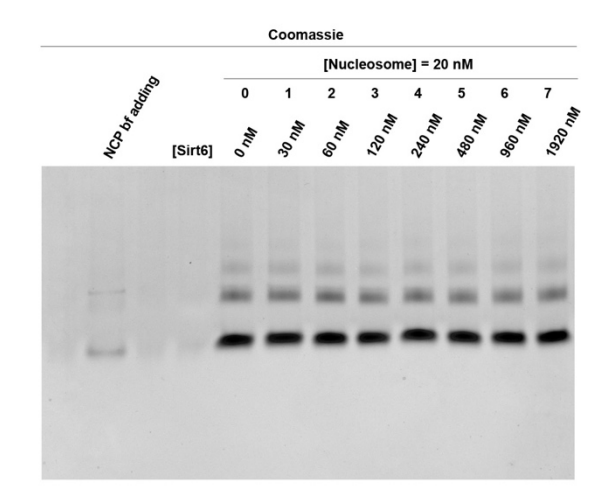
l H3K9ac Nucleosome-185 + Sirt6 acidic patch-binding tetra-mutant



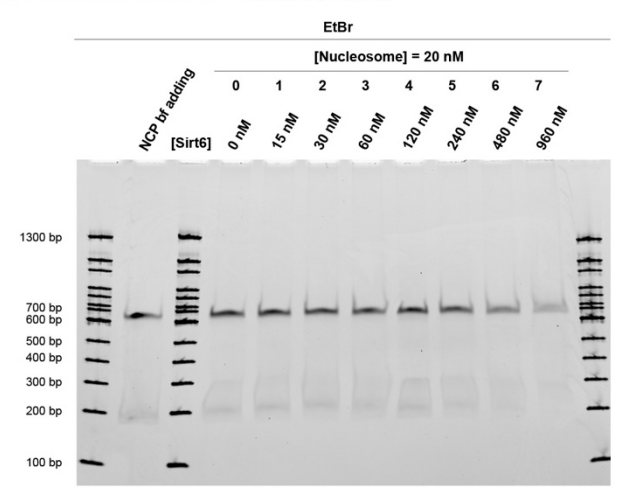


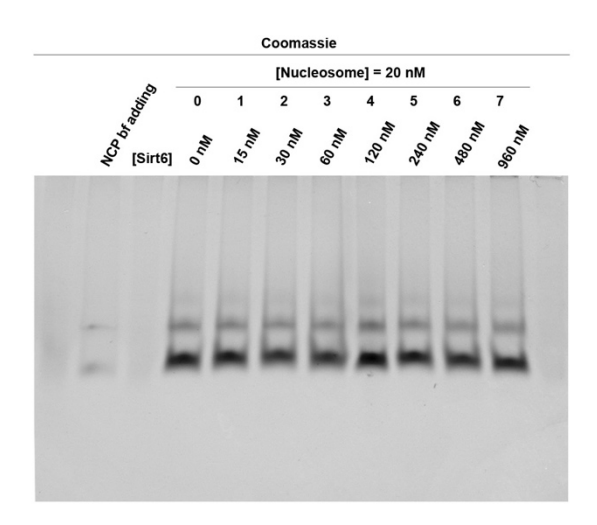
J H3K9ac Nucleosome-185 + Sirt6 R231A/R232A



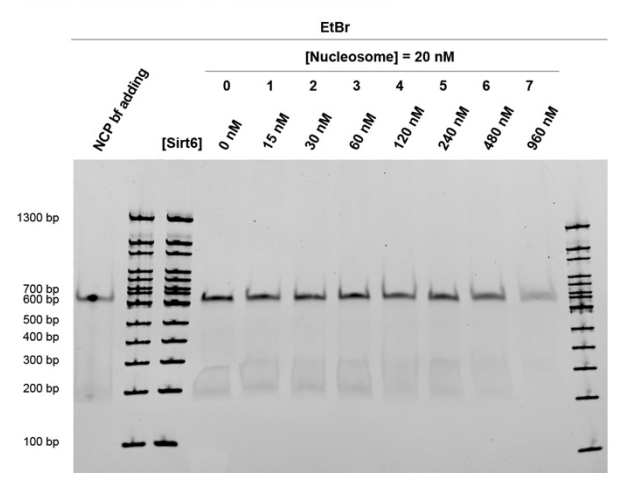


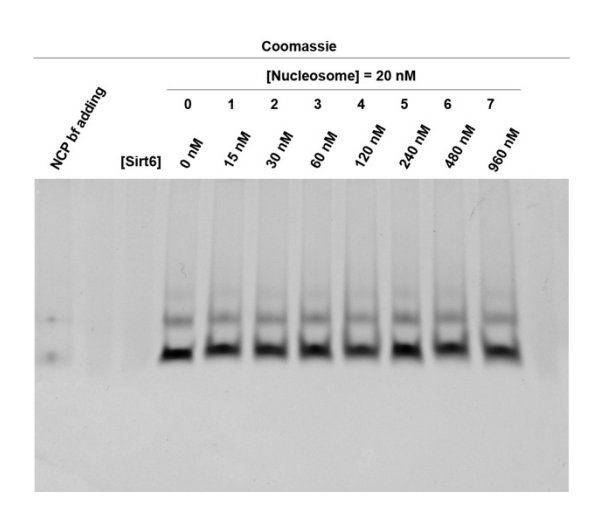
K H3K9ac Nucleosome-185 + Sirt6 R231A/R232A



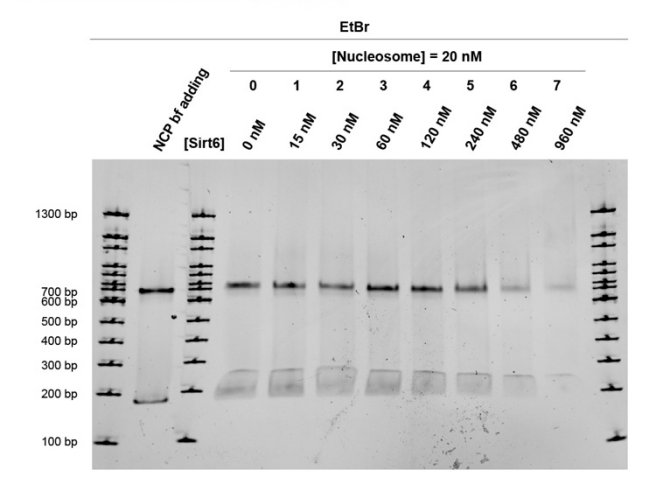


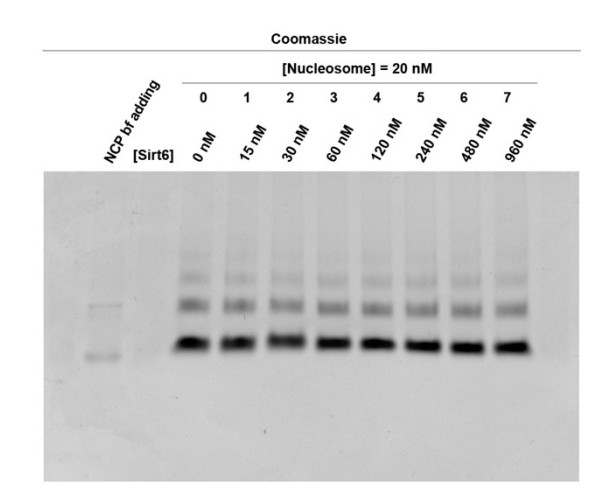
L H3K9ac Nucleosome-185 + Sirt6 R231A/R232A



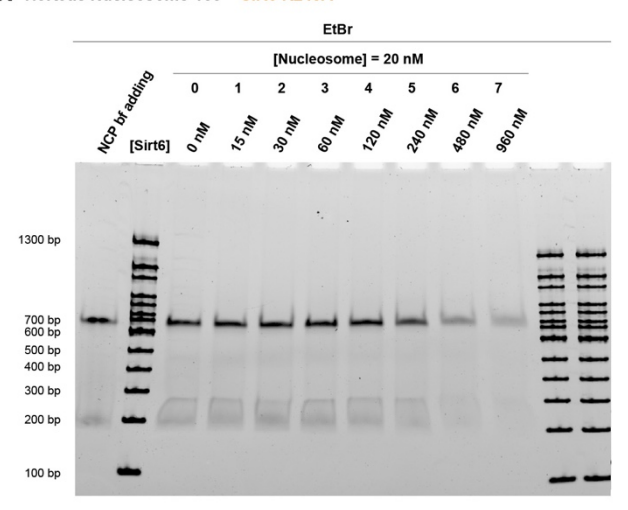


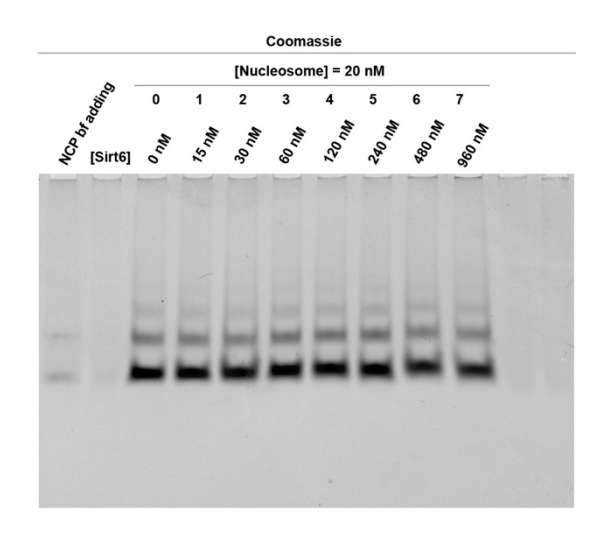
M H3K9ac Nucleosome-185 + Sirt6 R248A



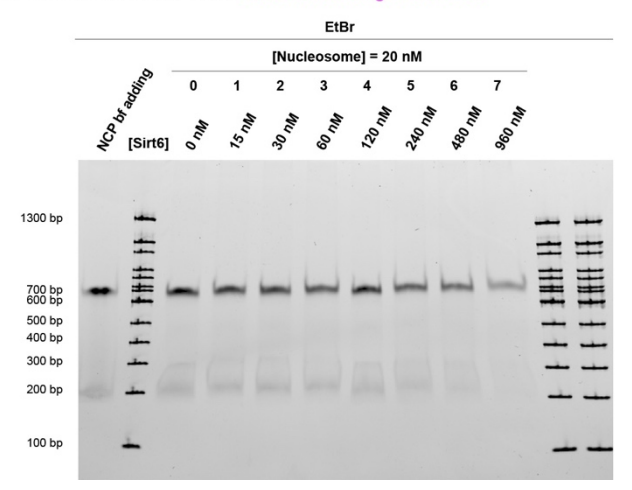


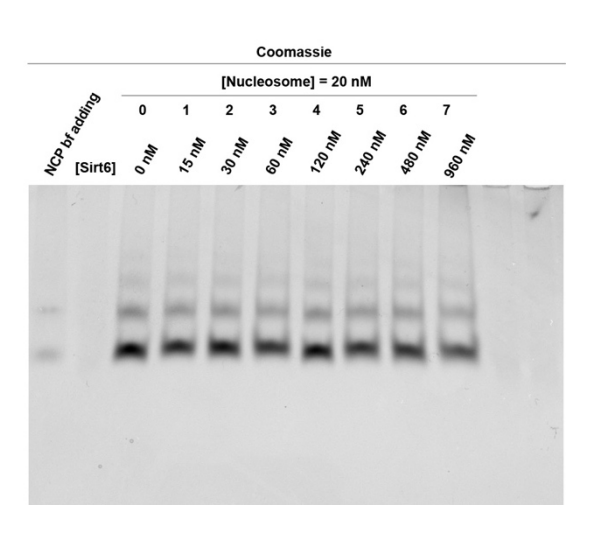
N H3K9ac Nucleosome-185 + Sirt6 R248A





O H3K9ac Nucleosome-185 + Sirt6 DNA-binding tetra-mutant





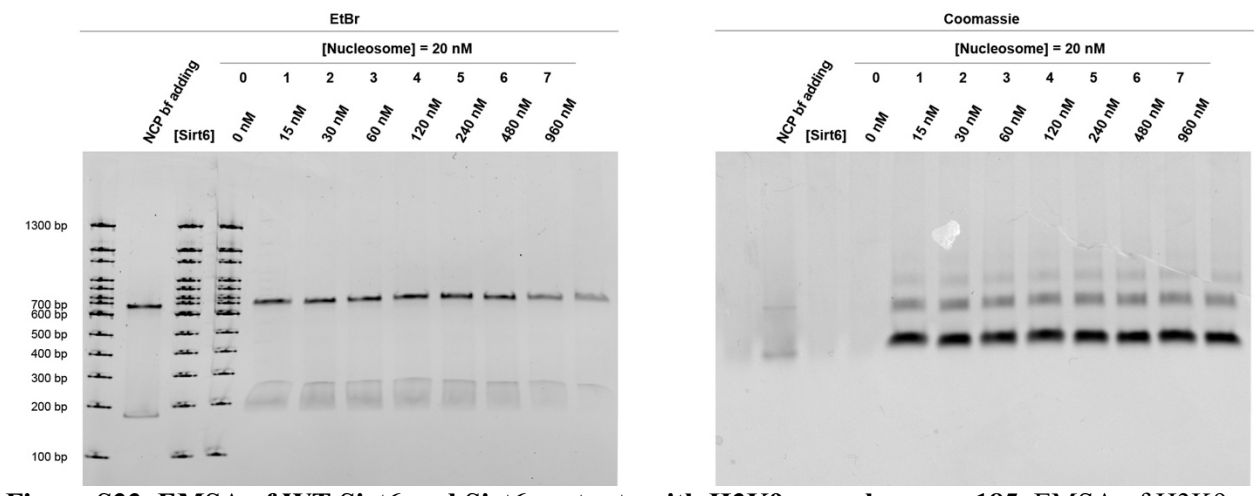


Figure S23. EMSA of WT Sirt6 and Sirt6 mutants with H3K9ac nucleosome-185. EMSA of H3K9ac nucleosome-185 binding with (A)(B) WT Sirt6. (C)(D)(E) Sirt6 R172A. (F)(G) Sirt6 R175A. (H)(I) Sirt6 acidic patch-binding tetra-mutant. (J)(K)(L) Sirt6 R231A/R232A. (M)(N) Sirt6 R248A. (O)(P) Sirt6 DNA-binding tetra-mutant.

Table SI 1-3

Table S1 All the calculated V/[E] for deacetylation assays

Table ST All the calculat	eu v/[E] for deacetyla	ation assays	
H3 Nucleosome sites	V/[E] (min ⁻¹)	H3 Protein sites	Normalized V/[E] (min ⁻¹)
H3K9ac	0.10±0.0068	H3K9ac	< 0.01
H3K14ac	0.0012±0.00030	H3K14ac	< 0.01
H3K18ac	0.043±0.0031	H3K18ac	< 0.01
H3K23ac	0.011±0.00059	H3K23ac	< 0.01
H3K27ac	0.040±0.0036	H3K27ac	< 0.01
H2B Nucleosome sites	V/[E] (min ⁻¹)	H2B Protein sites	Normalized V/[E] (min ⁻¹)
H3K9ac	0.10±0.068	H3K9ac	< 0.01
H2BK11ac	< 0.001	H2BK11ac	< 0.01
H2BK12ac	< 0.001	H2BK12ac	< 0.01
H2BK20ac	< 0.001	H2BK20ac	< 0.01
H2BK46ac	< 0.001	H2BK46ac	< 0.01
NAD (μM)	V/[E] (min ⁻¹)	NaCl (mM)	V/[E] (min ⁻¹)
0	0	0	0.10±0.010
56.95	0.030±0.0053	25	0.15±0.0089
227.8	0.076±0.0065	50	0.071±0.0042
1000	0.102±0.010	100	0.023±0.0015
1139	0.0997±0.0068	250	0.00077±0.00061
Nucleosome-147 (nM)	V/[E] (min ⁻¹)	Nucleosome-185 (nM)	V/[E] (min ⁻¹)
0	0	0	0
10	0.053±0.0072	10	0.065±0.0043
20	0.054±0.0096	20	0.058 ± 0.0033
50	0.096 ± 0.012	50	0.093±0.012
100	0.10±0.0048	100	0.11±0.0099
200	0.115±0.011	200	0.13±0.017
400	0.111±0.0057		
log[MDL-800(nM)]	V_0/V_m	Sirt6 mutants	V/[E] (min ⁻¹)
5	4.1±0.80	R172A	0.057±0.0049
4	3.6±0.57	R175A	0.048 ± 0.0050
3	1.8±0.38	acidic patch-binding tetra-mutant	0.044±0.0020
2	1.5±0.39	R231A/R232A	0.046±0.0062
1	1.6±0.25	R248A	0.060±0.0038
0	1.0±0.19	DNA-binding tetra-mutant	0.038±0.0033

Table S2 Cryo-EM data collection, refinement, and validation statistics

	Sirt6-nucloeosome (map A) PDB 8F86 EMDB 28915	Sirt6-nucleosome (map B)				
Data collection and processing						
Magnification	105,000	105,000				
Voltage (kV)	300	300				
Electron exposure (e ⁻ /Å ²)	50.45	50.45				
Defocus range (µm)	0.7-1.7	0.7-1.7				
Pixel size (Å)	0.83	0.83				
Symmetry imposed	C1	C1				
Initial particles images (no.)	4,064,579	4,064,579				
Final particle images (no.)	95,205	81,315				
Map resolution (Å)	3.1	3.3				
FSC threshold	0.143	0.143				
Map resolution range (Å)	3-6	3-8				
Refinement						
Initial models used (PDB code)	3LZ0, 5Y2F					
Map sharpening <i>B</i> factor (Å ²)	-69.3	-52.3				
Model composition						
Non-hydrogen atoms	14400					
Protein residues	1054					
Nucleotides	296					
Ligands	LIG: 1					
	ZN: 1					
B factors (Å ²) Protein	124.09					
Nucleotide	186.18					
Ligand	145.68					
R.m.s. deviations						
Bond lengths (Å) Bond angles (°)	0.004 (0)					
	0.638 (4)					
Validation						
MolProbity score	1.78					
Clashscore	7.47					
Poor rotamers (%)	0.00					
Ramachandran plot						
Favored (%)	94.67					
Allowed (%)	5.14					
Disallowed (%)	0.19					

Table S3 Input structural models and confidence

Domain/complex	Chain id	Input model	Level of confidence
Nucleosome	A-J	3LZ0	Atomic, side chains resolved
H2A	C,G	3LZ0	Atomic, side chains resolved
H2B	D,H	3LZ0	Atomic, side chains resolved
Н3	A,E	3LZ0,5Y2F	Atomic, side chains resolved
H3 tail (residues 3-13)	A	5Y2F	Atomic, side chains resolved
H4	B,F	3LZ0	Atomic, side chains resolved
DNA	I,J	3LZ0	Atomic, phosphate backbone resolved
SIRT6	K	5Y2F, AlphaFold2	Atomic, rigid body docked, AlphaFold2 modeled; partially side chains resolved or clear secondary structures resolved
SIRT6 (residues 2-16)	K	AlphaFold2	Rigid Body docked
SIRT6 (residues 17-83)	K	5Y2F	Rigid body docked
NAD analog	A	5Y2F	Rigid Body docked, density matches shape